Modeling cortical development and microcephaly in human pluripotent stem cells using combinatorial pathway inhibition

Dissertation

to obtain the academic degree
Doctor rerum naturalium (Dr. rer. nat.)

submitted to the Department of Biology, Chemistry and Pharmacy of
Freie Universität Berlin

by
Naresh Mutukula

2019

The research work for this dissertation was performed from July 2014 to May 2019 under the supervision of Dr. Yechiel Elkabetz at the Max Planck Institute for Molecular Genetics in Berlin, Germany. The dissertation was submitted in May 2019 to the Department of Biology, Chemistry and Pharmacy of the Freie Universität Berlin, Germany.

1st Reviewer: Dr. Yechiel Elkabetz
Max Planck Institute for Molecular Genetics, Berlin.

2nd Reviewer: Prof. Dr. Sigmar Stricker
Freie Universität Berlin

Date of disputation: 18th Nov, 2019

Acknowledgements

First and foremost, I would like to express my deep gratitude to my supervisor Dr. Yechiel Elkabetz for giving me the opportunity to work in his lab and introducing me to the very exciting world of pluripotent and neural stem cell biology research. I am very grateful to him for his excellent supervision, constant support and immense patience he has shown in both good and bad times during all these years of my PhD. I would like to thank him for all the teachings and discussions including non-academics during the last few years.

Secondly, I would like to thank Prof. Dr. Sigmar Stricker for accepting to be the second reviewer of my PhD dissertation.

I am very thankful to my good friend Rotem Volkman from Tel Aviv University, who was there for me during the initial phase of my PhD. I always admired his views and suggestions. I would like to thank Dr. Yakey Yaffe for teaching pluripotent and neural stem cell culture techniques and sharing his everlasting infectious enthusiasm towards science. It was a pleasure working with both of them and will always remember the great times we have shared. Toda raba!!

I would like to thank Daniel Rosebrock for all the help with the computational analysis for the manuscript and this dissertation. I would also like to thank Amèlia Aragonés Hernández for sharing her views and thoughtful discussions.

I would like to thank my wife and colleague Sneha Arora for helping me with the generation of microcephaly mutant cell lines. A huge hug and special thanks for putting up with me all these years of my PhD. Dhanyavaad!!

I would like to thank FACS, RNA-Sequencing and Imaging facility of MPIMG, Berlin and Tel Aviv University for all the help and support. I would also like to thank all the previous members of Elkabtez's group for all the support whenever needed and for being such great people.

Finally, I would like to thank my family — my father – Ananda Rao, my mother – Swaroopa Rani and my brothers – Mahesh Kumar and Suresh Kumar for their unconditional love and support during the ups and downs of my life. This wouldn't have been possible without your constant support. Words fall short to express my love and gratitude to you.

Table of Contents

Acknowledgements ... 3
Table of contents ... 5
Abstract (English) ... 8
Abstract (Deutsch) ... 10
1. Introduction ... 13
1.1 Early mammalian embryonic development ... 13
1.2 Neurulation ... 13
1.3 In vivo neural induction and patterning ... 15
1.4 Role of morphogens in neural induction and patterning ... 18
1.4.1 Transforming Growth Factor (TGF)-β Superfamily ... 18
1.4.1.1 Bone morphogenetic protein (BMP) Signaling ... 19
1.4.1.2 Activin/Nodal TGF- β Signaling ... 20
1.4.2 Fibroblast growth factor (FGF) Signaling ... 20
1.4.3 WNT Signaling ... 21
1.4.4 Retinoic acid (RA) Signaling ... 21
1.4.5 Sonic Hedge Hog (SHH) Signaling ... 21
1.5 Pluripotent stem cells (PSCs) – a powerful platform to study embryogenesis ... 22
1.6 Neural stem cells (NSCs) ... 23
1.7 NSCs in cerebral cortex development ... 24
1.8 Recapitulating in vivo neural induction and patterning in vitro using PSCs ... 27
1.9 Notch signaling and rosette formation - a tool for measuring efficiency of cortical specification ... 31
1.10 Modeling cortical neuro developmental disorders ... 32
2. Materials and methods ... 35
2.1 Cell lines ... 35
2.2 Reagents ... 35
2.3 Molecular biology application kits ... 37
2.4 Reagents preparation ... 37
2.5 Generation and culture of human embryonic stem cells (hESCs) ... 39
2.6 Generation and culture of induced PSCs (iPSCs) ... 40

2.7 Neural induction and rosette formation of PSCs using the small EBs (sEBs) protocol 41
2.8 Derivation of cerebral organoids from human pluripotent stem cells 44
2.9 RNA isolation 48
2.10 Preparation and Sequencing of RNA Sequencing (RNA-Seq) Libraries 49
2.11 Description of processed RNA-Seq datasets of human brain transcriptomes 49
2.12 RNA-Seq data processing and normalization for single and pooled organoids 50
2.13 Combined RNA-Seq data analysis for organoid and human brain datasets 50
2.14 Correspondence analysis 51
2.15 Differential Expression and Gene Set Enrichment analysis of organoid data sets 51
2.16 Single cell RNA-Seq (scRNA-Seq) procedures 52
2.16.1 Organoid dissociation 52
2.16.2 Single cell library preparation 52
2.16.3 Single cell RNA-Seq data processing 52
2.16.4 Single cell gene mapping and UMI counting 53
2.16.5 Single cell dataset alignments, tSNE analysis and cell-subpopulation identification 53
2.17 Immunostaining and confocal imaging 54
2.18 Quantitative PCR (qPCR) analysis 56
2.19 Measurements and statistical analysis 57
3. Results **58**
3.1 Neural induction platforms 59
3.2 Molecular analysis of 3D organoids and 2D neural rosettes derived by various inhibition paradigms 59
3.2.1 Correspondence analysis for RNA-Seq profiles of organoids derived by different methods 59
3.2.2 Integrated RNA-Seq analysis of organoids generated under different inhibition paradigms and human embryonic brain samples reveals substantially distinct human brain regional signatures 61

3.2.3 Correspondence analysis for RNA-Seq profiles of 2D neural rosettes generated under different inhibition paradigms 68
3.3 Cellular analysis of 3D organoids and 2D neural rosettes generated under different inhibition paradigms 71
3.3.1 Radial organization of NSCs is a hallmark for transition of PSCs towards cortical fates 71
3.3.2 Radial Organization of NSCs derived under combined dual SMAD and WNT inhibition coincides with dorsal cortical markers 76
3.4 Combined dual SMAD and WNT inhibition allows standardized modeling of microcephaly 90
3.4.1 Significant reduction in cortical gene expression and massive apoptosis in microcephaly organoids occurs only when derived under combined inhibition ... 94
3.5 Single cell RNA Sequencing of organoids reveals enrichment for cortical fates in organoids derived by combined dual SMAD and WNT inhibition 99
3.6 Cortical layer markers appear more homogeneously under combined dual SMAD and WNT inhibition 109
4. Discussion **113**
5. Bibliography **122**
6. Abbreviations **139**
7. List of publications **141**

Abstract (English)

Pluripotent stem cells have an enormous potential to self-renew indefinitely and differentiate into ectoderm, mesoderm and endoderm, the three germ layers of the body. This striking ability has turned PSCs throughout the years to be a major driver of regenerative medicine research and applications that utilize such cells for generation of cell types of interest thereby including disease modeling, drug screening and cell replacement-based therapies. However, creating PSC-based differentiation platforms that ensure derivation of homogenous cultures for desired clinically relevant cell types is critical for meaningful understanding and usage of such cells for therapy. Currently, cell heterogeneity is still one of the major hurdles for cell replacement-based therapy even following decades of stem cell research. Therefore one of the major goals of the field is to develop strategies for generating homogenous cell types from PSCs.

Our lab is mainly interested in studying PSC-based central nervous system (CNS) development, with particular focus on the development of the cerebral cortex. The cerebral cortex (or neocortex) is the newly evolved and most complex structure of human brain, which is the site for higher order functions such as sensory perception, cognition and emotions. Methods for deriving cortical progenitors from PSCs are highly diverse and largely lack robust readouts, and hence are prone to yield heterogeneous populations that contain both cortical and non-cortical CNS cell types among other non-neural cell types. Combining knowledge from *in vivo* cortical developmental studies and previous findings from our lab on *in vitro* studies of neural differentiation from PSCs, in this study we show a streamlined strategy to generate homogenous cortical progenitors from PSCs by inhibiting WNT pathway on top of routinely used dual SMAD inhibition. We perform a systematic comprehensive comparison, at both molecular and cellular levels, of previously the major known cortical differentiation paradigms side by side with our combined WNT and dual SMAD inhibition (Triple-i) paradigm in both 2D monolayer and 3D organoid culture platforms.

We employ bulk RNA-Sequencing and analysis of 10,000 differentially expressed genes among single organoids and human brain samples to reveal that combined WNT and dual SMAD inhibition exclusively reproduces neocortical fates, dual SMAD inhibition induces diencephalic-mid-hindbrain fates, and inhibition-free conditions promote mixed fates. Further employing Single cell RNA-Sequencing we confirm the brain regional heterogeneity observed in bulk RNA-Seq, highlighting enriched cortical stem cell population in organoids derived under combined WNT and dual SMAD inhibition. On the other hand, we find that dual SMAD-i and inhibitor-free organoids are heterogeneous consisting of both cortical and non-cortical populations. Single cell RNA-Sequencing also confirm the presence of the major cortical cell types including neural stem cells, intermediate progenitors and neurons in organoids derived by both dual SMAD-i and Triple-i.

In this study we also revisit the role of radial organization (rosette formation) – conventionally known to mark general neural fate conversion - and assign it as unique feature of cortical NSCs. We particularly show that enhanced Notch activation (stemness) and efficient radial organization are integral and overlapping hallmarks of homogeneous neocortical specification. We also show that this feature is dramatically streamlined under Triple-i in both 2D (rosettes) and 3D (organoids) systems, thus functionally linking stemness, cell polarity and the robust acquisition of cortical fates under combined inhibition. In support to this finding, inhibitor-free cultures exhibit weak Notch activation not necessarily overlapping radial organization, while SMAD cultures show Notch activation in non-radially organized regions enriched for non-cortical fates. We therefore propose these features – when overlapping – could be used as reliable readouts for efficient cortical differentiation.

As a proof of concept for the utility of our findings for regenerative medical research and applications, we use brain organoid technology as platform to model neurodevelopmental disorders such as microcephaly. Microcephaly is a genetically heterogeneous cortical developmental disorder characterized by abnormalities in the development of the cortex resulting in smaller brain size. We derive microcephaly organoids by generating hESCs harboring defects in the centrosomal protein STIL, and show that such organoids display apoptosis within Notch active and radially organized vesicles, arrest in cell cycle, premature differentiation and loss of cortex

specific marker expression only when derived by combined WNT and dual SMAD inhibition, demonstrating cortex-specific etiology. Thus, combined WNT and dual SMAD inhibition is indispensable for standardized modeling of corticogenesis in health and disease.

Abstract (Deutsch)

Pluripotente Stammzellen (PSCs) haben ein enormes Potential zur unbegrentzen Selbsterneuerung und Differenzierung zu den drei Keimschichten des Körpers: ektoderm, mesoderm und endoderm. Diese auffällige Kapazität hat dazu geführt, dass PSCs eine wichtige Rolle in der regenerativen Medizinforschung spielen. Ihr Potential, verschiedene Zellenarten zu generieren, ermöglicht ihre Verwendung in vielen Bereichen, zum Beispiel Krankheitsmodellierung, Drogenscreening und Zellensubstitutionstherapien. Um die PSCs erfolgreich für diese Therapien anzuwenden, braucht man Differenzierungsplatformen, die Herleitung homogener Zellkulturen für klinisch relevante Zellenarten sicherstellen. Auch nach Jahrzehnten der Stammzellforschung ist die Zellenheterogenität derzeit eine der größten Hürden für Zellensubstitutionstherapien. Deshalb ist eins der größten Ziele dieses Forschungbereichs Strategien für die Generierung homogener Zellenarten aus PSCs zu entwickeln.

Unser Labor interessiert sich hauptsächlich dafür, die Herstellung vom Zentralnervensystem (ZNS), besonders von der Großhirnrinde, von pluripotenten Stammzellen zu studieren. Die Großhirnrinde (der Neocortex) ist die neuentwickelte und komplizierteste Struktur des Menschengehirns, das für Funktionen höherer Schichten, z.B. die Sinneswahrnehmung, Kognition, und Emotion, verantwortlich ist. Die Methoden, die zurzeit für die Herstellung von Kortikalprogenitorzellen angewendet werden, sind sehr vielfältig und haben einen Mangel an robusten Auslesungen. Deswegen haben diese Methoden das Problem, dass sie heterogene Populationen von kortischen und nicht kortischen Zellenarten des ZNS und dazu nicht neurale Zellenarten herstellen. Durch die Kombination des Wissens von *in vivo* Studien über die kortische Entwicklung und vorherigen *in vitro* Ergebnissen unseres Labors über Neuraldifferenzierung von PSCs, zeigen wir in dieser Studie eine stromlinienförmige Strategie. Diese Strategie erschafft homogene Kortikalprogenitorzellen von PSCs durch die Inhibition von dem WNT Signalweg und

die routinemäßig benutzten dual SMAD Inhibition (Triple-i). Wir führen einen systematisch umfassenden Vergleich in molekularen und zellularen Ebenen durch. Wir vergleichen die bisherigen Methoden, die für den kortischen Differenzierungsprozess angewendet sind, mit unserer Triple-i Methode in 2D Monoschichten und 3D organoidzüchtungplatformen.

Wir benutzen bulk RNA Sequenzieren und die Analyse von 10.000 differentiell exprimierten Genen zwischen organoids und Proben von Menschengehirnen. Wir stellen fest, dass die Kombination der Inhibition von dem WNT Signalweg und dual SMAD Inhibition das neokortische Zellschicksal ausschließlich erschafft. Wir zeigen auch, dass die dual SMAD Inhibition diencephalic-mid-hindbrain Zellschicksalen ermöglicht und dass keine Inhibition gemischte Zellschicksale fördert. *Weiterhin bestätigen wir mit der Einstellung Einzel-Zell RNA Sequenzieren (single cell RNA-Sequencing) die regionale Heterogenität zwischen organoid Entwicklungsmethoden, die wir in bulk RNA-Seq gesehen haben. Durch die Analyse von scRNA-Seq Daten von Gehirnorganoids finden wir dazu eine hochangereichte kortische Stammzellpopulation in Triple-i organoids. Wir finden aber auch, dass dual SMAD-i organoids und organoids unter keiner Inhibition mehr heterogen sind. Diese organoids enthalten kortische und nicht kortische Zellpopulationen. Single cell RNA-Sequencing bestätigt die Anwesenheit wichtiger kortischer Zellenarten inklusive Nervenstammzellen, Kortikalprogenitorzellen und Nervenzellen in dual SMAD-i und Triple-i organoids.

In dieser Studie untersuchen wir u.a. die Rolle von der radialen Organisation (Rosettebildung), die eine wichtige Rolle in dem Nervenzellschicksal spielt. Diese Organisation wird dann als einzigartige Eigenschaft den kortischen Nervenstammzellen zugewiesen. Insbesondere zeigen wir die integrale Rolle von vergrößerter Notch Aktivierung für effiziente radiale Organisation. Diese beiden Charakterisierungen sind Eigenschaften für die homogene neokortische Spezifizierung. Wir zeigen zudem, dass diese Eigenschaft in 2D (Rosetten) und 3D (organoids) Systemen, die mit der Triple-i Methode entwickelt worden, dramatisch stromlinienförmig gemacht wird. Dadurch verbinden wir Stammzelleigenschaften mit Zellpolarität in der kortischen Zellschicksalprozess unter Triple-i. Um diese Ergebnisse zu unterstützen, finden wir eine schwache notch Aktivierung und ihre

Überschneidung mit radialer organistation in Systemen, die mit keiner Inhibition entwickelt worden. Dazu finden wir eine hohe notch Aktivierung in nicht radial organisierten Regionen, die nicht kortische Zellschicksale in Zellkulturen anreichern, die mit dual SMAD Inhibition entwickelt worden. Deswegen schlagen wir Folgendes vor: wenn diese Eigenschaften in Überschneidung zu sehen sind, können sie als eine zuverlässige Auslesung für eine effiziente kortische Differenzierung gelten.
Um diesen Konzeptnachweis zu veranschaulichen, besonders im Forschungsgebiet der regenerativen Medizinforschung und ihrer Anwendungen, benutzten wir die Gehirnorganoidtechnologie als platform, neural Entwicklungsstörungen zu modellieren, insbesondere Mikrozephalie. Mikrozephalie ist eine genetisch heterogene kortische Entwicklungsstörung, die durch Abnormitäten im kortischen Entwicklungsprozess gekennzeichnet ist und zu einer kleineren Gehirngröße führt. Wir entwickeln mikrozephalische organoids von embryonischen Stammzellen von Menschen (hESCs) mit einer mutation im zentrosomischen Protein STIL. Diese organoids zeigen apoptosis in notch aktiv und radial organisierten Vesikel, Zell-Zyklus Arrest, frühzeitige Differenzierung und Verlust der Expression von kortisch spezifischen Genen, wenn diese von Triple-i Methoden entwickelt worden. Das zeigt eine kortisch spezifische Ätiologie, die nur in Triple-i organoids zu finden ist. Auf diese Weise beschließen wir, dass die Kombination von WNT Inhibition mit dual SMAD Inhibition für die Standardisierung der Modellierung von der Kortikogenese auf Gesundheit und Krankheit unverzichtbar ist.

1. INTRODUCTION

1.1 Early mammalian embryonic development

Embryonic development starts with the fertilization of an oocyte by a sperm cell leading to the formation of a zygote. This single celled zygote now starts its journey from fallopian tubule to uterus, simultaneously undergoing several cell divisions to form the blastocyst, which gets implanted into the endometrium of uterus. The blastocyst consists of two distinctive cell types i) inner cell mass (ICM) which gives rise to the embryo and ii) an outer layer of trophoectoderm (TE) which generates extra embryonic tissues [1] (Figure 1). Post implantation, ICM cells differentiate into three germ layers known as the ectoderm, mesoderm and endoderm in a highly coordinated step known as gastrulation.

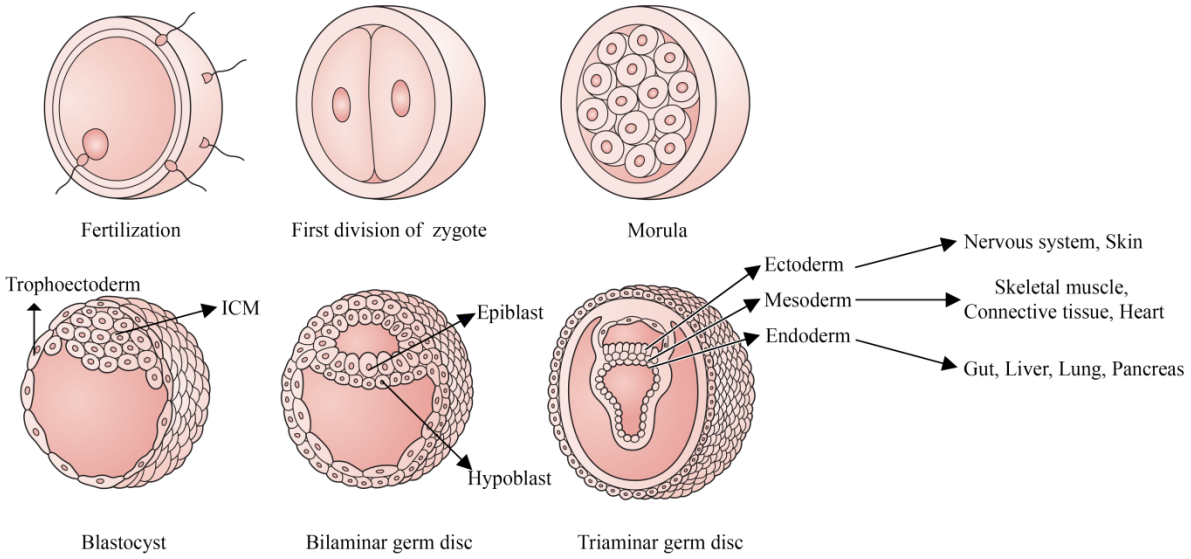

Figure 1: Stages of mammalian embryogenesis from fertilization to gastrulation.

Following fertilization, the zygote undergoes a series of cell divisions to from the blastocyst. The inner cell mass (ICM) of the blastocyst give rise to all three germ layers (ectoderm, mesoderm and endoderm). These three germ layers eventually generate different tissues of the body. Adapted from Neuroanatomy text book (Maria A Patestas and Leslie P. Gartner)

1.2 Neurulation

Neurulation refers to the process of formation of neural tube from the ectoderm subsequent to gastrulation. This process starts with thickening of the ectoderm to

form the neural plate, followed by bending of the neural plate to generate neural folds flanking the neural groove. Finally, these two neural folds fuse together leading to closure of the neural tube that then detaches from the overlying ectoderm (Figure 2).

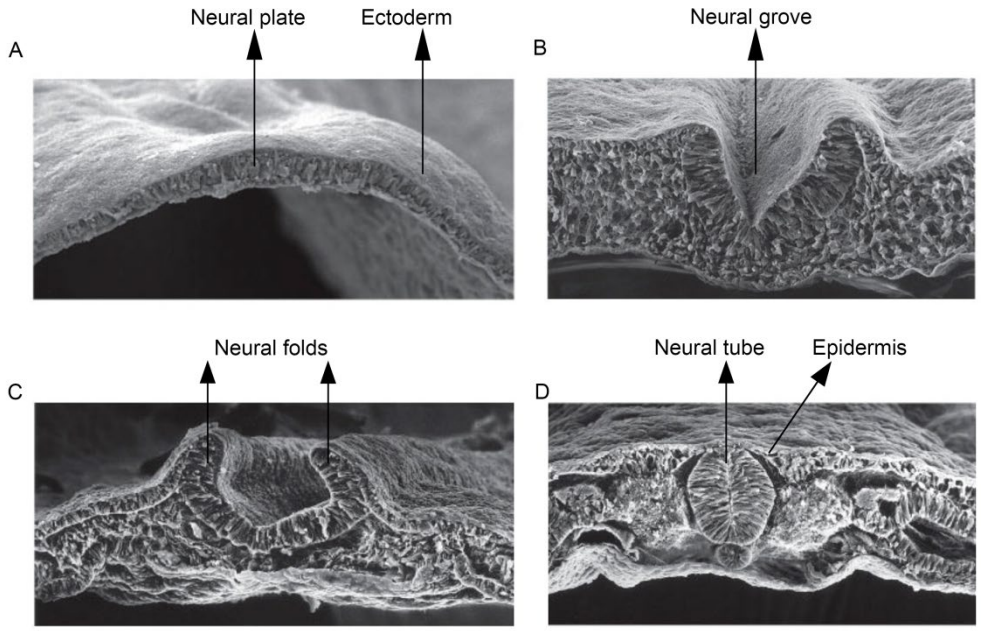

Figure 2: Steps in neurulation process

A) Thickening of ectodermal cells to from the neural plate. B) Elevation of neural folds giving rise to the neural groove. C) Convergence of neural folds to form the neural tube. D) Closure and detachment of the neural tube from the overlying epidermis. Adapted from Gilbert 2014

The early mammalian neural tube is a straight structure that eventually undergoes expansion leading to the formation of sac-like vesicles. The early neural tube is specified into three primary vesicles of the central nervous system (CNS): forebrain (prosencephalon), midbrain (mesencephalon) and hindbrain (rhombencephalon). The neural tube continues to develop and differentiate to secondary vesicles where the prosencephalon sub-divides into anterior telencephalon (future neocortex) and posterior diencephalon, which will form the thalamic and hypothalamic structures of the brain. The rhombencephalon also further divides into anterior metencephalon (cerebellum) and posterior mylencephalon (medulla) (Figure 3).

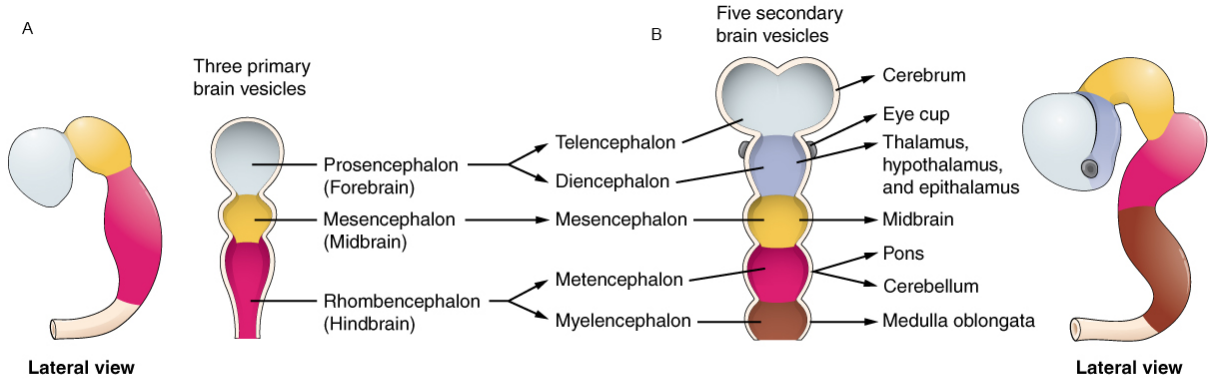

Figure 3: Primary and secondary brain vesicles development.

Expansion of the neural tube results in fluid filled vesicles. A) Primary vesicle stage has three brain regions. B) Brain continues to develop resulting in the formation of secondary vesicles which has five regions. Adapted from the Anatomy and Physiology book (Open Stax resource)

1.3 *In vivo* neural induction and patterning

Early development of the CNS is accompanied by regional patterning of the neural tube along the anterior-posterior (A-P) and dorsal-ventral (D-V) axes [2, 3]. The first classical experiments done by Hans Spemann and Hilde Mangold in 1924 [4] elucidated the role of organizers in inducing neural tissue. They transplanted a tissue from the dorsal region (the dorsal blastopore lip consisting of the future notochord, mesoderm and endoderm cells) of a pigmented newt gastrula embryo into the ventral region (future epidermis) of a non-pigmented newt gastrula embryo, and found that the donor tissue induced a second nervous system in the host (Figure 4). This dorsal tissue that has the capacity to induce the whole nervous system is known as the Spemann organizer. Later studies [5-7] revealed that this organizer secreted bone morphogenetic protein (BMP) pathway inhibitors which induce neural tissue in the surrounding ectoderm. Spemann and Mangold experiments also revealed that early gastrula grafts gave rise to the whole nervous system while late gastrula organizer grafts could induce only posterior regions. This led them to postulate the existence of separate organizers in space and time for inducing different regions of the nervous system along the A-P axis [8-10]. However Pieter Nieuwkoop later postulated an alternate activation-transformation theory, which states the default acquisition (activation) of neural tissue with anterior fate (forebrain character). In the subsequent transformation step, this anterior neuroectoderm would gradually make

more posterior regions in the presence of caudal transforming factors [11-13]. Although growing evidence favors Nieuwkoop's theory [3, 14], this issue still remains unclear. Thus, anterior fates are thought to form by default, while posterior fates are actively induced by caudalization factors such as FGF, WNT and retinoic acid (RA) signals [2, 7, 15-17].

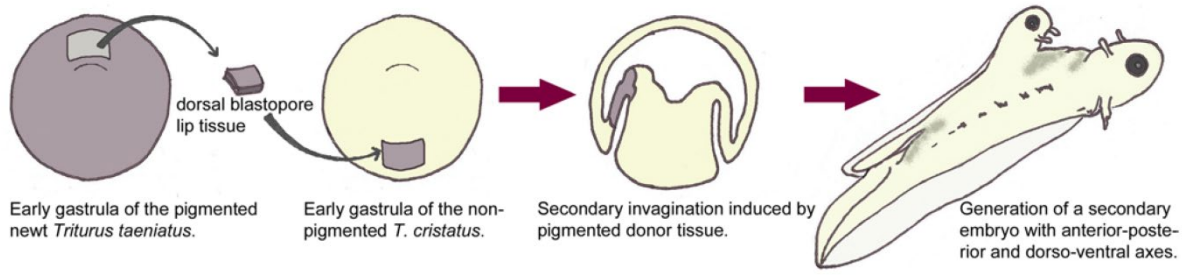

Figure 4: Transplantation experiments demonstrating organizer activity of newt dorsal blastopore lip tissue

Transplantation of dorsal blastopore lip tissue of pigmented newt *Triturus taeniatus* to non-pigmented newt *Triturus cristatus*. The transplanted donor tissue exerts an organizing activity on the surrounding host tissue and induces a whole new secondary axis in the host embryo. Adapted from Andoniadou, C.L et al - [18].

Structures similar to the Spemann organizer in xenopus are also found in other vertebrates such as chick (known as Henson node), zebrafish (known as embryonic shield) and mouse (known as node). Similar results were observed in experiments carried out in chick and mouse embryos, highlighting the evolutionarily conserved role of this organizer [19, 20]. However, in mice, the transplantation of the early gastrula organizer (node) could give rise to the neural axis with only posterior regions, lacking anterior forebrain tissue [20, 21], indicating that the mouse early organizer does not contain all the information for inducing an entire axis. Numerous studies support the idea of requiring an additional organizer like the anterior visceral endoderm (AVE), an extra embryonic structure for anterior neural tissue development [22-25]. At around mouse embryonic day E5.5, a group of cells from the distal region of the embryo known as the distal visceral endoderm starts migrating to the future anterior region of the embryo, establishing the AVE. This group of cells starts expressing several genes like Otx2, Lhx1, Cerebrus1, Lefty1 and Dkk1 which are important for head/anterior forebrain formation (Figure 5) [26-

31]. Noggin, Cerberus/Lefty and Dkk1 are inhibitors of BMP, TGF-β and WNT pathways, respectively, and thus help in establishing anterior neural fates. Mouse AVE equivalents are also found in xenopus (yolk cells), chick (hypoblast) and zebrafish (dorsal syncytial layer) [32-34]. However, other studies also have shown that anterior neural fate is not exclusively dependent on AVE, but works in synergy with signals from other organizers like the Spemann organizer (Node) and axial mesendoderm. Studies in chick embryos show that AVE/hypoblast cannot induce neural tissue from epiblast but can only transiently induce anterior neural markers such as Six3 and Otx2 [35]. This study shows that the AVE organizer is required for inducing a pre-neural/pre-forebrain like fate in first step, after which the anterior fate is established/stabilized by signals from the Node organizer. The AVE also protects the tissue that has acquired anterior fate from caudalizing in the second step. The caudal signals from the non-axial mesoderm then transform the tissue distant from the AVE to posterior regions in the third step. Thus, this study postulates a three-step model of neural induction and patterning, which is a closure to Nieuwkoop's model. Although it has not been clarified which of these models best represents early neural development, all of these studies contributed a lot in understanding early neural induction and patterning events.

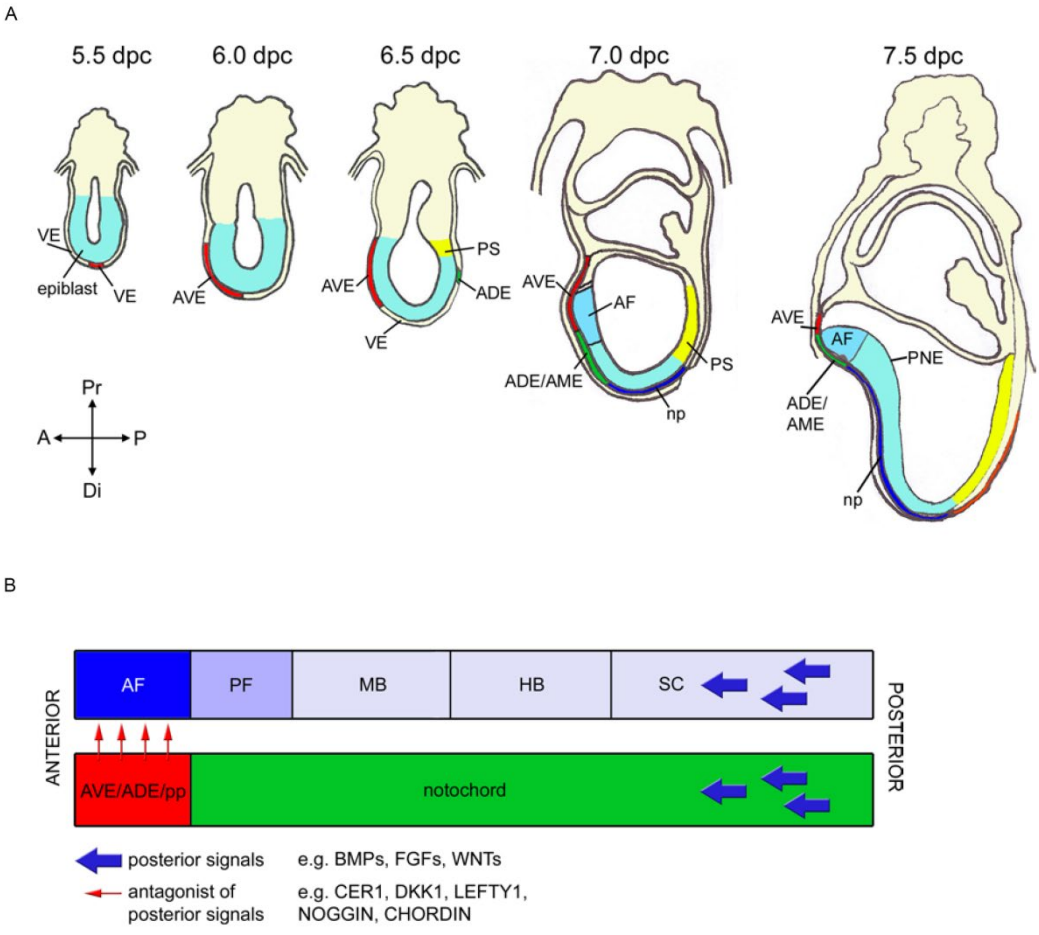

Figure 5: Specification of anterior to posterior brain regions in post implanted mouse embryo
A) Formation and migration of AVE from distal to anterior site in around 5.5-6.0 dpc embryos. Around 6.5-7.0 dpc, PS elongates and displaces ADE/AME which intermingle with the AVE. Future anterior and posterior forebrain is specified in the neuroectoderm tissue overlying AVE and ADE/AME whereas posterior brain regions are specified in neuroectoderm overlying notochord plate tissue. B) A host of signals conferring anterior to posterior brain regional fates. VE visceral endoderm, AVE anterior visceral endoderm, ADE anterior definitive endoderm, AME anterior mesendoderm, np notochordal plate, PS primitive streak, AF anterior forebrain primordium, PNE posterior neural ectoderm, PF posterior forebrain, MB midbrain, HB hindbrain, SC spinal cord, pp prechordal plate. Adapted from Andoniadou, C.L et al - [18].

1.4 Role of morphogens in neural induction and patterning

1.4.1 Transforming Growth Factor-β Superfamily

Broadly, TGF-β Superfamily signaling includes BMP and Activin/Nodal signaling pathways. These signaling pathways initiate with the binding of ligand to a heterodimeric receptor complex consisting of type I and type II receptor with a serine/threonine kinase domain. Following ligand binding, the type II receptor phosphorylates and activates the type I receptor which then phosphorylates Smad proteins initiating a Smad protein dependent signaling cascade. Eight Smad proteins operate in this signaling pathway, of which five Smad proteins (Smad1, Smad2, Smad3, Smad5 and Smad8) are receptor regulated Smads known as R-Smads. Smad2 and Smad3 are activated by Activin/Nodal signals whereas Smad1, Smad5 and Smad8 are activated in response to BMP signals. These activated R-Smads now bind to a common Smad i.e., Smad4 forming RSmad/Smad4 complex, which then translocates to the nucleus and regulates gene expression. The other Smads such as Smad6 and Smad7 acts as inhibitory Smads inhibiting the signalling pathway (Figure 6).

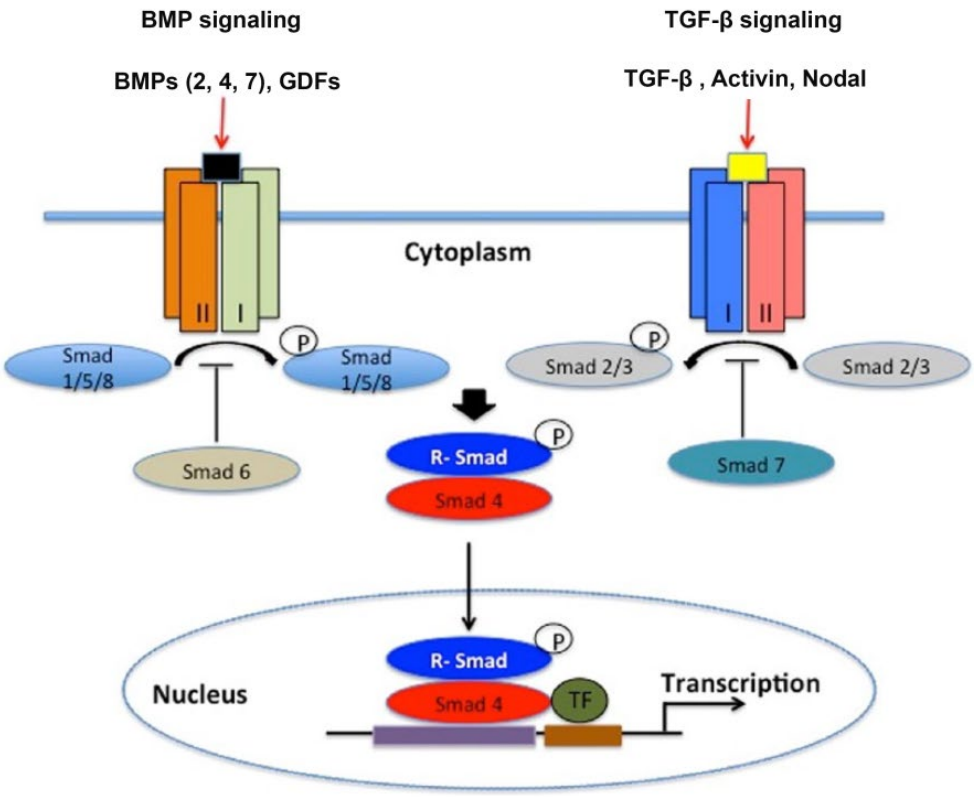

Figure 6: TGF-β superfamily including BMP and TGF- β signaling pathways

Binding of ligands, either BMPs or TGF-β to the respective type I and type II heterodimer receptors triggers the activation of Smad1/5/8 in the case of BMP signaling and Smad2/3 in the case of TGF β signaling. Activated R-Smads then bind to Smad 4 and translocate into the nucleus and drive the transcription of targeted genes. Adapted from Brzica, H et al [36].

1.4.1.1 Bone morphogenetic protein (BMP) Signaling

Inhibition of BMP signaling is a prerequisite for the induction of neural plate from ectoderm. Studies identified the ability of the Spemann organizer or the notochord in neuralizing the overlying ectoderm is due to the expression of BMP antagonist proteins like Noggin, Follistatin and Chordin, which prevent the binding of BMPs especially BMP-4 to its receptor, thereby inhibiting the BMP pathway [37]. Studies done in xenopus and zebrafish embryos treated with morpholinos against Noggin, Follistatin and Chordin result in loss of neural tissue [38, 39]. Mice with deficient BMP receptor ($Bmpr1a^{-/-}$) exhibit a premature neural induction at the pre gastrula stage [40] and $Noggin^{-/-}Chordin^{-/-}$ mutant mice fail to form proper forebrain [41]. Altogether these studies imply the inhibition of BMP is indispensible for the neural induction process.

1.4.1.2 Activin/Nodal TGF- β Signaling

Although numerous studies show the importance of BMP inhibition in neural induction, it is not the sole player in this process. There are studies which also established the role of other TGF-β members like Nodal signaling in neural induction. Nodal signaling inhibits neural induction [42] and Nodal$^{-/-}$ mouse mutants show increased neuroectoderm specification [43]. TGF-β signaling inhibits neural induction as mouse ESC mutants for Cripto$^{-/-}$ (co-receptor for TGF- β / Nodal signaling) and over expression of Cerberus and lefty — inhibitors of TGF-β pathway display increased neural induction [28, 44, 45, 46]. Collectively, these studies reveal the requirement for the inhibition of TGF-β signaling in achieving neural induction.

1.4.2 Fibroblast growth factor (FGF) Signaling

Fibroblast growth factors are a family of secreted ligands that bind to their specific FGF receptors (FGFR1-4), following which they initiate a number of signaling cascades such as MAPK/ERK and PLC/Ca^{+2} pathways, which exhibit diverse roles during embryonic development. The role of FGFs in neural induction is not clear yet, possibly due to species-specific differences. While the default model of neural induction is solely dependent on inhibition of BMPs in xenopus embryos, is not entirely so in chick and zebrafish embryos. In chicks, epiblast cells express BMP4 and BMP7 ligands early on and decrease their expression after specification to neural fates, with the concomitant expression of FGF3. Blocking FGF signaling with the inhibitor SU5402 results in decreased neural specification, indicating an important role of FGF in neural induction [47]. In zebrafish, activating FGF signaling indirectly inhibits BMP expression, leading to dorsalization of the embryo, whereas blocking FGF signaling causes increased BMP expression, resulting ultimately in ventralization of the embryo [48]. FGFs have also been shown to caudalize neural tissue in xenopus, chick and mouse embryos [49, 50]. FGF/MAPK signaling reduces the efficacy of BMP signaling directly through the degradation of Smad1 and indirectly by inducing the transcription factor ZEB2, which in turn represses the transcriptional activity of Smads [51, 52]. Thus, these studies support the notion that FGFs promote neural induction and patterning by attenuating BMP signaling.

1.4.3 WNT Signaling

WNT signaling is also an important pathway for neural induction as well as for the axis patterning process. It has roles in both cell proliferation and fate specification. Inhibition of WNT pathway establishes anterior fates. Studies in mice mutants of the WNT co-receptors Lrp5 and Lrp6 show the expansion of the anterior neuroectoderm [53]. Loss of the WNT inhibitor Dickkopf 1 (Dkk1) in mouse prevents the formation of forebrain [54]. Wnt1 is expressed in caudal midbrain-hindbrain regions, and in accordance, loss of Wnt1 in mouse embryos leads to defects in midbrain and anterior hindbrain formation [55], while Wnt8c overexpression causes the expansion of midbrain fates on the expanse of anterior forebrain fates [56]. In chicks, ectoderm explants fated to become anterior forebrain structures are transformed into posterior neural fates when exposed to WNT molecules [57]. A GSK3 mutant zebrafish was shown to exhibit increased WNT levels, resulting in the transformation of telencephalon and eye tissues to posterior diencephalic fates [58].

1.4.4 Retinoic acid Signaling

RA plays an important role in posterior neural fate specification, especially in the formation of hindbrain and anterior spinal cord structures, by regulating the expression of Hox genes [59, 60, 61]. Retinol dehydrogenase, an enzyme required for RA synthesis, is found to be highly expressed in posterior neural regions. Enzymes degrading RA such as CYP26 and cytochrome P450 are also expressed highly in anterior neural regions and thus regulate the levels of RA along the A-P axis [60, 62]. In zebrafish, FGF and WNT pathways posteriorize neural ectoderm tissue by suppressing anterior fate specific genes independently of RA, resulting in induction of posterior fate specific gene expression in an RA-dependent process [60]. RA is also important for dorso-ventral (D-V) patterning, where RA along with BMP antagonist Follistatin are expressed in response to SHH in the regulation of ventral patterning.

1.4.5 Sonic Hedge Hog Signaling

SHH plays a key role in assigning the dorso-ventral axis of the neural tube. In the anterior neuraxis, structures such as the pallium (cerebral cortex) and subpallium (basal ganglia) are present on the dorsal and ventral regions, respectively. In the posterior neuraxis, such as the spinal cord, motor neurons reside ventrally and

sensory neurons dorsally. Broadly, the D-V axis identity is determined ventrally by activation of Nodal and SHH and dorsally by BMP/Wnt [63]. SHH is secreted from the notochord and induces the ventral structures along the neural tube as well as the floor plate [64]. Mice Shh null mutants show an absence of ventral structures, small diencephalon and midbrain structures [65] and miss the ventral half of the spinal cord, while retaining the dorsal half [66]. Ectopic Shh expression in mouse dorsal neural tube and Patched1 (SHH receptor) mutant mice show hyper proliferative phenotypes [67, 68], indicating the role of SHH in cell proliferation.

1.5 Pluripotent stem cells – A powerful platform to study embryogenesis

Embryonic development starts with the formation of an unspecialized zygote, which eventually gives rise to an embryo consisting of hundreds of specialized cell types. As development proceeds, cells undergo restriction in their developmental potential. Embryonic stem cells are pluripotent cells derived from the inner cell mass of the blastocyst, which are able to self-renew and differentiate into the three germ layer cells – ectoderm, endoderm and mesoderm. A mouse ESC was first generated in 1981 by isolating the ICM from the blastocyst [69, 70], and later in 1998, a human ESC line was established [69, 70] and later in 1998 human ESC line was established [194]. The enormous capacity of ESCs to maintain differentiation potential towards distinct cell types makes them an indispensable tool for developmental studies, disease modeling and regenerative medicine applications [71, 72, 73]. It should be noted that the use of hESCs is limited due to ethical, technological and tissue availability reasons. Also, issues related to immune rejections following cell replacement therapies further complicate the use of ESCs in stem cell therapy.

Earlier studies demonstrated the ability of somatic cells to regain the pluripotency state using somatic cell nuclear transfer [74, 75] and fusion with ESCs [76, 77], indicating the presence of factors in oocytes and ESCs that can reprogram somatic cell to a pluripotent cell state. In 2006, ground-breaking work done by Takahashi and Yamanaka resulted in successful reprogramming of mouse fibroblasts to embryonic stem-like cells known as induced pluripotent stem cells using four transcription factors Oct3/4, Sox2, c-Myc and Klf4 [78]. IPSC technology holds great promise due to its ability to generate patient-specific PSCs that are highly useful for potential cell replacement based therapies, disease modeling and drug development and

tolerability tests [79, 80]. IPSCs also have the advantage of circumventing the major ethical issues concerning the use of ESCs. Although they behave similarly to ESCs to a large extent, iPSC lines still require a rigorous characterization as their complete epigenetic reprogramming is still in question [81, 82]. However, the full harnessing of ESCs or iPSCs for regenerative medicine applications depends mainly on the availability of efficient differentiation protocols to generate cells of interest at high purity. The main challenge of any differentiation scheme is to obtain an enriched target cell population. This depends on many factors such as cell density, type of differentiation platform: monolayer, EBs or 3D organoids; how well defined the types or batches of knock-out serums used are, the degree and extent of use of morphogens or small molecule inhibitors, which contribute as well to high variability in terms of cell types generated. Nonetheless, PSCs provide a powerful and unlimited source to generate and study different cell types such as neural lineage stem cells, which our lab is mainly interested in, thus enabling the experimental study of otherwise inaccessible cell types.

1.6 Neural stem cells

NSCs are multipotent cells that can self-renew and differentiate into neurons, astrocytes and oligodendrocytes [83, 84]. The neural tube consists of a one cell thick layer of early NSCs known as neuroepithelial cells (NE) whose nuclei are arranged at different height's ranging from the inner luminal site to the outer surface leading to a pseudostratified epithelial arrangement [85]. NSCs emerge during the development of the nervous system and continue to exist in adults [83, 84]. Heterochronic transplantation studies have revealed the loss in stem cell potency as development proceeds, i.e., early NSCs have the broad potency to give rise to all neural cell types whereas later derived NSCs have restricted potency and are incapable to give rise to early cell types [86, 87, 88]. Embryological transplantation studies in xenopus, chick and mice elucidated the role of morphogens (discussed above in detail) in the patterning of NSCs across the A-P and D-V axes during the nervous system development. Together, these findings suggest that the potential of NSCs is restricted both spatially and temporally and this dynamic changing nature of NSCs during developmental progression plays a key role in producing the enormous neural cell type heterogeneity in the central nervous system [88]. Therefore, more work

needs to be accomplished for further dissecting heterogeneity *in vivo* and *in vitro* based on novel distinct markers.

1.7 NSCs in cerebral cortex development

The cerebral cortex or neocortex is the largest and most complex structure of the mammalian brain and is involved in higher order brain functions such as perception, cognitive abilities, language, memory and consciousness. The neocortex is specified in the most anterior and dorsal region of the early embryonic neural tube, whose development starts with the generation of a single layer of epithelial cells from the ectoderm known as neuroepithelial cells arranged in a pseudo-stratified manner. NE cells are early NSCs that are highly polarized in nature showing apico-basal polarity, with their apical sites facing the lumen of the neural tube forming ventricular zone (VZ) and basal site towards the basal lamina. The nuclei of NE cells undergo a unique migration process along the apico-basal sites during the cell cycle known as Interkinetic nuclear migration (INM) (Figure 7) [89, 90]. In this process, during G1-S phase of cell cycle, nuclei migrate from apical to basal site and undergo 'S phase-DNA replication' at the basal site. Then the nuclei migrate back to the apical site during G2 phase and finally undergo mitosis/cell division at the apical site of lumen.

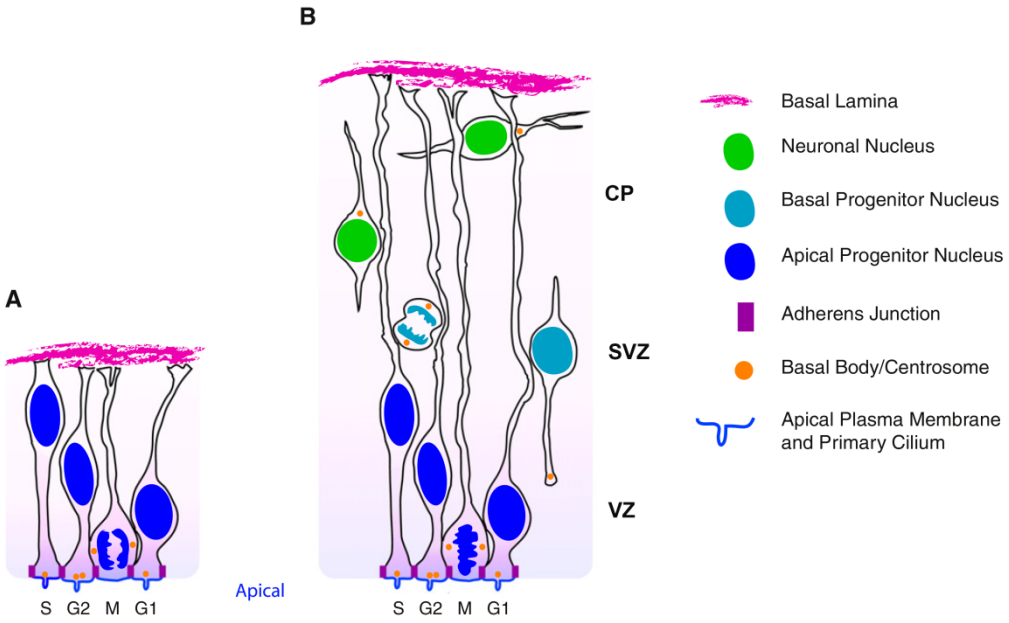

Figure 7: Interkinetic nuclear migration of neural stem cells

Nuclei of neuroepithelial (A) and radial glial cells (B) exhibiting migration from apical to basal site depending on the phase of their cell cycle. During G1 phase nuclei migrate from the apical-basal site with DNA replication (S-phase) occurring at the basal site. In contrast nuclei returns to the apical site during G2 phase with cell division (mitosis) taking place at the apical site. VZ ventricular zone, SVZ sub-ventricular zone and CP cortical plate. Adapted from Taverna, E et al [89].

During cortical development, NE cells first divide symmetrically giving rise to two identical daughter stem cells resulting in expansion of the NSC pool. This phase is then followed by asymmetric cell divisions that generate one stem cell and an intermediate progenitor (IP) or a neuron, resulting in decreased NSC ratios [91]. During this phase, NE cells transform into a distinct fate restricted NSC type with astro-glial characteristics known as radial glial (RG) cells [92, 93]. RG cells still maintain polarity, perform INM and undergo cell division in the VZ, although they already start to express astroglial markers [91, 92]. On the other hand, the generated IP daughter cells detach and migrate basally, forming the sub-ventricular zone (SVZ) through consecutive cell divisions. IP cells lack apico-basal polarity and undergo few rounds of proliferative divisions yielding more IPs, and finally produce neurons. Another class of RG cells known as basal radial glial (bRG) cells were found in the outer SVZ (oSVZ), which lacks apical attachment with the VZ but still maintains the basal process and is thought to contribute to expansion and gyrification of the cortex in large-brain primates [94-96]. Neurons generated either from NE, RG or IP cells migrate basally to the SVZ and accumulate in a timely manner, forming the cortical plate (CP) in a process known as cortical lamination. The neocortex is a highly complex structure with hundreds of neuronal cell types distributed across six layers (Layer I - Layer VI), formed in an inside-out fashion, where the oldest neurons (Layer VI) accumulate in the deep layers and the youngest neurons (Layer II) migrate past these oldest neurons and accumulate in the superficial layers (Figure 8) [97].

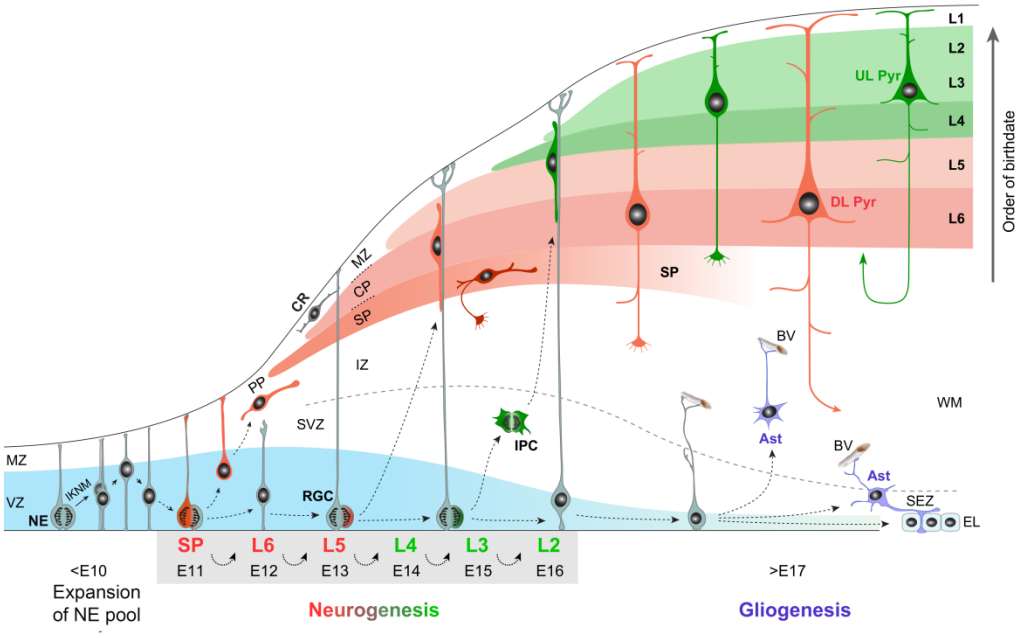

Figure 8: Cortical lamination in mouse neocortex

NE cells residing in the VZ initially undergo symmetrical cell division to expand its pool and then attain radial glial morphology. RGC divides asymmetrically to generate either IPC which occupies SVZ or neurons reaching CP in a time dependent manner. Subplate neurons are generated first, followed by DL neurons destined to L6/L5 and finally UL neurons destined to L2/3/4. Once neurogenesis is completed RGC then becomes gliogenic and give rise to astrocytes and oligodendrocytes and then transforms into adult neural stem cells known as ependymal cells occupying SEZ. NE neuroepithelial cells, RGC radial glial cells, VZ ventricular zone, SVZ sub-ventricular zone, IPC intermediate progenitor cells, MZ marginal zone, SP subplate, CP cortical plate, CZ Cazal Retzius cells, BV, blood vessel; CR, Cajal-Retzius neuron; DL Pyr, deep-layer pyramidal neuron; IZ, intermediate zone; UL Pyr, upper-layer pyramidal neuron, WM, white matter, EL ependymal cells, SEZ subependymal zone, Ast astrocytes. Adapted from Kwan, K.Y et al [98]

The neurons generated earliest during cortical neurogenesis are Cajal-Retzius and subplate neurons. Cajal-Retzius neurons are the main source of reelin, a secreted protein important for normal cortical lamination [99]. The deep cortical layers (layer V-VI) consist of corticofugal projection neurons, of which Layer VI neurons project their axons to the thalamus (corticothalamic neurons) and Layer V neurons interact with the midbrain tectum (corticotectal neurons), brainstem or pons (corticopontine neurons) and spinal cord (corticospinal motor neurons). Studies in mice revealed that these deep layer cortical neurons are characterized by marker transcription factors such as Tbr1, Ctip2 and Fezf2, by showing that their absence leads to improper cortical lamination process [100, 101, 102]. Upper layer neurons (Layer

II/III, IV) consist of callosal projection neurons, which project axons within the cortex (intracortical)-connecting both cerebral hemispheres via the corpus collasum and expressing transcription factors such as Cux1 and Cux2, Brn1 and Brn2, and Satb2 (Figure 9) [103 -109]. Once the upper layer neurons are generated, radial glia stem cells now switch their neurogenic fate to gliogeneic fate, thereby giving rise to glial cells such as astrocytes and oligodendrocytes. Astrocytes nourish the neurons by supplying nutrients and oxygen, maintaining CNS homeostasis, whereas oligodendrocytes coat the axons of neurons with a lipid rich myelin sheath providing insulation and thereby enhancing transduction of nerve electric impulses. Altogether, these mechanisms are fundamental for the generation of distinct types of NSCs and their progeny that account for the enormous cellular diversity of the cortex.

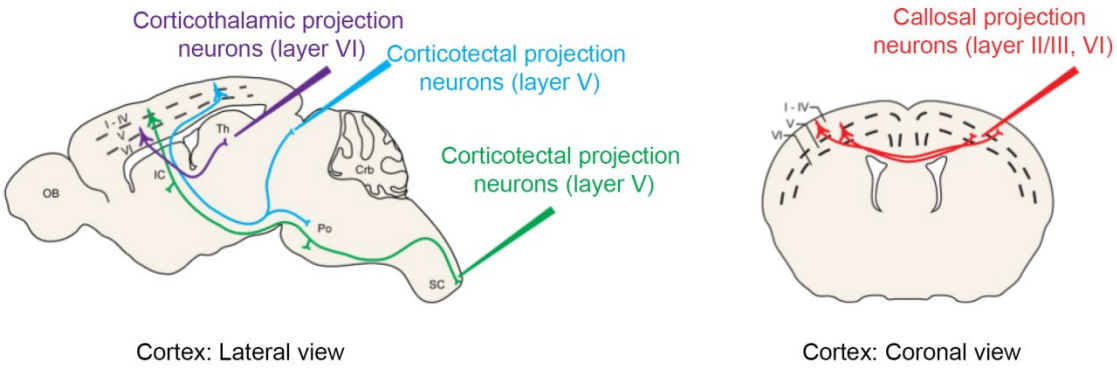

Figure 9: Schematic representation of cortical projection neurons connections

Deep layer cortical neurons (Layer V/VI) project their axons into the thalamus, midbrain tectum, brainstem (pons) and spinal cord. Upper layer neurons (Layer II/III/IV) connect both cerebral hemispheres via the corpus collasum. Adapted from Molyneaux, B.J et al [110].

1.8 Recapitulating *in vivo* neural induction and patterning *in vitro* using PSCs

The advent of PSC biology has led us to utilize these cells and generate in vitro models for early development, poorly understood diseases and target cell populations for regenerative cell therapies. In vitro neural induction experiments are dated back to the early 1990s, where the xenopus animal cap (future ectoderm) explants cultured in simple pond saline water produced epidermal fates. However when these explants were dissociated and plated as single cells, they gave rise to neural fates [111], although they did restore epidermal fate when exposed to BMP-4

ligand [112], indicating that the loss of cell-cell contact diluted BMP/TGF-β signaling that in turn specified them to neural fates. Thereafter, studies showing the necessity of the inhibition of BMP/TGF-β signaling in mammalian PSCs to achieve neural induction are continuously emerging, showing the evolutionarily conserved mechanism.

Neural induction methods using both mouse PSCs (mPSCs) and human PSCs (hPSCs) have undergone many modifications to date, starting from culturing PSCs as embryoid bodies (EBs) in serum, through culture on a feeder layer, then in a chemically defined medium with small molecule inhibitors, to the recently developed organoid technology (Figure 10) [113]. Early studies that involved screening of feeder layers revealed that bone-marrow derived stromal cells could promote strong neural induction in mPSCs, although the exact role of stromal cells remains unclear [114]. Mouse PSCs cultured under low density-mimicking xenopus experiments-generated neural progenitors albeit with less efficiency (0.2%), but in the presence of Noggin and Cerebrus (mCer1) and with Smad4-/- null mESCs (resistant to BMP/TGF-β signaling) showed an increased neural progenitor derivation [115]. These studies confirm the default neural induction process also holds true for mammalian systems.

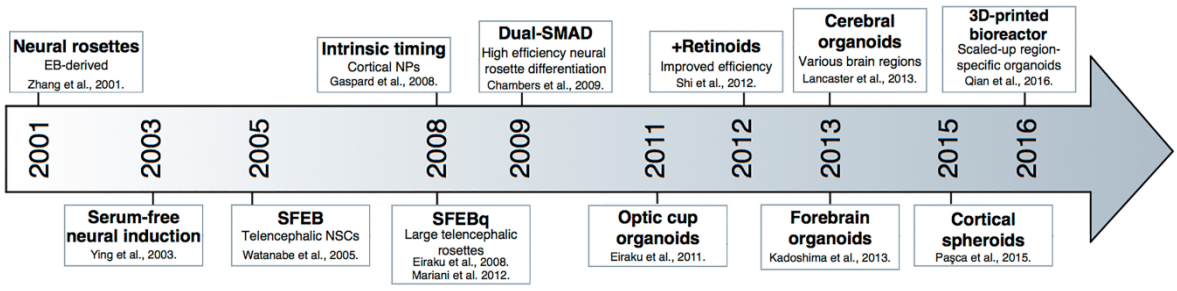

Figure 9: Timeline of *in vitro* neural induction protocols from human or mouse PSCs
Schematic showing different neural induction protocols for the generation of neural/cortical tissue. Adapted from Kelava, I et al [113].

Zhang and colleagues first reported the generation of neural tube like structures known as neural rosettes by culturing hPSCs as EBs in the presence of FGF2 [116]. These neural rosette precursors generated neurons, astrocytes and

oligodendrocytes upon mitogen removal. Another study from Ying et al. reported the neural induction by plating mPSCs as adherent monolayer culture instead of EBs, in the absence of serum and other neural inductive signals [117]. The method launched by the Sasai group utilized Nodal and WNT pathway antagonists for derivation of general telencephalic fates from mouse PSCs [118]. We later recapitulated this default neural induction mechanism in human PSCs and isolated neural rosette-forming NSCs corresponding to early radial glial like NSCs with anterior/cortical character using the BMP antagonist Noggin [119, 120]. This method was significantly improved by the same group by adding TGF beta inhibition – becoming the widely accepted dual SMAD inhibition protocol in human PSCs [121]. Parallel studies showed a time-dependent sequential production of cortical neurons by diverse methods using SHH antagonist and relying on intrinsic signals [122], to using different combinations of TGF, BMP and WNT signaling inhibition with or without FGF signaling modulation [123-125]. WNT and dual SMAD inhibition were also used in combination with SHH activation to accelerate specification of cortical interneurons [126]. We recently used dual SMAD inhibition to recapitulate the generation of the building blocks of corticogenesis from human PSCs based on their Notch activation state using a Notch activation reporter as readout [127]. We showed that the timed and ordered production of deep followed by superficial layer neurons and then glia could be remarkably recapitulated by consecutively isolated Notch active progenitors. While this latter paradigm yielded cells that were enriched but not restricted to cortical fates, these building blocks of corticogenesis were very well reiterated in vitro due to high stem cell state present in each of the isolated progenitor populations due to Notch activation enrichment. However, the use of many successful yet distinct approaches over the years reflected inconsistency in recapping cortical differentiation principles in vitro. We reasoned that this diversity mirrors a general lack in robust and direct readout to assess efficiency of differentiation already at early phases of differentiation, rather than assessing fate potential throughout hundred days and more in culture, urging for a more standardized method for efficient derivation of specified dorsal telencephalic (neocortical) neuroepithelial cells and their progeny.

Parallel to 2D differentiation systems, in recent years there has been an astounding increase in the use of brain organoid models, enabling an in vivo-like view of

fundamental neurodevelopmental features and processes. This in turn evoked, again, an explosion of methods to derive these 3D structures for modeling development and disease, with protocols ranging from inhibitor-free conditions [128, 129, 130] to dual SMAD inhibition [131, 132] or TGF/WNT inhibition [133-136]. Nonetheless, organoids are complex structures and are inherently heterogeneous. Heterogeneity is postulated to be reflected in both the robustness of neural induction as well as the bias in regional identity, possibly due to the fact that organoids can well form in the absence of defined extrinsic cues, allowing inherent differences in local inductive signals within individual organoids. Nevertheless, a major hindrance for regenerative medicine is still the poor ability of such protocols to generate homogenous cortical neural stem cells and their progeny, an essential component for future cell replacement based therapies, as well as for gaining a better understanding of disease etiology and progression. As the biology of cerebral organoids is only beginning to unravel, these observations together urge for both further improving strategies for developing more defined 3D organoid systems alongside with continuous efforts to enhance the homogeneity of the more simplified 2D cultures that yield cells in a more single cell or clonal level.

Collectively, this continuously evolving diversity in differentiation paradigms also causes inconsistencies in the way cortical differentiation principles and disease modeling phenotypes are interpreted and conceived by the community. We reasoned that this diversity mirrors a general lack in robust and direct readout to measure specification efficiency during early phases of differentiation, namely accurately capturing the purity of the starting population. Second is the scarcity of specific genes that unequivocally mark cortical cell populations. Furthermore, assuming expression of very late markers appearing after more than a hundred days in culture as gold-standard probes to assess differentiation adds controversy on how results with such markers should be interpreted. Finally, different methods are not run in parallel in the same study, questioning the validity of disease phenotypes. These concerns urge for more standardized methods for efficiently assessing homogeneity of neocortical neuroepithelial cells and their progeny.

1.9 Notch signaling and Rosette formation - a tool for measuring efficiency of cortical specification

The Notch signaling pathway plays a major role in nervous system development by regulating cell fate decisions. The Notch gene encodes receptor transmembrane proteins (Notch1-4) consisting of an extra cellular domain (NECD), transmembrane domain (TM) and intra cellular domain (NICD). Signal conveying cells express ligands such as Delta-like (Dll1, Dll3 and Dll4), Jagged (Jag1 and Jag2), and bind to the Notch receptors on signal receiving cells. Ligand binding results in two proteolytic events. First NECD is cleaved from TM-NICD, mediated by TACE (TNF-α ADAM metalloprotease converting enzyme). Second NICD is cleaved from TM, mediated by γ-secretase. Ligand bound to NECD is then endocytosed and recycled in signal sending cells. In signal receiving cells, the cleaved NICD then translocates to the nucleus and binds with transcription factor complex CSL (CBF1/Su(H)/Lag-1) in drosophila / RBP-Jk in mammals resulting in the activation of Notch target genes like Hes family genes, MYC, p21 etc.,

The basic helix-loop-helix (bHLH) genes Hes1 and Hes5 are important notch effectors that are crucial for the maintenance of neural progenitors in the mammalian neural tube. In mice deficient of Hes1 [137-138] and Hes5 [141] premature neural differentiation was observed along with severe abnormalities in neural tube formation, anencephaly and eye formation. Similar precocious neural differentiation phenotype at the expense of progenitor maintenance was observed in Notch1 and RBP-Jk deficient mice [139]. Conversely, activation of Notch signaling by over expression of NICD or Hes genes (Hes1 and Hes5) overexpression in neural progenitors resulted in the inhibition of neural differentiation and promoted radial glia identity [140, 141]. The expression of Hes5 correlates with the expression of Notch1 in the nervous system [142] and also shows better correlation with neural stem cell potential compared to Hes1 [143]. Thus, Notch activation, in turn the expression of downstream targets like Hes1 and Hes5 are important for neural stem/progenitor cell maintenance during nervous system development.

Formation of neural rosettes is a critical morphogenetic event occurring during nervous system development. Differentiation of PSCs into cortical lineages is reflected by the formation of neural rosette structures comprising of NSCs that are

radially organized, thus creating a lumen resembling the VZ of a developing cortex. Moreover, rosettes NSCs undergo cell division at the rosette apical sites resembling *in vivo* apical mitosis in the VZ [144, 145]. Our earlier studies identified a novel type of NSCs from PSC termed as rosette neural stem cells (R-NSCs) with anterior/cortical character. These R-NSCs have considerable self-renewing abilities and broad potency towards CNS fates [119]. We showed that Notch activation is essential for radial organization (rosette formation) which in turn is abrogated in the presence of Notch signaling inhibitors [119]. We further coupled Notch activation and radial organization to cortical neurogenesis by showing that only cells obtained from mechanically isolated Notch active radially organized structures (i.e. rosettes) could give rise to cortical neurons in a time and cortical layer dependent manner [127]. We also validated this correlation at the molecular level by revealing transcriptional and epigenetic factors associated with corticogenesis that drive Notch activation at the rosette stage [146]. Finally, we also demonstrated that Notch active cells within rosettes performed interkinetic nuclear migration – the hallmark phenomenon of cortical differentiation and then used this feature as a cytoarchitectural quantitative readout for cortical differentiation at the rosette stage [147]. This quantitative readout has the potential to serve for functional molecular studies, drug screening, and may be implicated to gain novel insights into biology of NSCs in health and disease. Taken together, our recent data propose that radial organization and Notch activation are linked hallmarks of the transition of PSCs into anterior/ cortical fates – and hence could be used as readouts for improving methods for streamlining cortical fates and also help better understanding of cortical disorders involving defects in NSC proliferation and differentiation such as microcephaly.

1.10 Modeling cortical neurodevelopmental disorders

Autosomal recessive primary microcephaly (MCPH) is a neuro developmental disorder in which patients are born with reduced brain size and show mild to severe mental retardation. Clinically, microcephaly is defined as having a head circumference more than two standard deviations (>-2 std.dev) below the mean for a patient's given age and sex. Microcephaly is a genetically heterogeneous disease and there are at least 10 loci in proteins such as *Microcephalin, ASPM, CDK5RAP2, CENPJ* and *STIL* which are associated with microcephaly [148-152]. Most of these proteins have functions related to centrosome, mitotic spindle, DNA repair etc,

linking the disease due to a disruption in cell cycle and cell division activities. It is predicted that these microcephaly mutations cause disturbances in NSC proliferation, differentiation and cell death kinetics that would impair stem cell pool, thereby leading to the generation of a lesser number of neurons and thus to a small brain phenotype. The recent outbreak of Zika virus (ZIKV) in South America with its suspected link to causing microcephaly in new-borns has put stem cells at the forefront of neuro developmental disorder research. ZIKV transmits from infected mother to foetus causing congenital defects like microcephaly to infected new-born babies [153]. Recent studies show that ZIKV readily infects cortical neural stem cells and affects their cell cycle progression, causing death of both cortical stem cells and neuronal cell types [132, 154-156].

In this thesis, we have worked on a microcephaly disease model caused due to mutations in *STIL* gene. The *STIL* gene (or *SIL*; SCL/TAL1 interrupting locus) was initially found to be associated with the chromosome rearrangement site causing T-cell acute lymphoblastic leukaemia [157] and later studies found that it is involved in centriole duplication. Indeed, STIL depletion blocks centriole duplication whereas its overexpression leads to centrosome amplification [158-160]. $Stil^{-/-}$ knock out mice display numerous abnormalities such as neural tube defects, loss of left-right axis symmetry and die after E10.5 [161]. *STIL* mutations linked with primary microcephaly are predicted to generate truncated proteins (p.Val1218X and p.Gln1239X) causing loss of 49 and 69 amino acids from the C-terminus. The STIL protein has several conserved domains like proline rich CR2 domain that interacts with other centrosomal proteins such as CPAP/CENPJ, the coiled-coil (CC) domain, which interacts with PLK4 and CDK1 proteins [162, 163], and is important for STIL oligomerization [164], the STAN domain interacting with SAS-6 protein and important for centriole duplication [163], and the KEN domain at the C-terminus, which is important for its degradation mediated by anaphase promoting complex/cyclosome (APC/C). Arquint and Nigg found that STIL microcephaly mutations generate truncated proteins with the loss of the KEN domain making them resistant to APC/C mediated degradation. Thus, the protein stabilizes and represents a gain of function phenotype [165]. However, it is not clear how the mutation in a centrosomal protein affects NSC population and their progeny ultimately leading to a small brain phenotype.

Although conventional animal models like rodents have been a source for understanding many human disease etiologies, modeling neuro developmental and psychiatric disorders like microcephaly, autism and schizophrenia in animals is difficult, due to the inherent species-specific differences in size, architecture, cell types and functions of brain. The recent emergence of PSC derived human brain 3D organoid technology which mimics in vivo brain development and architecture provides a good platform to investigate the etiology of these neuro developmental disorders. However the diversity in the 3D organoid derivation methods ranging from using inhibitor free methods to different combinations of pathway inhibitors (as described above) mirrors the lack of a unified or gold standard method to derive homogeneous cortical organoids that can best be used to interpret the cortical disease phenotype.

2. MATERIALS AND METHODS

2.1 Cell lines

- HES5::eGFP H9 human Embryonic stem cells (hESCs), Wicell Research Institute (WA-09, XX)
- Microcephaly STIL mutant HES5::eGFP H9 human Embryonic stem cells (hESCs), Wicell Research Institute (WA-09, XX)
- ZIP8K8 induced pluripotent stem cells
- Mitotic-arrested mouse embryonic fibroblasts (MEFs), Globalstem

2.2 Reagents

- DMEM/F12 (Gibco)
- Knock-out DMEM (Invitrogen)
- Neurobasal medium (Gibco)
- mTeSR1 medium (Stem Cell Technologies)
- Knockout serum (KSR, Gibco)
- 1mM Glutamine(Gibco)
- GlutaMAX (Invitrogen)
- Penicillin-streptomycin (Gibco)
- MEM non-essential amino acids (MEM-NEAA, Gibco)
- Beta-Mercaptoethanol (Invitrogen)
- Fetal bovine serum heat inactivated (FBS, Gibco)
- Di methyl sulphoxide (DMSO, Sigma)
- Insulin (Sigma)
- Apotransferin (Sigma)
- Sodium Selenite(Sigma)
- Putrescine(Sigma)
- Progesterone(Sigma)
- D-Glucose(Sigma)
- Sodium bicarbonate(Sigma)
- Gelatin powder (Sigma)
- Matrigel (BD Biosciences)

- Polyornithine (Sigma)
- Fibronectin (BD Biosciences)
- Laminin (BD Biosciences)
- Paraformaldehyde (PFA; Sigma-Aldrich)
- Picric acid
- Sucrose (Sigma-Aldrich)
- Optimal cutting temperature compound (OCT, Tissue-Tek)
- Bovine serum albumin (BSA, Sigma)
- Triton-X100 (Sigma)
- Trypan blue (Gibco)
- D-PBS without calcium and magnesium (Gibco)
- Growth factors and small molecule inhibitors
- Basic fibroblast growth factor 2 (bFGF2, R&D)
- Transforming growth factor-β1 (TGF-β1,Peprotech)
- Noggin (R&D)
- SB-431542 (Tocris)
- XAV (Tocris)
- Fibroblast growth factor 8 (FGF8, R&D)
- Brain derived growth factor (BDNF, R&D)
- Epithelial growth factor (EGF, R&D)
- L-Ascorbic acid (Sigma)
- B27 – vitamin A supplement (Gibco)
- B27 + vitamin A supplement (Gibco)
- ROCK inhibitor (Y27632, Tocris)
- Neutral protease (Dispase, Worthington)
- Accutase (Sigma-Aldrich)
- Deoxy ribonuclease (DNase I, Worthington)
- Papain dissociation system (Worthington)
- trypLE (Gibco)
- 0.5M EDTA (Invitrogen)
- HBSS (Gibco)

2.3 Molecular biology application kits

- DNeasy Blood & Tissue Kit (Qiagen)
- Plasmid Plus Midi Kit (Qiagen)
- miRNeasy Mini Kit (Qiagen)
- RNase Free DNase Set (Qiagen)
- High Capacity cDNA Reverse transcription Kit (Applied Biosystems)
- FastStart Universal SYBR Green Master (ROX, Roche)
- Phusion High-Fidelity PCR Kit (New England Biolabs)

2.4 Reagents preparation

hESC medium (500 ml)

To 386.5 ml of DMEM/F12, add 100 ml of KSR, 2.5 ml of GlutaMAX, 5 ml of MEM-NEAA, 5 ml of Penicillin-Streptomycin and 0.5 ml of beta-mercaptoethanol. Filter it using a vacuum-driven 0.2-µm filter unit, store at 4°C and use at room temperature (RT).

mTESR1 medium (500 ml)

To 400 ml of mTESR1 basal medium, add 100 ml of mTESR1 5X supplement and 5 ml of Penicillin-Streptomycin. Filter it using a vacuum-driven 0.2-µm filter unit, store at 4°C and use at room temperature (RT).

KSR medium (500 ml)

To 409.5 ml of Knockout DMEM, add 75 ml of KSR, 5 ml of GlutaMAX, 5 ml of MEM-NEAA, 5 ml of Penicillin-Streptomycin and 0.5 ml of beta-mercaptoethanol. Filter it using a vacuum-driven 0.2-µm filter unit, store at 4°C and use at room temperature (RT).

Neurobasal medium (500 ml)

To 484.5 ml of Neurobasal medium, 5 ml of GlutaMAX, 5 ml of MEM-NEAA, 5 ml of Penicillin-Streptomycin and 0.5 ml of beta-mercaptoethanol. Filter it using a vacuum-driven 0.2-µm filter unit, store at 4°C and use at room temperature (RT).

N2 medium (500 ml)

To 490 ml of DDW, add 6.5 g of DMEM/F-12 powder, 0.775 g of D-Glucose, 1 g of Sodium bicarbonate, 5 mg of Apo-transferrin, 12.5 mg of insulin, 30 µl of 500µM Sodium selenite, 100 µl of 830nM Putrescine, 100 µl of 100µM Progesterone and 5 ml of Penicillin-Streptomycin. Filter it using a vacuum-driven 0.2-µm filter unit, store at 4°C and use at room temperature (RT).

Dispase solution

Reconstitute 50 mg of dispase powder with indicated activity of C units/mg dry weight (=50C units) in a desired volume (=50C/4) of hESC medium to get a working activity of 4 units/ml. Filter the solution using a vacuum-driven 0.2-µm filter unit, store at -20°C and use at RT.

EDTA solution

Add 200 µl of 0.5M EDTA to 200 ml of DPBS and filter it using a vacuum-driven 0.2-µm filter unit, store and use at RT

Fixing and staining solutions

4% PFA and 0.15% Picric acid solutions (250 ml)

Heat 200 ml of PBS to 58-60°C in a beaker on a magnetic heating plate and add 10g of PFA with continuous stirring with magnetic stirrer and add few drops of 1N NaOH for complete dissolving of PFA. Once the PFA is dissolved and the solution is clear, make up the rest of the volume to 221 ml with PBS and let it stand to come to room temperature. Add 28.8 ml of 1.3% Picric acid and adjust the pH to 7.4 by using 10N NaOH. Store it at -20°C and use at RT.

PB (PBS/BSA, 500 ml) and PBT (PBS/BSA/Triton X100, 200 ml) solutions

To 539 ml of DDW, add 7 g of BSA, 70 ml of 10X PBS and 70 ml of FBS and stir continuously on a magnetic plate with a magnetic stirrer inside until the solution is completely dissolved and appear clear. Take 485 ml of PB solution, add 15 ml of PBS and filter it using a vacuum-driven 0.2-µm filter unit. Store at 4 oC and use at RT. To the remaining 194 ml of PB solution, add 6 ml of 10% Triton X100 and mix well. Filter it in to a separate 200 ml bottle using a vacuum-driven 0.2-µm filter unit. Store at 4°C and use at RT.

2.5 Generation and culture of hESCs line

The BAC transgenic HES5::eGFP Notch activation human ES cell reporter line has been derived from the H9 (WA-09, XX) human ES cell line (Wicell) and described previously [166]. Undifferentiated HES5::eGFP hES cell lines were cultured on mitotically inactivated mouse embryonic fibroblasts (Globalstem) and maintained in medium containing DMEM/F12, 20% KSR, 1mM Glutamine, 1% Penicillin/Streptomycin, non-essential amino acids, beta-mercaptoethanol and supplemented daily with 10 ng/ml FGF2 (R&D), and passaged weekly using Dispase (Worthington) to maintain their undifferentiated state.

The microcephaly STIL HES5::eGFP Notch activation reporter line was generated using clustered regularly interspaced short palindromic repeat (CRISPR)/Cas9 genome editing system to introduce a nonsense mutation at the STIL locus in the H9 (WA09)-derived HES5::eGFP hESC reporter line. This nonsense mutation mimics the microcephaly STIL1218 (designated in this study as MC) mutation in which deletion of the nucleotide (nt) G (at 3655 nucleotide position) leads to a premature stop codon (Val1219X). A 21-nt guide RNA (gRNA) sequence and a 150-nt ssDNA oligo (IDT, PAGE purified) were designed to target and generate double-strand breaks within the STIL ultimate exon (exon no.17) upstream to the KEN domain and result in the generation of a truncation mutation via non-homologous end-joining (NHEJ) and homology-directed repair (HDR). This gRNA was cloned into pSpCas9 (BB)-2A-GFP (PX458, Addgene) plasmid downstream of U6 promoter using the Gibson assembly cloning method. hESCs (400,000 cells) were nucleofected (Amaxa) with 1.5 µg of SpCas9 plasmid cloned with gRNA and 1 µg of the ssDNA. Ninety-six hours after nucleofection, cells were sorted for GFP signal by FACS. Sorted cells were replated at clonal density (5K) on MEFs supplemented with MEF-conditioned media and 10 µM ROCK inhibitor with daily fresh 10 ng/ mlFGF2. Individual colonies were manually picked and cultured in 24 well plates for a week and later expanded in 6 well plates as individual clones. Genomic DNA was extracted from each clone and targeted genomic region was sequenced. The microcephaly STIL mutant human ES cell reporter line were cultured on mitotically inactivated mouse embryonic fibroblasts (Globalstem) and maintained in medium containing DMEM/F12, 20% KSR, 1mM Glutamine, 1% Penicillin/Streptomycin, non-

essential amino acids, beta-mercaptoethanol and supplemented daily with 10 ng ml−1FGF2 (R&D), and passaged weekly using Dispase (Worthington) to maintain their undifferentiated state.

2.6 Generation and culture of iPSC line

The ZIP8K8 iPSC line was derived from Human dermal fibroblast (HDF) cells were obtained from a 40 year old Caucasian male with no history of genetically inherited, neurological or metabolic disorders using a 3 mm punch biopsy. Briefly, biopsy material was segmented into smaller fragments, plated onto tissue culture-treated plastic dishes and maintained in HDF medium containing DMEM Glutamax, 1% Penicillin/Streptomycin and 20% fetal calf serum at 37°C and 5% CO2. HDF medium was changed every other day to obtain a 90% confluent monolayer until the cells were passaged at a 1:3 ratio using trypsin. Pluripotent stem cell lines were induced using episomal plasmids following a published protocol with minor modification [167]. All plasmids were a gift by Shinya Yamanaka and obtained via Addgen (http://www.addgene.org). Briefly, 2 µg of pCXLE-hSK (#27080), pCXLE-hUL (#27078) and pCXLE-hOCT3/4-shp53F (#27077) were transfected into 106 HDFs using the Neon microporator device with 100 µl electroporation tips (Settings: 1.650 V, 10ms, 3 timed pulses; Thermo Fisher Scientific) according to the manufacturer's protocol. Transfected cells were resuspended in 10 ml fibroblast medium containing 90% 1x MEM (Thermo Fisher Scientific) supplemented with 10% FCS, and 2.5x104 HDF/cm2 were reseeded onto Matrigel coated (0.5 mg/ml) six-well plates. Two days post transfection, fibroblast medium was replaced with TeSR-E7 (Stemcell Technologies) and cells were fed every other day with 2 ml TeSR-E7/well. On day 26-30, post transfection emerging hiPSC colonies were picked and transferred onto Matrigel-coated plastic dishes (Corning; 0.5 mg/ml) in TeSR-E8 medium (Stemcell Technologies) for further expansion. Enzyme-free colony expansion using EDTA was performed every 3-4 days at a 1:6 ratio based on a protocol previously described [168]. Expression of pluripotency markers as well as tri-lineage differentiation markers for this iPSC line was confirmed by qPCR, immunostaining and FACS sorting assays.

The Fragile X FX1 iPSC line was derived by infection and STEMCCA-OKSM lentivirus Dox induction of Fragile X patient (male) obtained fibroblasts (Cat.

#GM05131, Coriell Inst.), generated by the Hanna Lab and described previously [169]. FX1 iPSCs were cultured on feeder-free matrigel coated plates (1:100) and grown in mTeSR™1 medium (Stemcell Technologies), supplemented with 1% Penicillin/Streptomycin and daily complemented with 8 ng/ ml FGF2 (R&D) and 2 ng/ml TGF-β1 (Peprotech), and passaged every 4-5 days using trypLE (Gibco) to maintain their undifferentiated state, as described previously [169].

2.7 Neural induction and rosette formation from pluripotent stem cells using the small EBs protocol

Day 0

For Feeder dependent pluripotent stem cells (hESC growing on MEF feeder layer)

- hESC medium was collected from the confluent hESC culture dish into a 15ml falcon tube.
- 1ml of Dispase (4U/ml) was added to the culture dish and incubated for 10 min at 37°C in the incubator (incubation time could change according to the enzyme activity, so care was taken to not to over digest).
- The culture dish was tapped gently to detach the colonies from MEF and neutralized the dispase by adding 4ml of hESC medium collected in the first step.
- All the colonies were collected into a 15 ml falcon tube and let it wait till all the cells sink to bottom of the tube.
- Supernatant was aspirated and again washed the cells with 5 ml of hESC medium and let the cells to sink down.
- Supernatant was aspirated and 1 ml. of Accutase was added along with ROCK inhibitor (10μM) and kept in 37°C water bath for 4 min.
- With p1000 pipette, colonies were triturated for 15-20 times and observed for single cells under microscope.
- Neutralized the accutase by adding 10 ml of hESC medium and centrifuged at 1400 rpm for 5 min.
- Aspirated the supernatant and again washed with ½ KSR + ¼ N2 + ¼ NB medium and ROCK inhibitor (10μM) and centrifuged at 1400 rpm for 5 min.

- Aspirated the supernatant, resuspended the pellet in ½ KSR + ¼ N2 + ¼ NB medium with ROCK inhibitor (10μM) and counted the cells with haemocytometer.
- Plated 750K cells per each well of a 6-well low-attachment plate in 2 ml of ½ KSR + ¼ N2 + ¼ NB medium + ROCK inhibitor (10μM) + B27-RA (1%) and kept the plates in incubator at 37 ^{o}C and 5% CO_2.
- Day 0 media: ½ KSR+ ½ (N2+NB) medium + ROCK inhibitor (10μM) + B27-RA (1:100)

For Feeder independent pluripotent stem cells (iPSC growing on matrigel coated plates)

- mTESR1 medium was aspirated from the confluent iPSC culture dish and washed the cells once with 3 ml of EDTA and aspirated out.
- 1ml of EDTA was added to the culture dish and incubated for 3-4 min at 37°C in the incubator.
- EDTA solution was aspirated gently without disturbing the colonies and added 2 ml of accutase and kept back in the incubator for another 3 min.
- Detached the colonies with 2 ml of mTESR1 and then transferred the 4 ml to a 15 ml falcon and triturated them and observed under microscope for single cells and then added 2 ml of mTESR1 medium.
- Centrifuged the cells at 270g for 5 min.
- Supernatant was aspirated and washed with 4 ml of ½ KSR+ ½ N2+NB medium with ROCK inhibitor (10 μM) and centrifuged at 270g for 5 min.
- Supernatant was aspirated and resuspended the cells in 3 ml of ½ KSR+ ½ N2+NB medium with ROCK inhibitor (10 μM) and cells were counted.
- Plated 750K cells per each well of a 6-well low-attachment plate in 2 ml of ½ KSR + ¼ N2 + ¼ NB medium + ROCK inhibitor (10 μM) + B27-RA (1%) and kept the plates in incubator at 37 ^{o}C and 5% CO_2.
- Day 0 media: ½ KSR+ ½ (N2+NB) medium + ROCK inhibitor (10 μM) + B27-RA (1%)

Day 1

- EBs were allowed to form and in order for them to not attach to plate, each well was scrapped using cell scraper gently
- For day 3 EB transfer, New 6 cm dishes were coated ahead with 2ml of polyornithine/DPBS solution (15 µg/ ml polyornithine) -- 2 X 6 cm dishes were coated for each well of 6-well plate

Day 2

- EBs were scraped and collected in a 15ml falcon and waited for 15 mins for them to settle down. Centrifuged for 1 min at 200rpm and made sure whether the supernatant is clear and all EBs were settled down
- Supernatant was aspirated and then resuspended the EBs in 2ml of day 2 medium with inhibitor molecules SB-431542 (10 µM), Noggin (250 ng/ml) and XAV939 (3.3 µM) as required and replate the EBs in same wells. EBs were either untreated (denoted as Inhibitor-free), or treated with SB-431542 and Noggin (denoted dual SMAD-i), or treated with XAV-939 (denoted WNT-i), or their combination (denoted Triple-i).
- Washed the PO plates prepared on Day1 with PBS twice and again coated with Fibronectin (1 µg/ml) and Laminin (1 µg/ml).

Day 2 medium: ¼ KSR+3/4 (N2 + NB) + Rock inhibitor (10 µm)+ 1:100 B27-RA

Day 3

- Laminin plates were dried using 2 ml pipette encircling on the edges of the plate (Just make 1 big drop)
- EBs were scraped in each well using cell scraper, collected and distributed to 2 X 6 cm plates.
- Plates were kept for 10 mins in the incubator for the EBs to attach and then day 3 media was added.
- Medium was not changed for next 4 days.

Day 3 medium: ¼ KSR+ ¾ (N2 + NB) + Rock inhibitor (10 µm) + B27-RA (1%)

Day 7

- Medium was changed with ½ N2 + ½ NB medium along with inhibitor molecules SB-431542 (5 µM), Noggin (125 ng/ml) and XAV939 (3.3 µM)

Day 9

- Medium was replaced, all inhibitors were omitted and replaced with ½ N2 + ½ NB + FGF8 (100ng/ml) + BDNF (5ng/ml) + B27-RA (1%)

Rosettes were allowed to form till day 12, following which cells were fixed, harvested for analysis, or subjected to terminal differentiation. Neural induction and direct rosette formation could be also obtained by adherence on Matrigel-coated plates as previously described [127], with the modifications defined for this study (such as XAV-939 addition etc.). Long term propagation of cortical neural progenitors was performed by a weekly mechanical harvesting of rosettes followed by re-plating on Po/Lam/FN coated dishes and culture with ½ N2 + ½ NB medium containing 1% B27 without retinoic acid and with either FGF8 and BDNF (till day 28), or 20ng/ml of FGF2, EGF and BDNF (day 28 and on).

2.8 Derivation of cerebral organoids from human pluripotent stem cells

Organoids derivation was performed according to the Lancaster et al. protocol [170] with slight modifications as following.

Day 0

For Feeder dependent pluripotent stem cells (hESC growing on MEF feeder layer)

- hESC medium was collected from the confluent hESC culture dish into a 15ml falcon tube.
- 1ml of Dispase (4U/ml) was added to the culture dish and incubated for 10 min at 37°C in the incubator (incubation time could change according to the enzyme activity, so care was taken to not to over digest).
- The culture dish was tapped gently to detach the colonies from MEF and neutralized the dispase by adding 4ml of hESC medium collected in the first step.

- All the colonies were collected into a 15 ml falcon tube and let it wait till all the cells sink to bottom of the tube.
- Supernatant was aspirated and again washed the cells with 5 ml of hESC medium and let the cells to sink down.
- Supernatant was aspirated and 6 ml. of trypsin was added along with ROCK inhibitor (10 µM) and kept in 37°C water bath for 4 min.
- With p1000 pipette, colonies were triturated for 5 times and neutralized with 6 ml of trypsin inhibitor and triturated again for 10 times and observed for single cells under microscope.
- Washed twice by adding 10 ml of hESC medium + FGF2 (4 ng/ml) and centrifuged at 1400 rpm for 5 min.
- Aspirated the supernatant and cell pellet was resuspended in hESC medium + FGF2 (4 ng/ml) + ROCK inhibitor (50 µM) and counted the cells.
- Plated 9000 cells in 150 µl of hESC medium + FGF2 (4 ng/ml) + ROCK inhibitor (50 µM) per each well of a 96-well U-bottom low-attachment plate and kept the plates in incubator at 37 ^{o}C and 5% CO_2.

For Feeder independent pluripotent stem cells (iPSC growing on matrigel coated plates)

- mTESR1 medium was aspirated from the confluent iPSC culture dish and washed the cells once with 3 ml of EDTA and aspirated out.
- 1ml of EDTA was added to the culture dish and incubated for 3-4 min at 37°C in the incubator.
- EDTA solution was aspirated gently without disturbing the colonies and added 2 ml of accutase and kept back in the incubator for another 3 min.
- Detached the colonies with 2 ml of mTESR1 and then transferred the 4 ml to a 15 ml falcon and triturated them and observed under microscope for single cells and then added 2 ml of mTESR1 medium.
- Centrifuged the cells at 270g for 5 min.
- Supernatant was aspirated and washed twice by adding 10 ml of hESC medium + FGF2 (4 ng/ml) and centrifuged at 270g for 5 min.
- Aspirated the supernatant and cell pellet was resuspended in hESC medium + FGF2 (4 ng/ml) + ROCK inhibitor (50 µM) and counted the cells.

- Plated 9000 cells in 150 µl of hESC medium + FGF2 (4 ng/ml) + ROCK inhibitor (50 µM) per each well of a 96-well U-bottom low-attachment plate and kept the plates in incubator at 37 ^{o}C and 5% CO_2.

Day 1

- Checked the plate under microscope and observed that EBs were started to form at the center of the plate along with some single cells surrounding the EB

Day 2

- 75 µl of medium was gently aspirated without disturbing the EB at the center and 150 µl of fresh hESC medium was added with inhibitor molecules SB-431542 (10 µM), Noggin (250 ng/ml) and XAV939 (3.3 µM). Continued adding FGF2 (4 ng/ml) and ROCK inhibitor (50 µM) until the size of the EBs were around 350-400 µm in diameter. EBs were either untreated (denoted as Inhibitor-free), or treated with SB-431542 and Noggin (denoted dual SMAD-i), or treated with XAV-939 (denoted WNT-i), or their combination (denoted Triple-i).

Day 4

- Organoid size was measured under microscope. If the organoid size is above 350um, FGF2 and ROCK inhibitor were not supplemented to the medium.
- From each well, 150 µl of medium was gently aspirated and 150 µl of fresh hESC medium was added with inhibitor molecules SB-431542 (10 µM), Noggin (250 ng/ml) and XAV939 (3.3 µM).

Day 6

- Organoid size and morphology was checked under microscope. If the organoid size is greater than 400 µm and have brighter and smooth edges, then they were transferred to N2 neural induction medium. If the organoids were smaller in size, this step should be postponed for one day.
- 500 µl of N2 medium supplemented with the inhibitor molecules (SB-431542 (10 µM), Noggin (250 ng/ml) and XAV939 (3.3 µM)) were pre-added to each

well of 24 well low attachment plates and then kept in incubator at 37 ^{o}C for 15-20 minutes.

- Using clipped 200 µl pipette tip, organoids were transferred from each well of 96 well plate to each well of 24 well plates with neural induction medium (one organoid per well).

Day 8

- 300 µl of media was aspirated from each well, and 300 µl of fresh medium, (similar to day 6 medium), was added to each well of 24 well plate.

Day 10

- 300 µl of media was aspirated from each well, and 300 µl of fresh medium, (similar to day 6 medium), was added to each well of 24 well plate.
- Organoid size and morphology was checked under microscope. Observed organoids were brighter on the outside and began to show radial organization of pseudostratified epithelium indicating formation of neuroepithelium.

Day 11

- Matrigel was thawed on ice for about 1 hour for making matrigel droplets.
- Parafilm was cut and sterilized with ethanol and dimples were made using empty 200 µl tip box tray.
- Organoids were transferred into parafilm dimples by looking under the microscope using a clipped 200 µl pipette tip. Excess media was aspirated very gently and 30 µl of matrigel was added on top of each organoid and were gently pushed into the center of matrigel drop with a 10 µl tip to ensure complete embedding.
- Organoids were then kept in incubator at 37 ^{o}C for 30 minutes and once the matrigel was solidified (gel), gently transferred using spatula into low attachment 6-well plate with N2 + NB + B27-RA (1%) medium. 4 organoids were transferred to each well of 6 well plate with 2.5 ml of medium.

Day 12

- Checked the organoids under microscope and neuroepithelial vesicle outgrowths were started to appear. Differences between different inhibitor conditions were obvious at this stage.

Day 13

- 1.5 ml of media was aspirated carefully without touching the organoids within in the matrigel droplets and then 1.5 ml of fresh media (similar to day 11 medium) was added.

Day 15

- 1.5 ml of media was aspirated carefully and then 1.5 ml of fresh media now with 1% B27+RA (containing retinoic acid) was given. Plates were now transferred to an orbital shaker shaking with 86 rpm.
- For long term organoid culture, medium was changed every 2 days. Organoids were fixed in 4% paraformaldehyde, 0.15% picric acid for 20-40 minutes (RT) depending on their culture age, and then cryoprotected and processed as described under Immunostaining and confocal imaging section.

2.9 RNA isolation

RNA was isolated using the miRNeasy™ RNA Mini Kit (Qiagene) according to the manufactures protocol briefed below.

- 700 µl of QIAzol lysis reagent was added to the sample and were vortexed for 1 min to get a homogenized mixture.
- Homogenate was then incubated at room temperature (15-25 ^{o}C) for 5 min.
- 140 µl of chloroform was added and shaked vigorously for 15s and incubated at room temperature for 2-3 mins and centrifuged for 15 mins at 12000g at 4^{o}C.
- Sample forms an organic and aqueous phase after centrifugation. 300 µl of aqueous phase was collected without touching the organic phase and transferred to a new collection tube and 450 µl of 100% ethanol was added and mixed thoroughly by pipetting up and down.

- 700 µl of sample was transferred into RNeasy mini column placed in a 2 ml collection tube. Centrifuged at 8000g for 15 s at room temperature and flow through was discarded.
- 350 µl of buffer RWT (prepared with isopropanol) was added into the RNeasy mini spin column and centrifuged for 15s at 8000g and flow through was discarded.
- 10 µl of DNase I stock solution was added to 70 µl of buffer RDD and mixed gently by inverting the tube.
- DNAse I incubation mix (80 µl) was pippeted directly onto the RNesay mini spin column membrane and incubated for 15 min at room temperature.
- 500 µl of RWT buffer (prepared with iso-propanol) was added into RNeasy mini spin column and centrifuged for 15 s at 8000g. Flow through was kept and reapplied into the RNeasy mini spin column and centrifuged again at 8000g for 15 sec. Flow through was discarded.
- 500 µl of RPE buffer was added to RNeasy mini column. Centrifuged for 15 sec at 8000g. Discarded the flow through.
- Again 500 µl of buffer RPE was added to the column and centrifuged for 2 min at 8000g. Discarded the flow through.
- Transferred the RNeasy mini columns to a new 1.5 ml collection tube and eluted the RNA in 30 µl of RNase free water.
- Eluted RNA quality and concentration was measured using nanodrop.

2.10 Preparation and Sequencing of RNA-Seq Libraries

RNA-seq libraries for human samples were generated using the Illumina TruSeq RNA Library Preparation Kits, and pooled sampled were sequenced on the Illumina HiSeq 2500 sequencer as 100bp paired-end reads.

2.11 Description of processed RNA-Seq datasets of human brain transcriptomes

Gene expression data for different brain regions was retrieved from BrainSpan Atlas of the Developing Human Brain (http://human.brain-map.org/) based on extensive RNA-Seq study done by Šestan and colleagues [171]. Among the samples collected for that study, for our analysis we utilized datasets obtained from 16 brain regions

dissected from 8 to 37 gestational weeks, out of which 11 obtained from different neocortical regions and 5 others collected from the hippocampal primordia (future hippocampus), sub-cerebral regions including the diencephalon (future thalamic structures) and the sub-pallium (future striatum), as well as posterior brain regions (cerebellum). The file “RNA-Seq Gencode v10 summarized to genes” containing RPKM values (available at http://www.brainspan.org/static/download.html) was downloaded on 3.08.2017. A detailed description of data processing procedures for generating the above file by the authors is available at (http://help.brain-map.org/display/devhumanbrain/Documentation).

2.12 RNA-Seq data processing and normalization for single and pooled organoids

Raw RNA-Seq reads were mapped to the human reference genome hg19 using STAR mapper [172]. Generated bam files were filtered for uniquely mapped reads using Samtools [173] and read counts were generated using HTSeq [174] (parameters: -m intersection-strict --nonunique all -r pos -s reverse). For further analysis, all mitochondrial genes were removed from the data. RPKM values were calculated by dividing the number of counts by gene length and sequencing depth, followed by multiplying by 10E9. For data normalization, only RefSeq-annotated genes were considered and their RPKM values were normalized by bringing the samples to the same RPKM sum. For generating heatmaps, a pseudocount of 1 was added to RPKM values, and a log2 base was then taken. Afterwards, all rows (genes) of heatmap matrices were scaled to a range (-0.5, 0.5).

2.13 Combined RNA-Seq data analysis for organoid and human brain datasets

Since raw RNA-Seq datasets for human brain regions have not been accessible, combined comparative analysis of BrainSpan and cerebral organoid samples together was re-processed so as to minimize the processing differences between both datasets. This was achieved first by re-processing organoid datasets similar to as described above for processing organoid datasets alone, such that HTSeq parameter -s was changed to “no”. In addition, all values generated by merging both RPKM matrices were quantile normalized. To remove non-biological variations revealed by the correspondence analysis (see description below), the function ComBat [175] from the sva package [176] was applied. ComBat uses an empirical

Bayesian framework to adjust data for batch effects and other unmeasured sources of variation.

2.14 Correspondence analysis

Correspondence analysis (CA) [177] is a projection method that represents variables such as expression values of genes as vectors in a multidimensional space. Similar to principal component analysis (PCA), CA reveals also principal axes of the investigated space. This allows projecting data matrix into a low-dimensional subspace, thereby investigating the main variance in the data. Moreover, in contrast to PCA, CA can simultaneously account for samples in a gene-dimensional space and for genes in a sample-dimensional space - showing the information in a so-called biplot. The interpretation of CA biplot is such that one finds the genes characteristic for a (group of) sample(s) in the direction of this sample (group). The farther away from the center the genes lie, the more characteristic they are for the respective sample(s).

Both correspondence analyses from our study were conducted using the 10,000 genes with the highest expression variance across investigated samples. In the combined analysis of brain and organoid samples, we first merged both RPKM matrices and projected the new matrix into the three-dimensional subspace. The resulting CA plot shows very clearly that the first principal axis accounts for the technical variation between both datasets (data not shown). Hence, to remove the observed bias we applied ComBat, and the result of the final CA of the ComBat-transformed data is shown in Figure 12.

2.15 Differential Expression and Gene Set Enrichment analysis between organoids

From the Allen Brain Atlas dataset, we estimated markers for different brain regions during weeks 12-21, by comparing the log2 fold change of the raw RPKM expression in each regional sample compared to all other regions across weeks 12-21. Genes were defined as regional-specific if they had at least a log2 fold change of 2 when compared to all other regions, excluding striatal and amygdala samples, across all weeks. We furthermore filtered striatal and amygdala specific genes by removing genes with a log2 fold change of 2 in amygdala or striatal samples compared to all

other regions across weeks 12-21. To determine differential gene expression across brain organoids derived by different protocols, we ran DeSeq2 [Love et al., 2014] on three pairwise treatment comparisons, Triple-i vs Dual-SMADi, Triple-i vs Inhibitor-free, and Dual-SMADi vs Inhibitor-free, using 8 biological replicates of individual organoids from each protocol. Regional genes derived from the Allen Brain Atlas are subsequently highlighted in the volcano plot. A Gene Set Enrichment Analysis (GSEA) [citation] was then run to determine enrichment of the regional specific gene sets in each of the three comparisons. Furthermore, among we estimated z-scores of the expression in the Allen Brain Atlas.

2.16 Single cell RNA-Seq procedures

2.16.1 Organoid dissociation

D50 organoids (N=4) derived by different treatments were dissociated into single cells using papain dissociation kit (Worthington). Organoids were first incubated with papain and DNase I solution for 35 min and then triturated and filtered through 40-micron filter to obtain single cell suspension. Cells were centrifuged at 300g for 5 min, re-suspended in Hank's Balanced Salt Solution (HBSS), counted for viability (>80% were viable) and FACS sorted using FACS Aria III (Becton Dickinson), while excluding dead cells labeled with DAPI.

2.16.2 Single cell library preparation

Roughly 50,000 single organoid derived and sorted live cells were collected in PBS buffer (100 cells/μL) and subjected to an inDrop procedure [178, 179]. Briefly, collected cells were injected in the commercially available inDrop™ system from 1CellBio. Hydrogel bead-cell co-encapsulation, in-drop synthesis of barcoded cDNA and library preparation was performed according to the recommended procedures of the manufacturer. Obtained libraries were sequenced using Illumina short read sequencing.

2.16.3 Single cell RNA-Seq data processing

Two paired-end sequencing batches were generated using a NextSeq 500 sequencing device (Illumina). These two batches were treated separately until the dataset alignment was performed by applying the Seurat pipeline (Andrew et al, bioRxiv 2017). The alignment step described below is important to correct any

potential batch effects and normalize the data altogether. The sequencing data was converted to fastq by fastq-dump (v2.4.5) using default parameters. Read 1 was used to obtain the sample barcode and UMI (unique molecular identifiers) sequences; read 2 was then mapped to a reference transcriptome as described below. The reads were first filtered based on presence in read 1 of two sample barcode components separated by the W1 adaptor sequence. Read 2 was then trimmed using Trimomatic (Bolger et al., 2014) (version 0.36; parameters: LEADING:28 SLIDINGWINDOW:4:20 MINLEN:16). Barcodes for each read were matched against a list of the 3842 pre-determined barcodes from 1CellBio, and errors of up to two nucleotides mismatch were corrected. Reads with a barcode separated by more than two nucleotides from the reference list were discarded. The reads were then split into barcode specific files for mapping and UMI filtering. We kept barcodes with minimum 10000 UMIs.

2.16.4 Single cell gene mapping and UMI counting

The UMI alignment was done according to [180]. In summary, reads split into barcode-specific files were aligned using Bowtie (version 0.12.0, parameters: -n 1 –l 15 –e 300 –m 200 –best –strata -a) to the human transcriptome. Alignments from bowtie were filtered in order to choose the alignment closer to the end of the transcript. The resulting UMI counts tables were concatenated and loaded into R for analysis. Cells with less than 5000 mapped UMIs and less than 500 detected genes (at least one UMI) were discarded.

2.16.5 Single cell dataset alignments, tSNE analysis and cell-subpopulation identification

The UMI counts tables were then merged across all cells in organoids derived by Triple-i, dual-SMAD-i, and Inhibitor-free treatments. First, the counts were divided by the library size (number of UMIs in each cell) and then multiplied by a scaling factor of 10000, and log(x+1) transformed, using Seurat's "NormalizeData" function. The scaled z-score residuals were then estimated after regressing on the number of UMI and percent of mitochondrial counts per cell using Seurat's "ScaleData" function. Principal Component Analysis was then performed on the scaled z-score residuals of the most highly variable genes (log variance to mean ratio of UMI counts at least 0.5), 2868 genes in total. Clusters were determined using the graph-based clustering

approach “FindClusters” in Seurat on the first 6 principal components from PCA with a resolution of 0.6. The tSNE visualization was then generated using the first 10 principal components.

2.17 Immunostaining and confocal imaging

Cells were fixed in 4% paraformaldehyde, 0.15% picric acid, permeabilized and blocked with PBS, 1% bovine serum albumin (BSA), 10% FBS and 0.3% Triton solution. Organoids were similarly fixed, washed, cryoprotected with 30% sucrose overnight and then submerged in OCT. Fixed cells or sectioned organoids (10uM slices) were stained with indicated primary antibodies (see below) followed by Alexa Fluor secondary antibodies (Invitrogen). Following staining, cells were imaged in PBS, and organoid sections were mounted on Moviol (Sigma). Fluorescence images were obtained using a confocal microscope LSM710 (Carl Zeiss Micro Imaging, Germany). The confocal images were captured using 10X and 20X objectives (NA=0.3 and 0.8, Plan-Apochromat, respectively). Fluorescence emissions resulting from Ar 488, 543 and 633 nm laser lines for EGFP, CY3 and CY5, respectively, were detected using laser scanning settings and filter sets supplied by the manufacturer. For DAPI detection in all images as well as GFP detection for organoid images, we used our mode-locked Ti:Sapphire, fento second pulsed, multiphoton laser (Chameleon Ultra II, Coherent, Inc.) at a wavelength of 720 nm and 920 nm, respectively. Epi fluorescent and phase contrast images were obtained using Nikon Eclipse Ti-E microscope. Fluorescence emissions results from mercury arc lamp. Images were taken using 10X and 20X objectives. Images were generated and analyzed using either Zeiss ZEN 2011 software (Carl Zeiss, Inc.) or NIS elements software (Nikon). All images were exported in TIF and their color levels were identically adjusted per each staining procedure.

2.17.1 Table for antibodies list

Antibody name	Vendor	Dilution
CTIP2	ABCAM (ab18465)	1:250
CUX1	ABCAM (ab54583)	1:200
CUX2	ABCAM(ab130395)	1:100

EMX2	ABCAM(ab94713)	1:50
FEZF2	ABCAM(ab69436)	1:250
FOXG1	ABCAM(ab18259)	1:400
p-VIMENTIN	ABCAM(ab22651)	1:120
PERICENTRIN	ABCAM(ab4448)	1:1000
SATB2	ABCAM(ab51502)	1:50
NKX2.1	ABCAM(ab76014)	1:400
SOX1	ABCAM	1:1000
SOX2	ABCAM (ab79351),	1:500
TBR1	ABCAM(ab31940)	1:500
TBR2	ABCAM(ab23345)	1:200
HOXB4	DSHB (concentrated)	1:100
NKX2.2	DSHB(74.5A5,concentrated)	1:120
PAX6	DSHB(concentrated)	1:22
GAD65	R & D (AF2247)	1:40
OTX2	R & D(AF1979)	1:40
SOX1	R & D(AF3369)	1:40
SOX17	R & D(AF1924)	1:30
TUJ1	BD Biosciences (560340)	1:500
COUP-TF1	Millipore (ABE1425)	1:500
DCX	Millipore (AB2253)	1:500
RELN	Millipore(MAB5364)	1:200
β-3-Tubulin	Covance (PRB-435P)	1:500
FOXA2	Santa cruz biotechnology (SC-6554)	1:100
PTPRZ1	Sigma (HPA015103)	1:500
SP8	Atlas Antibodies (HPA054006)	1:50
CAS-3	Cell signaling (#9661)	1:500
GFAP	Dako	1:1000
Poly-Glutamylated TUBULIN	Enzo lifesceinces (GT335)	1:1000

2.18 Quantitative PCR (qPCR) analysis

RNA was extracted using miRNeasy kit (Qiagene) followed by cDNA reverse transcription kit (Applied Biosystems). 4-6ng of cDNA was subjected to qPCR using our homemade designed primers (see 'Primer set list'), FastStart universal SYBR green (Roche) and ViiA-7cycler (ABI). Threshold cycle values were determined in triplicates and presented as average relative fold over those of HPRT. Fold changes were calculated using the 2-Δct method.

2.18.1 Table for qPCR Primer set

Gene	Sequence
BRACHYURY_F	5'-ACCCAGTTCATAGCGGTGAC-3'
BRACHYURY_R	5'-CAATTGTCATGGGATTGCAG-3'
CTIP2_F	5'-TCCAGAGCAATCTCATCGTG-3'
CTIP2_R	5'-GCATGTGCGTCTTCATGTG-3'
CUX1_F	5′- CAACAAGGAATTTGCTGAAGTG -3′
CUX1_R	5′- CTATGGTTTCGGCTTGGTTC -3′
CUX2_F	5′- GAGCTGAGCATCCTGAAAGC -3′
CUX2_R	5′- AGGCCTCCTTTGCAATAAGC -3′
DCX_F	5'-CATCCCCAACACCTCAGAAGA -3'
DCX_R	5'-CGTTTGCTGAGTCAGCTGGA-3'
EGFR_F	5′- GATAGTCGCCCAAAGTTCCGT -3′
EGFR_R	5′- CTGAATGACAAGGTAGCGCTG -3′
FEZF2_F	5'-CCCAGGAAAAGCCACATAAAT-3'
FEZF2_R	5'-GGATGCGGATATGCGTGTT-3'
FOXA2_F	5'-CCGACTGGAGCAGCTACTATG -3'
FOXA2_R	5'-TGTACGTGTTCATGCCGTTC-3'
FOXG1_F	5'-AGGAGGGCGAGAAGAAGAAC-3'
FOXG1_R	5'-TGAACTCGTAGATGCCGTTG-3'
GFAP_F	5′- AGAGATCCGCACGCAGTATG -3′
GFAP_R	5′- TCTGCAAACTTGGAGCGGTA -3′
GLAST_F	5′-CCCTTGGGTTTTTATTGGAGG-3′
GLAST_R	5′-ATGGGTAGGGTGGCAGAACT-3′

HES5_F	5’-ACCAGCCCAACTCCAAGCT-3’
HES5_R	5’-GGCTTTGCTGTGCTTCAGGTA-3’
HPRT_F	5’-TGACACTGGCAAAACAATGCA-3’
HPRT_R	5’-GGTCCTTTTCACCAGCAAGCT-3’
OCT4_F	5’-CAGCAGATCAGCCACATC-3’
OCT4_R	5’-CGGTTACAGAACCACACTC-3’
PAX6_F	5’-CACACCGGTTTCCTCCTTCA-3’
PAX6_R	5’-GGCAGAGCGCTGTAGGTGTTT-3’
S100β_F	5′- GGAAATCAAAGAGCAGGAGGTT -3′
S100β_R	5′- TCCTGGAAGTCACATTCGCC -3′
SATB2_F	5′- TAGCCAAAGAATGCCCTCTC -3′
SATB2_R	5′- AAACTCCTGGCACTTGGTTG -3′
SOX1_F	5’-GCAAGATGGCCCAGGAGAAC-3’
SOX1_R	5’-CGGACATGACCTTCCACTCG-3’
SOX17_F	5’-AAGATGACTGGCAAGTCGT-3’
SOX17_R	5’-CTTCAGCCGCTTCACCTG-3’
TBR1_F	5’-GTCACCGCCTACCAGAACAC-3’
TBR1_R	5’-ACAGCCGGTGTAGATCGTG-3’
TBR2_F	5’-AACCACTGGCGCTTCCA-3’
TBR2_R	5’-AACATACATTTTGTTGCCCTG-3’

2.19 Measurements and statistical analysis

For all qPCR gene expression analysis obtained for neural induction, cortical specification, and iPSC characterization experiments, two-way ANOVA test followed by Tukey’s multiple comparison test were applied. Statistical analysis was performed using GraphPad software. For calculating organoid size, as well as neuroepithelial and luminal measurements (area, perimeter and luminal length) ImageJ or Nis-elements (Nikon) software was used. For neuroepithelium area calculation, luminal areas were subtracted from entire vesicle areas. For all size organoid/vesicle size measurements, for SOX2/DCX counting in organoids and rosette derived progenitors, and for P-VIM nuclei counting, t-Test was applied. Statistical analysis was performed using GraphPad software.

3. RESULTS

3.1 Neural induction platforms

We used PSC based two neural differentiation platforms – neural rosettes grown as 2D monolayer cultures and brain organoids grown as 3D cultures. We have used both hESC (HES5::eGFP hESC reporter line – in order to assess notch activation status) and hiPSC line (ZIP8K8 iPSC line– as an additional supporting cell line to confirm the results observed in hESC) and subjected these to 2D and 3D neural differentiation methods. In the case of 2D culture, we first modified a standard embryoid body (EB) protocol to generate small EBs formed by aggregation period of 3 days and followed by attachment and continued differentiation as monolayer/flattened adherent colonies on laminin coated plates. We reasoned that small EBs generated by short aggregation should combine preservation of early cell-to-cell mediated intrinsic inductive signaling together with maximized responsiveness to exogenous cues once they were flattened. This is in contrast to 3D systems, where intrinsic inductive signals are sufficient to enable self-organization ability of neuroepithelial cells into CNS fates (Lancaster et al., 2013). To compare the different inhibition paradigms on both systems, we employed inhibition-free conditions **(**denoted as **Inhibition-free)**, WNT inhibition alone using XAV 939 **(WNT-i),** TGF-β and BMP inhibition using SB-431542 and Noggin **(dual SMAD-i)** (Chambers et al., 2009), and combined dual SMAD-i and WNT-i **(Triple-i)**.

We employed these inhibitors starting on day 2 of differentiation, when EB formation was evident and continued till day 9. While dual SMAD-i is known to strongly induce CNS specification, WNT-i impairs early gastrulation events [181, 182] during early differentiation phases (days 2-5), and thus streamline dual SMAD inhibition-mediated CNS specification. Continued WNT inhibition through the neural induction period (days6-9) should allow preferential expansion of anterior neuroectodermal fates on the expanse of caudal fates during the neural patterning phase [53, 183]. WNT inhibition was omitted on day 9 prior to robust Notch activation [127] so as to allow cortical progenitors to utilize endogenous WNT activation required for their maintenance, once established [184, 185, 186]. In 2D system, inhibitor withdrawal on day 9 was complemented by addition of FGF8 for the proliferation of NE cells. In

case of 3D organoids, we followed the inhibitor-free method of Lancaster et al., [129] on top of which inhibitors were added from day 2 like in the 2D system and continued till neural induction period i.e., till the day of Matrigel embedding (day11-12). Following inhibitor withdrawal, organoids were supplemented with B-27 without retinoic acid till day 15 and then transferred to a moving orbital shaker for more oxygen penetration and now supplemented with B-27 with retinoic acid (Figure 10).

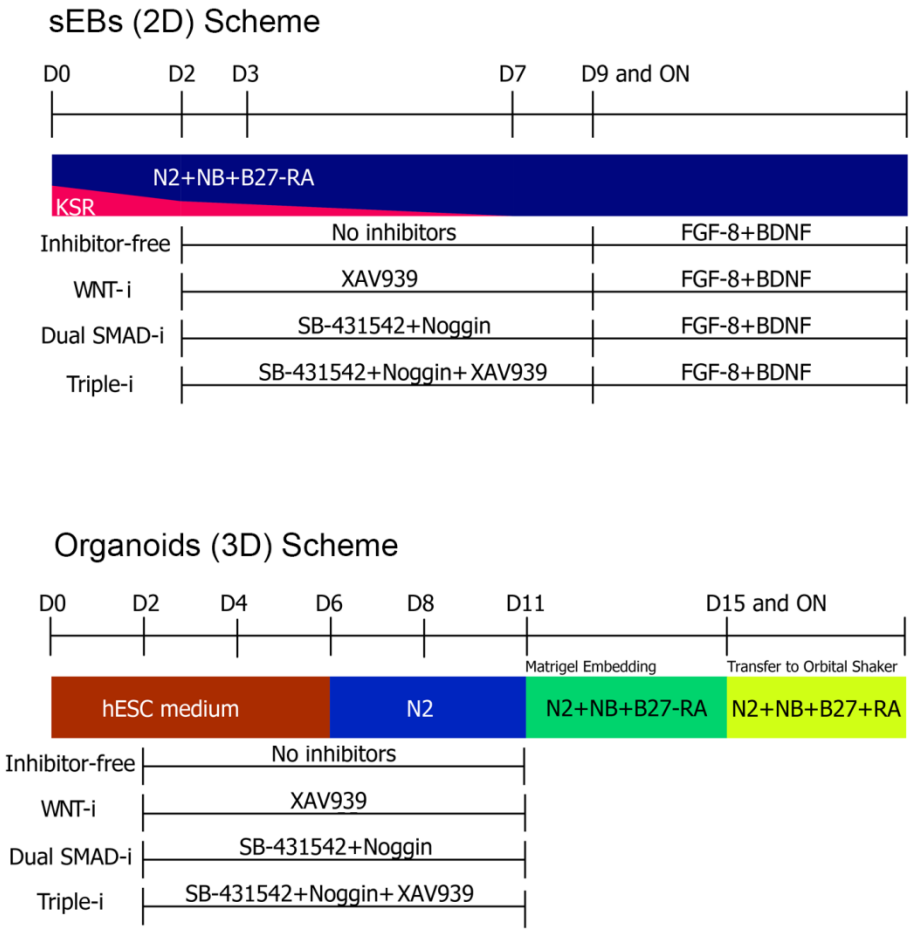

Figure 10: Differentiation scheme

Schematic showing generation and maintenance of 2D monolayer neural rosettes (above) and 3D cerebral organoids (below) from human pluripotent stem cells.

3.2 Molecular analysis of 3D organoids and 2D neural rosettes generated under different inhibition paradigms

3.2.1 Correspondence analysis for RNA-Seq profiles of organoids derived by different methods

We assessed the transcriptional signature of neural progenitors derived by various inhibitory paradigms under both 2D monolayer cultures and brain organoids grown as 3D cultures. We employed RNA-Seq on multiple, individually processed day 30 organoids (N=8) derived by either inhibitor-free, dual SMAD-i or Triple-i conditions. We also analyzed day 17 (N=3) and day 30 (N=3) organoids that were pooled and processed together. Correspondence analysis (CA) first confirmed that undifferentiated PSCs, day 17 organoids and day 30 organoids segregated as separate clusters, reflecting expected differences in general transcriptional identity during the transition from the undifferentiated state towards early and then later neural stages (Figure 11). Remarkably, while day 17 organoids appeared proximal to each other regardless of treatment, day 30 organoids further sub-segregated into three sub clusters corresponding to the three derivation paradigms, demonstrating that making organoids by different methods clearly creates distinct transcriptional signatures (Figure 11).

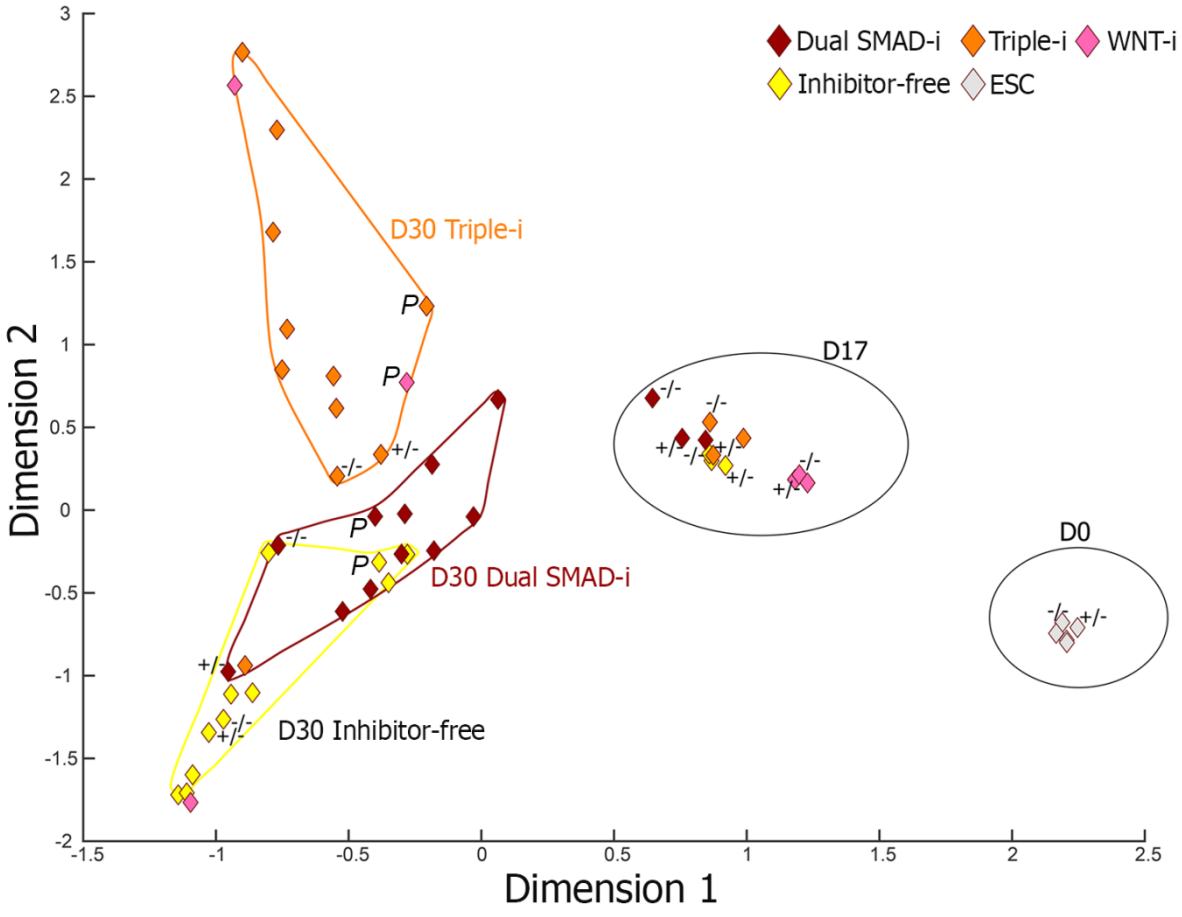

Figure 11: Correspondence analysis (CA) plot of 3D organoid RNA-Seq datasets

Correspondence analysis (CA) plot of RNA-Seq datasets obtained from undifferentiated PSCs (D0), day 17 organoids (D17) and day 30 organoids (D30) derived by indicated treatments. Transcriptome profiles were obtained from single, individually processed (N=8) D30 organoids, pool (≥3) processed D17 organoids and pool (≥3) processed D30 organoids derived under indicated treatments. Symbols: diamonds represent PSCs (Grey), inhibitor-free organoids (Yellow); dual SMAD-i derived organoids (Red), Triple-i derived organoids (Orange) and WNT-i derived organoids (Pink). P: Pooled organoids. -/- and +/-: homozygous and heterozygous microcephaly mutant organoids (discussed in detail under microcephaly result section).

3.2.2 Comparative correspondence analysis of organoid RNA-Seq profiles and human brain samples reveals substantially distinct human brain signatures

To gain a comprehensive look into the brain regions assigned by the differently derived organoids we integrated transcriptional datasets from the Allen Human Brain Atlas (http://human.brain-map.org/) done by Šestan and colleagues [171] in to organoid CA plots (Figure 11). For our analysis we utilized datasets obtained from 16 brain dissected regions from 8 to 37 gestational weeks, out of which 11 samples were obtained from different neocortical regions and 5 others collected from the medial pallium (future hippocampus), sub-cerebral regions including the diencephalon (future thalamic structures) and the sub-pallium (future striatum), as well as more posterior brain regions (cerebellum). These integrated CA plots showed first that embryonic brain samples clustered into three distantly located gestational week groups corresponding to week-8, weeks 12,16,21, and week-37. Yet, each cluster contained representatives of all forebrain sub-structures tested, (neocortical, hippocampal, sub-cerebral) excluding hindbrain regions, which clustered elsewhere than cortical regions (Figure 12). We interpreted this wide distribution of groups across developmental age as reflection for extensive transcriptional remodeling of forebrain/cortical cell identity and composition during development. Interestingly, day 17 organoids derived by all methods overlapped with week-8 forebrain/cortical cluster. However, among the three sub clusters representing day 30 organoids derived by the different treatments, only Triple-i derived organoids overlapped with forebrain/cortical embryonic structures, with a particular overlap with week-21 forebrain samples (Figure 12). These findings provide strong evidence that early exposure to combined dual SMAD and WNT inhibition (Triple-i) is critical for specification of growing organoids towards forebrain / neocortical fates.

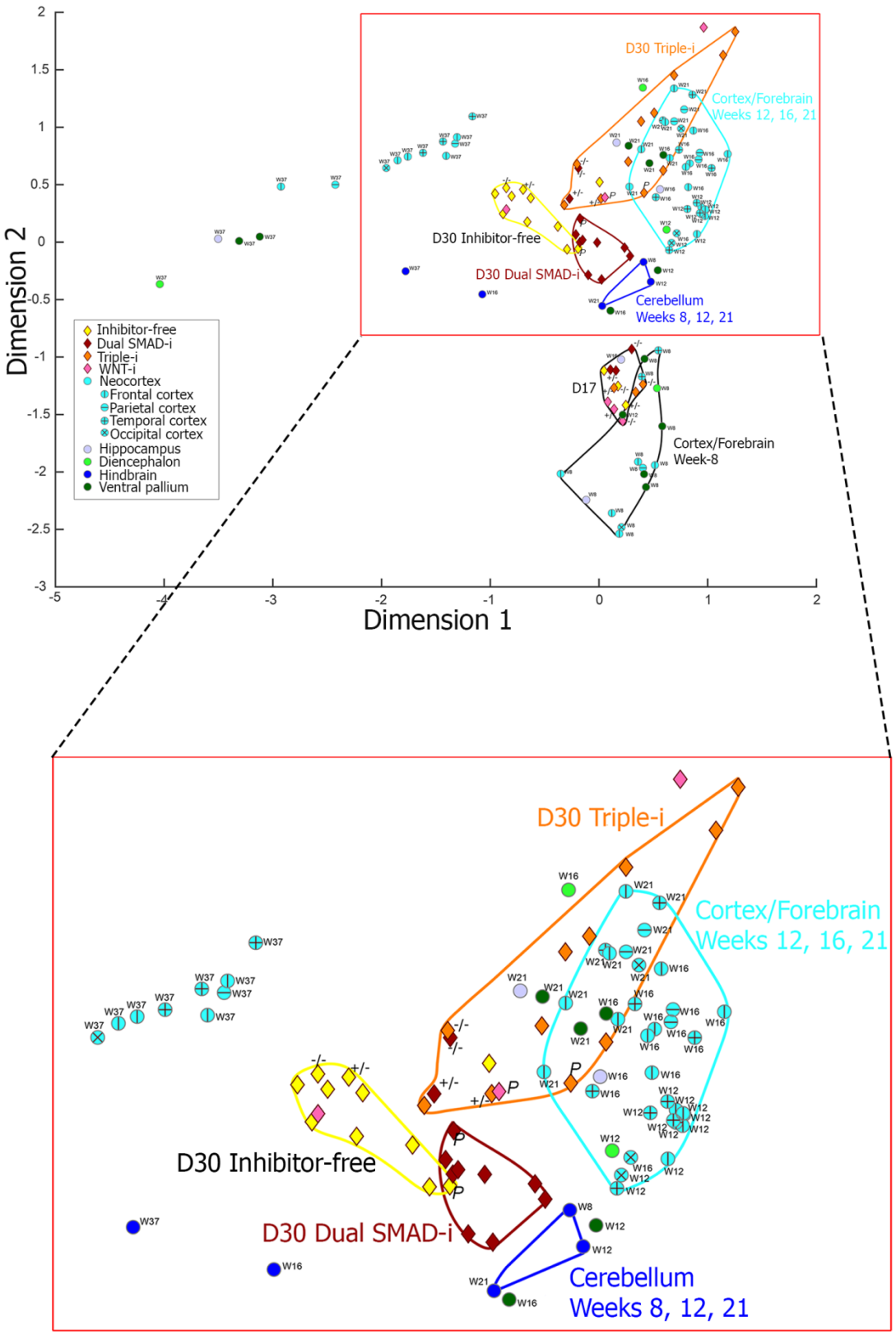
Dimension 2
Dimension 1
Inhibitor-free
Dual SMAD-i
Triple-i
WNT-i
Neocortex
Frontal cortex
Parietal cortex
Temporal cortex
Occipital cortex
Hippocampus
Diencephalon
Hindbrain
Ventral pallium
D30 Triple-i
Cortex/Forebrain
Weeks 12, 16, 21
D30 Inhibitor-free
D30 Dual SMAD-i
Cerebellum
Weeks 8, 12, 21
D17
Cortex/Forebrain
Week-8

Figure 12: Correspondence analysis (CA) plot of 3D organoid RNA-Seq datasets integrated with human brain regional transcriptomic dataset

CA plots calculated for RNA-Seq datasets obtained from (Figure 11) and then integrated with human brain region specific RNA-Seq datasets (Allen Human Brain Atlas: http://human.brain-map.org/) corresponding to 16 brain regions including 11 neocortical areas, hippocampus, ventral forebrain, diencephalon and cerebellum and collected across several developmental stages ranging from gestational week-8 to week-37. Symbols for organoid samples appear as in (Figure 11). Brain region-specific samples appear as circles representing cortical regions (Turquoise) further sub-divided to frontal cortex (vertical crossing line), parietal cortex (horizontal crossing line), temporal cortex (vertical and horizontal crossing line) and occipital cortex (diagonally crossing lines), as well as hippocampus (light purple), diencephalon (green), hindbrain (blue) and ventral pallium (dark green). Each cluster was encircled by its respective color. See methods for further sub-divisions according to Šestan and colleagues [171]. Note the close proximity of the Triple-i derived D30 organoids to week-21 human neocortex/forebrain samples. Large scale cluster distribution appears at the bottom.

While forebrain and hindbrain (cerebellum) structures well separated from each other in our CA plots, less separation between cortical, medial pallium or sub-cortical regions could be seen within the forebrain domain. We next identified biomarkers for the cortex, medial pallium, diencephalon, and cerebellum across weeks 12 through 21 in the Allen human brain data sets. We then did a differential gene expression analysis on the pairwise comparisons of different treatments i.e., Triple-i vs dual SMAD-i (Figure 13A), Triple-i vs Inhibitor-free (Figure 13B) and dual SMAD-i vs Inhibitor-free (Figure 13C) to identify the genes enriched in each treatment. This analysis revealed that Triple-i significantly enriches for cortical genes (Figure 13A and 13B) whereas dual SMAD-i shows a significant enrichment of diencephalon and cerebellum specific genes (Figure 13A and 13C) while Inhibitor-free shows a slight but not significant enrichment of medial pallium genes (Figure 13B).

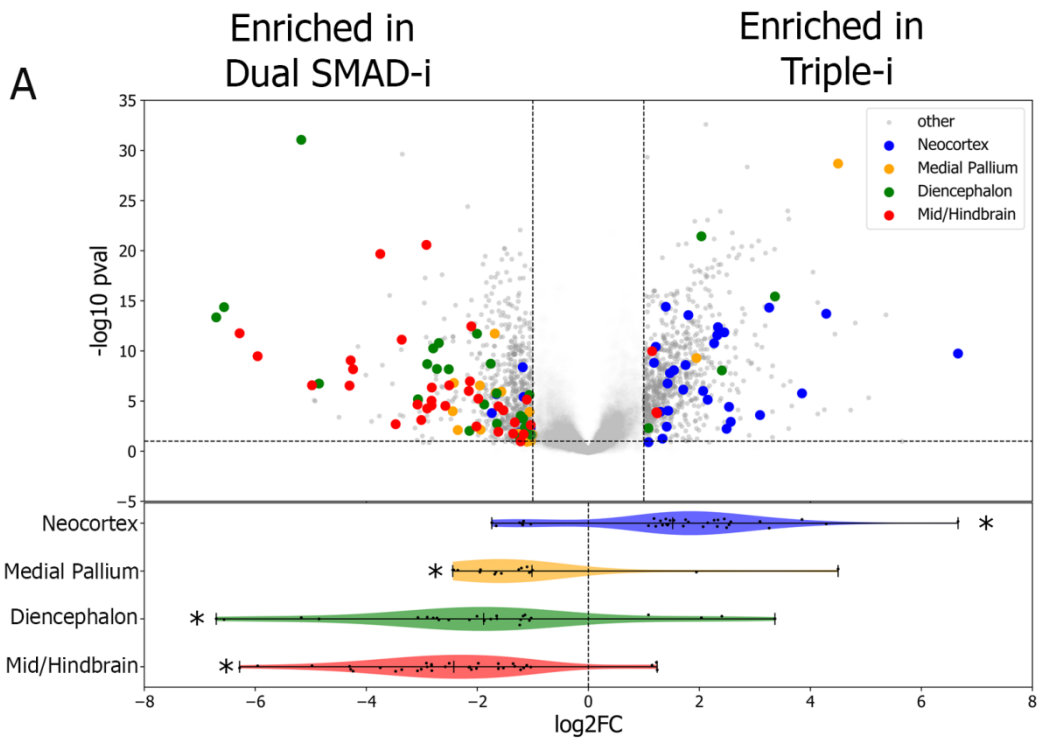
A
Enriched in
Dual SMAD-i
Enriched in
Triple-i
other
Neocortex
Medial Pallium
Diencephalon
Mid/Hindbrain
-log10 pval
Neocortex
Medial Pallium
Diencephalon
Mid/Hindbrain
log2FC

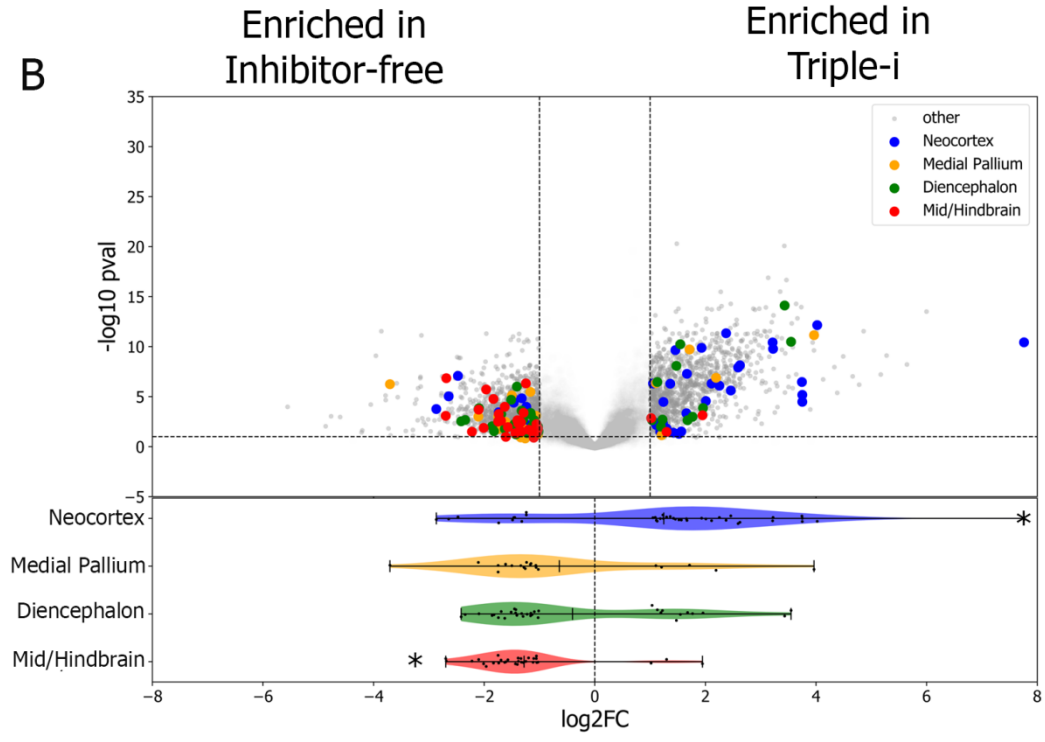
B
Enriched in
Inhibitor-free
Enriched in
Triple-i
other
Neocortex
Medial Pallium
Diencephalon
Mid/Hindbrain
-log10 pval
Neocortex
Medial Pallium
Diencephalon
Mid/Hindbrain
log2FC

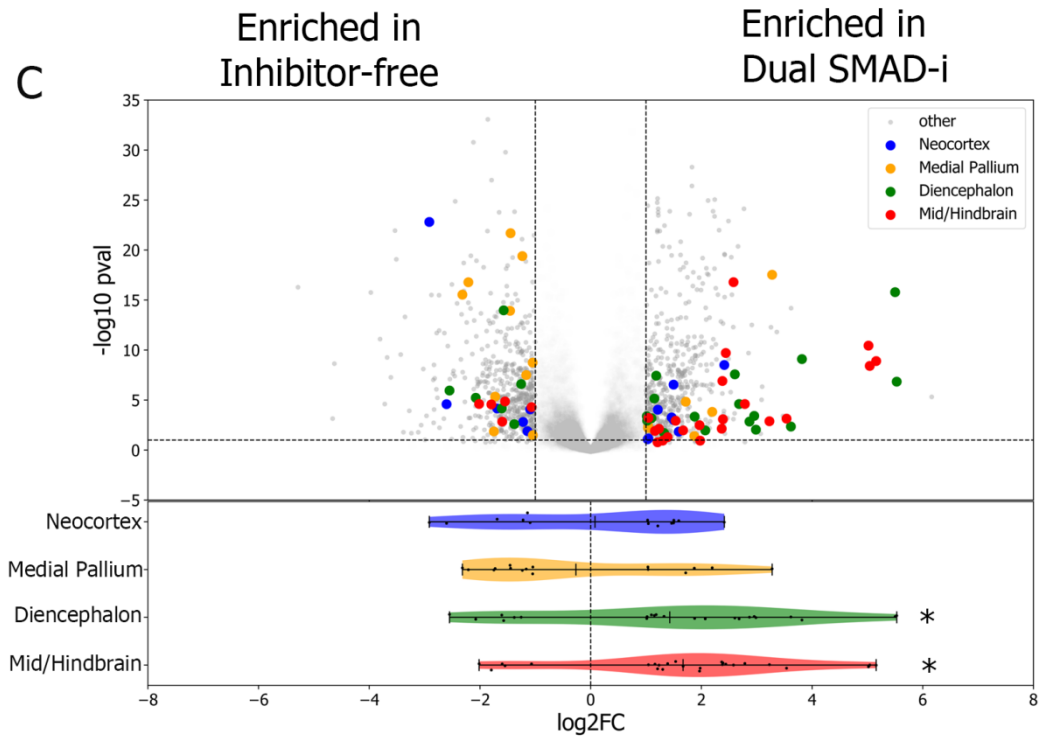

Figure 13: Differential gene expression and gene set enrichment analysis

A. Volcano plot of day 30 Triple-i organoids vs dual SMAD-i organoids. Log2 fold change is plotted on the x-axis and -log10 (Q-value) is plotted on the y-axis, estimated by DESeq2. Significant differential expression (DE) of region-specific genes of weeks 12-21 measured in the Allen human brain atlas dataset are highlighted in the plot. The distributions of significant DE regional genes are plotted in the violin plot beneath the volcano plot. The -log10(Q-value) after running a Benjamini-Hochberg correction of Gene Set Enrichment Analysis using regional gene sets derived from Allen Brain Atlas samples from weeks 12-21 for day 30 Triple-i organoids vs dual SMAD-i organoids. An asterisk is plotted at the peak of the bar to signify whether the GSEA test was significant using a Q-value of 0.1.

B. Volcano plot of day 30 Triple-i organoids vs Inhibitor-free organoids. See (A) for plot description.

C. Volcano plot of day 30 dual SMAD-i organoids vs Inhibitor-free organoids. See (A) for plot description.

We then compared the differentially expressed gene sets from the pairwise comparisons of day 30 organoids to the regional specific gene sets from weeks 12 through 21 in in-vivo human brain data. Among the 206 cortex specific genes, 23 were consistently upregulated in Triple-i organoids (upregulated in both Triple-i vs dual SMAD-i and in Triple-i vs Inhibitor-free) (Figure 14). When overlaying the relative expression levels of these genes in the Allen Bran Atlas samples, we observe that the Triple-i specific gene set has the highest expression level, followed

by the 12 genes enriched in both dual SMAD-i and Triple-i. All together these findings clearly show that Triple-i generated organoids are enriched for cortical fates.

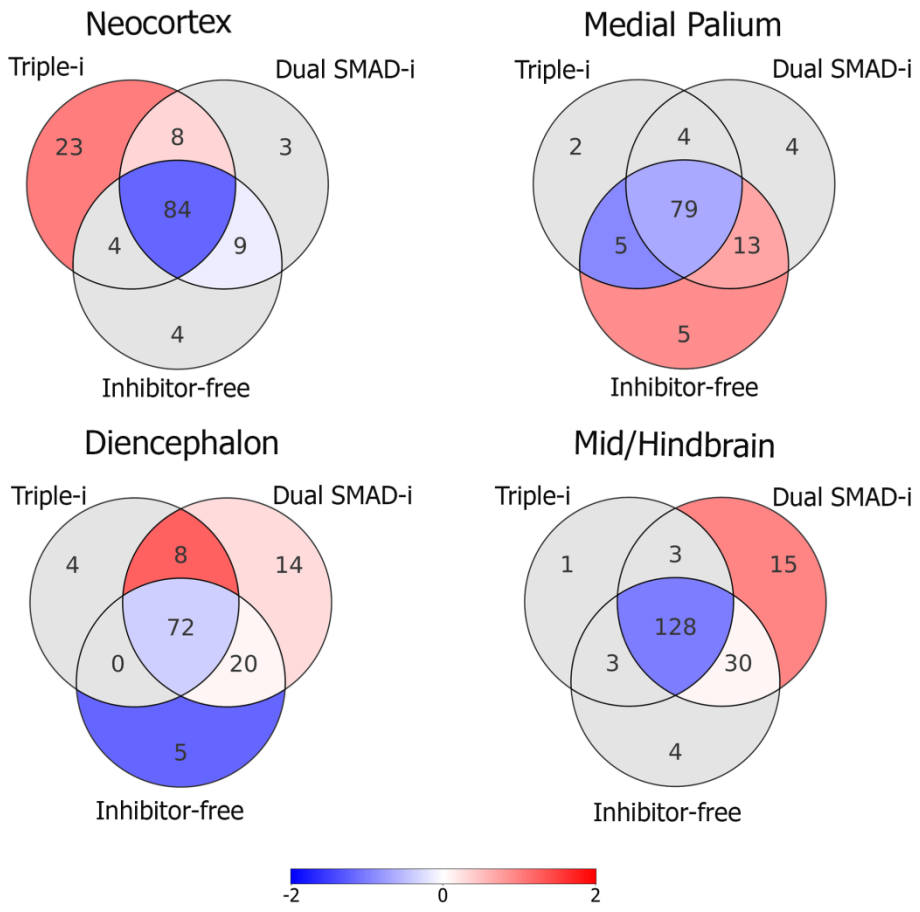

Figure 14: Differential gene expression and gene set enrichment analysis overlaid on Allen human brain regional biomarkers expression

Venn diagrams of treatment specific DE genes and Allen human brain regions specific gene sets. Color of Venn diagram sections represents the relative expression levels of genes across Allen human brain samples from weeks 12-21, calculated by estimating mean expression level across all samples from the respective region across weeks 12-21, estimating mean of these values, and calculating z-score from this value across all sections. Sections were only included with 5 or more genes present.

One of the limitations of current organoid methods is the existence of high variability between the organoids generated in the same experiment. In order to identify the molecular heterogeneity between the organoids derived under different inhibition paradigms, we examined the expression of a panel of brain region characteristic markers such as dorsal pallium (neocortical), medial pallium (cortical hem/hippocampal primordia) and diencephalic (thalamic), as well as more posterior

regions such as mid-hindbrain – all across different treatments (Figure 15). We found that genes expressed in neocortical region, were predominantly and homogenously induced by most Triple-i organoids (Figure 15). Intriguingly, medial pallium genes corresponding to the cortical hem and hippocampal primordia could be induced by any of the methods, including inhibitor-free conditions, indicating that the formation of this forebrain/cortical organizer is largely unaffected by WNT activation (or inhibition) levels modulated in this study. Third, sub-cortical and more posterior brain regions including diencephalon, midbrain and hindbrain, were exclusively and also heterogeneously induced by dual SMAD-i. Finally, induction of these posterior fates by dual SMAD-i coincided with enhanced NSC marker expression. This was compatible with a similar trend in human week-21 brains [171] – the in vivo embryonic counterpart of day 30 organoids – where higher expression level of NSC markers such as HES5, NOTCH1, NES and SOX2 is observed for cerebellar structures, when compared to other brain parts. To conclude, our results show that different derivation methods result in distinct global transcriptional identities in organoids. Moreover, the findings also particularly pinpoint combined WNT-i on top of dual SMAD-i as critical for yielding cortical fates. Last, since inhibition was employed during early days of differentiation (until day 10), our findings also suggest that shaping the identity of the starting population by exogenous cues in early days is critical and sufficient for inducing a lasting cerebral fate induction effect also after 20 more days in culture.

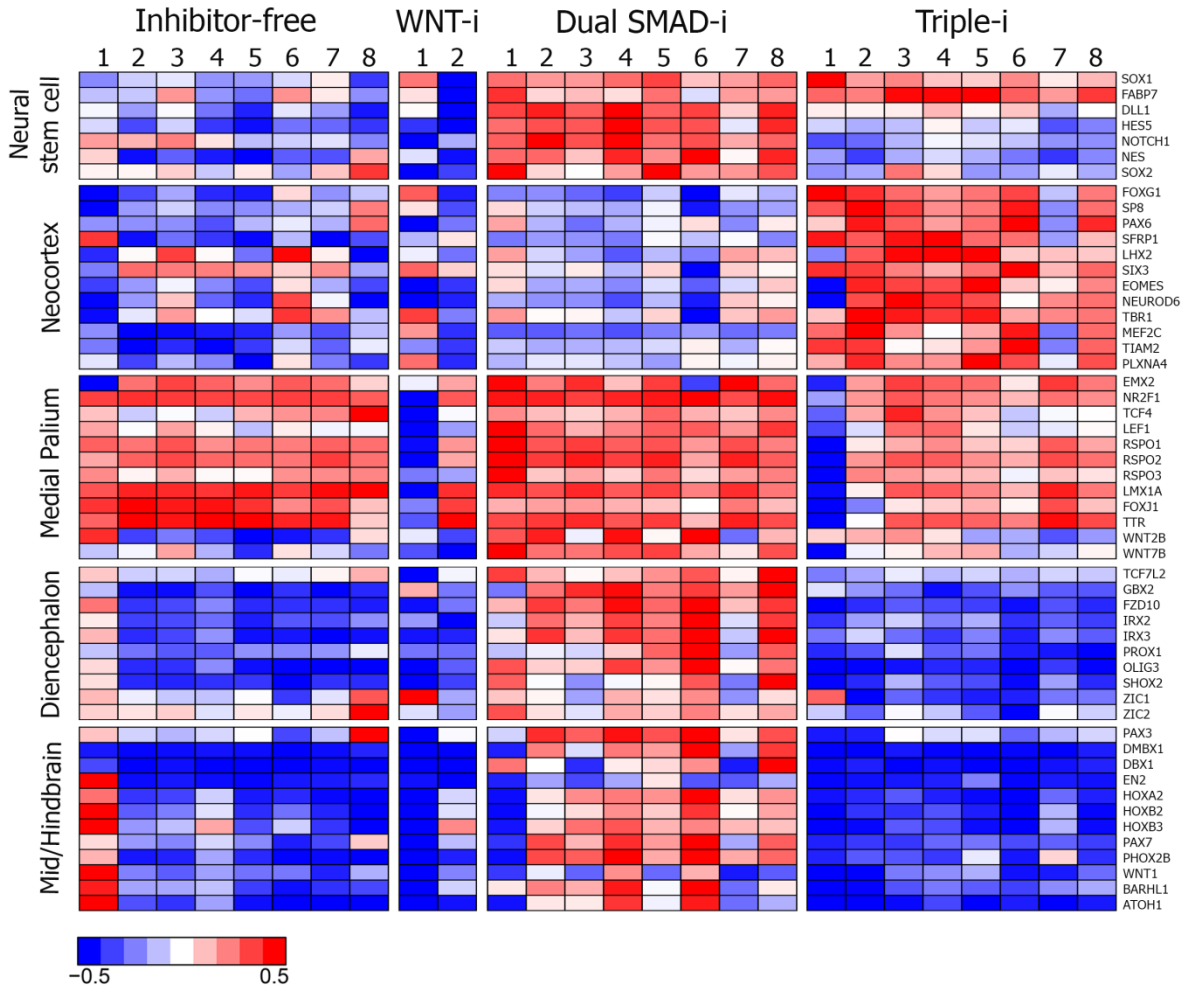

Figure 14: Brain regions specific gene expression among organoids across defined treatments
A heatmap representing expression values for selected genes categorized according to neural stem cell markers and additional groups of regional markers (neocortex, medial pallium, diencephalon and midbrain-hindbrain) in day 30 organoids derived under indicated treatments. Color-coded scale represents relative expression levels of each gene (row) across treatments.

3.2.3 Correspondence analysis for RNA-Seq profiles of 2D neural rosettes derived by different methods

The effects of inhibitors also worked similarly for 2D monolayer cultures despite the lack of certain cell-to-cell interactions and cytoarchitectural components required to efficiently recapitulate specification. CA plots generated for RNA-Seq obtained from day 8, 10 and 12 of monolayer cultures generated under different inhibitory paradigms (Figure 15A) reveals a clear distinction between dual SMAD-i and Triple-i derived samples on one hand, and WNT-i and inhibitor-free derived samples on the

other hand – segregating neural fate-favoring from -unfavoring conditions [121, 125]. Also, the differences between dual SMAD-i and Triple-i became greater as days progressed, with major change observed on day 12 of differentiation (Figure 15A). Consistently, differences in expression level of the same regional and NSC markers used to characterize organoids were most apparent between treatments on day 12 (Figure 15B). In addition, we interestingly observed that anterior/cortical genes were expressed on day 8 under both dual SMAD-i and Triple-i, but then peaked on day 12 under Triple-i, while declining under dual SMAD-i with concomitant upregulation of posterior/non-cortical genes. This was similar to reminiscent of studies in frogs where some anterior neural axis fates developed first, from which only later transformed to posterior fates [11, 12]. The upregulation of diencephalic and midbrain-hindbrain genes already on day 8 and consistently increased up to day 12 in dual SMAD-i treatment demonstrates that the early starting populations generated were heterogeneous with both cortical and non-cortical fates (Figure 15). Notably, some posterior markers were upregulated on earlier days also under inhibitor-free and WNT-i conditions, possibly reflecting early non-neural fates marked by the same genes. This was not recorded in inhibitor-free or WNT-i derived organoids, which again, could develop neural fates in the absence of inhibitors. While trends for forebrain and diencephalic-mid-hindbrain patterning genes were generally similar for 2D and 3D, medial pallium markers corresponding to the cortical hem/future hippocampus seemed to be induced by dual SMAD-i better than Triple-i, compared to the treatment-indifferent induction of this structure in organoids (Figure 15B). Nonetheless, these results still argue that also in 2D cultures Triple-i is critical for induction of homogenous neocortical fates.

A

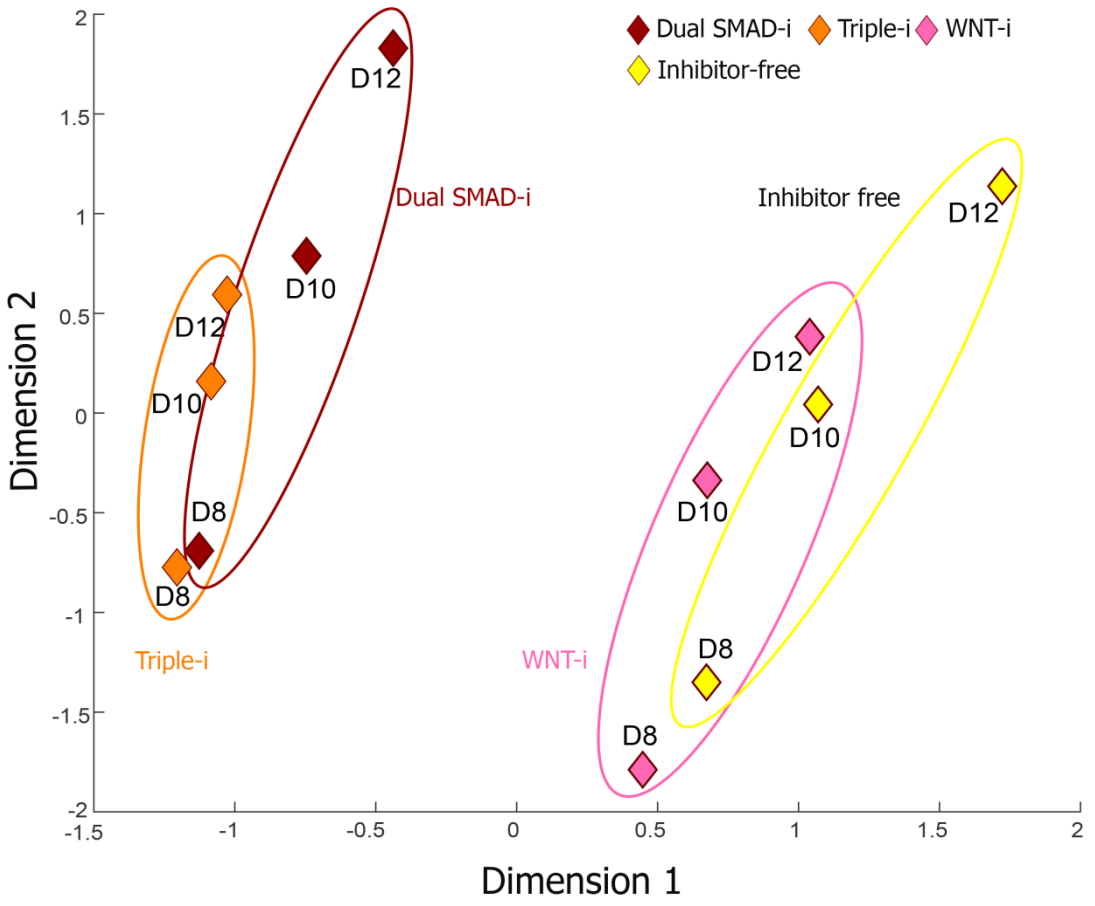
Dual SMAD-i
Triple-i
WNT-i
Inhibitor-free
Dimension 2
Dimension 1
Dual SMAD-i
Triple-i
WNT-i
Inhibitor free
D12
D10
D8
D12
D10
D8
D12
D10
D10
D8
D8
D12

B

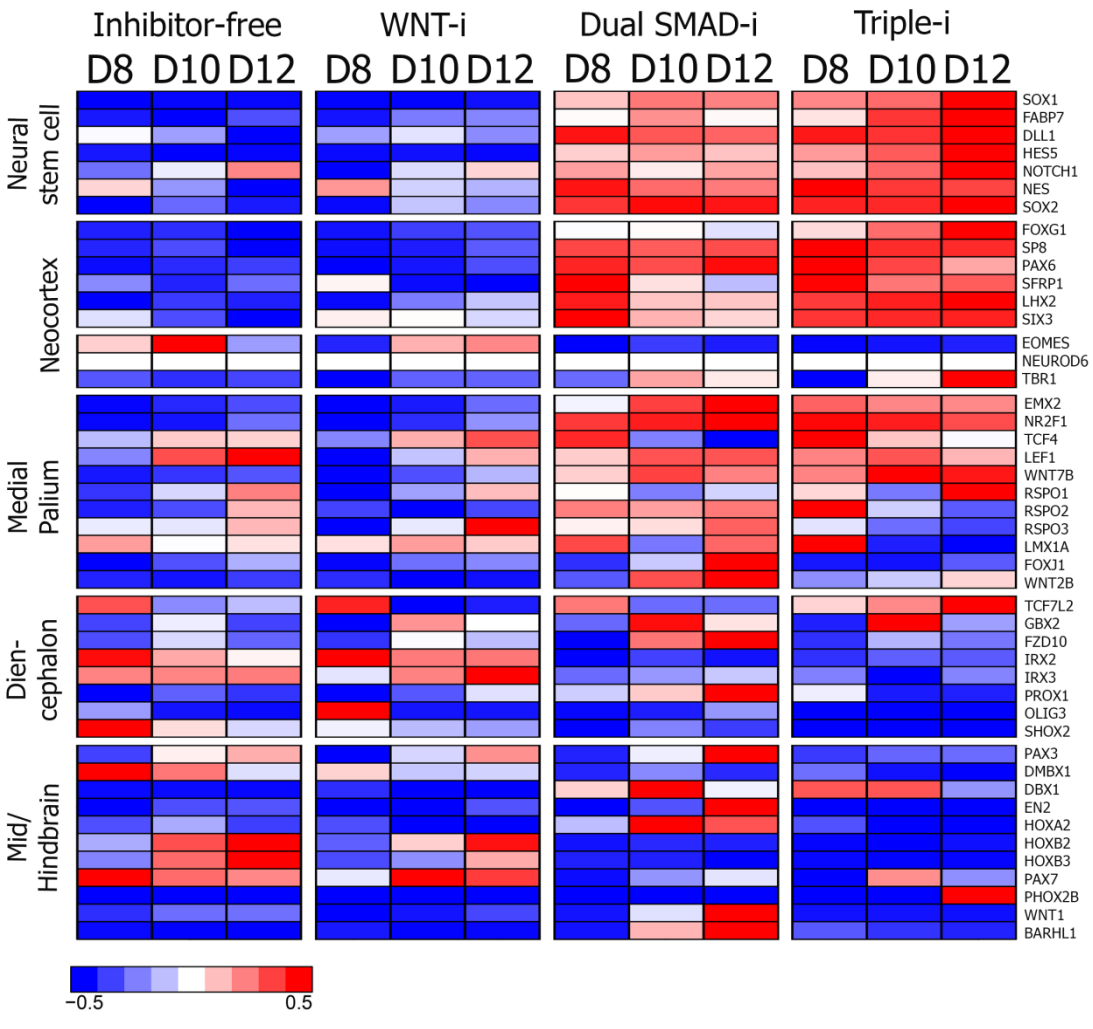
Inhibitor-free
WNT-i
Dual SMAD-i
Triple-i
D8 D10 D12
Neural stem cell
Neocortex
Medial Palium
Dien-cephalon
Mid/ Hindbrain
SOX1
FABP7
DLL1
HES5
NOTCH1
NES
SOX2
FOXG1
SP8
PAX6
SFRP1
LHX2
SIX3
EOMES
NEUROD6
TBR1
EMX2
NR2F1
TCF4
LEF1
WNT7B
RSPO1
RSPO2
RSPO3
LMX1A
FOXJ1
WNT2B
TCF7L2
GBX2
FZD10
IRX2
IRX3
PROX1
OLIG3
SHOX2
PAX3
DMBX1
DBX1
EN2
HOXA2
HOXB2
HOXB3
PAX7
PHOX2B
WNT1
BARHL1
−0.5
0.5

Figure 15: Correspondence analysis (CA) plot of 2D rosette RNA-Seq datasets generated under different treatments and their relative brain regions specific gene expression signature

A) CA plots of RNA-Seq datasets obtained from day 8 (D8), day 10 (D10) and day 12 (D12) monolayer neural progenitors derived by indicated treatments. Same symbols as in organoids apply to monolayer samples.

B) A heatmap representing expression values for selected genes categorized as in (Figure 14) and obtained for day 8, day 10 and day 12 monolayer neural progenitors derived under indicated treatments. Color-coded scale represents relative expression levels of each gene (row) across treatments and days.

3.3 Cellular analysis of 3D organoids and 2D neural rosettes generated under different inhibition paradigms

3.3.1 Enhanced Notch activation and robust radial organization are hallmarks for transition of PSCs towards cortical fates

The molecular analysis draw a clear dichotomy between the specification of distinct cortical and non-cortical (posterior) identities both in 2D and 3D systems based on the addition or exclusion of a single pathway inhibitor for WNT signaling (on top of a dual SMAD-i background). Nevertheless, as cortical stem cell markers can be somewhat unambiguous such as known SOX2, SOX1 and PAX6 markers are present in both cortical (neocortex) and non-cortical (diencephalon, mid/hindbrain) cell types, so one main concern is how to assess - already at the early neural starting population level - the efficiency of cortical differentiation. In search for such reliable readouts, based on evidence from our lab, we reasoned that Notch activation and radial organization (rosette formation) capacity - when overlapping - may serve as a potential readout for efficient early specification towards cortical identity. Our earlier studies showed that radial organization (rosette formation) of early telencephalic neural progenitor cells is abrogated in the presence of Notch signaling inhibitors [119]. We further coupled Notch activation and radial organization to cortical neurogenesis by showing that only cells obtained from mechanically isolated Notch active radially organized structures (i.e. rosettes) could give rise cortical neurons in a time and cortical layer dependent manner [127]. We also validated this correlation at the molecular level by revealing transcriptional and epigenetic factors associated with corticogenesis that drive Notch activation at the rosette stage [146]. Finally, we demonstrated that Notch active cells within rosettes performed

interkinetic nuclear migration – the hallmark phenomenon of cortical differentiation [147], and then used this feature as a cytoarchitectural quantitative readout for cortical differentiation at the rosette stage.

Here we revisited the ability of Notch activation and radial organization to project cortical cell identity within starting populations. We used the same *HES5::eGFP* human embryonic stem cell reporter line [166] used for RNA-Seq to correlate Notch activation and radial organization capacity to cortical fate specification in 2D and 3D systems. In 2D cultures, Notch activation (*HES5::eGFP* expression) and rosette formation were completely absent from inhibitor-free and WNT-i derived progenitors, observed to some extent and not necessarily overlapping in dual SMAD-i derived progenitors, and were both highly enhanced in Triple-i derived progenitors (Figure 16 A). However, in addition to their enhancement under Triple-i conditions, they impressively overlapped (Figure 16A), suggesting a strong link between efficient radial organization and Notch activation cellularly, and the acquisition of cortical fates transcriptionally.

In organoids on the other hand, the generation of vesicle-like neuroepithelial protrusions – a 3D counterpart of rosettes -were naturally occurring under all treatments (Figure 16B), in line with other studies [129, 131-133, 136]. However, under inhibitor-free organoids, radially organized structures exhibited weak Notch activation through entire organoid sections in multiple organoids (N=9) (Figure 16B), suggesting attenuated stemness. In correlation, inhibitor-free organoids developed non-neuroepithelial extensions similar to previous observations [129]. WNT-i alone increased radially organized protrusions in organoids (N=9), improved their Notch activation, and eliminated non-neuroepithelial extensions (Figure 16B). This was in contrast to the poor ability of WNT-i alone to drive Notch activation or radial organization in monolayers (Figure 16A), emphasizing the potential of 3D systems to utilize a WNT-depleted cellular environment to streamline self-acquisition of neural fates. Nonetheless, radial organization in organoids derived by WNT-i often remained in a small scale, and Notch activation was not first-rate (see HES5::eGFP images for Triple-i). In correlation, WNT-i derived organoids were transcriptionally heterogeneous (Figure 11), and often did not endure the long-term culture. These findings possibly reflect altogether the critical role of SMAD inhibition in cell

expansion and lumen growth. Dual SMAD-i was sufficient to yield regions with strongly enhanced Notch activation alongside radially organized regions in organoids (N=9) (Figure 16B). However, areas of high Notch activation did not coincide with those of radial organization. In addition, non-neuroepithelial extensions were still present. Together with our transcriptional analyses, these results show that the posterior fates derived by dual SMAD-i potentially exhibit high Notch activation not compatible with capacity for radial organization.

Only when combined, dual SMAD-i and WNT-i treatments led to robust radial organization that well overlapped with enhanced Notch activation within organoids (N=9) (Figure 16B). This also correlated with significantly increased organoid size under this treatment (See Figure 24 for size comparison under different treatments). Moreover, non-neuroepithelial extensions were entirely eliminated. High-power confocal Z-stacks of organoids across treatments demonstrate the superior effect of Triple-i conditions on Notch activation and radial organization (vesicle formation) (Figure 17). We interpret the increase in these two features under Triple-i as readout for enhancement of NSC identity (stemness) and establishment of robust cell polarity, respectively. We also propose that acquisition of these features may be a critical step in the process of corticogenesis in vitro. More generally, these results demonstrate that early pathway inhibition had a robust effect on shaping the identity, homogeneity and maintenance of the starting population in both 2D and 3D systems.

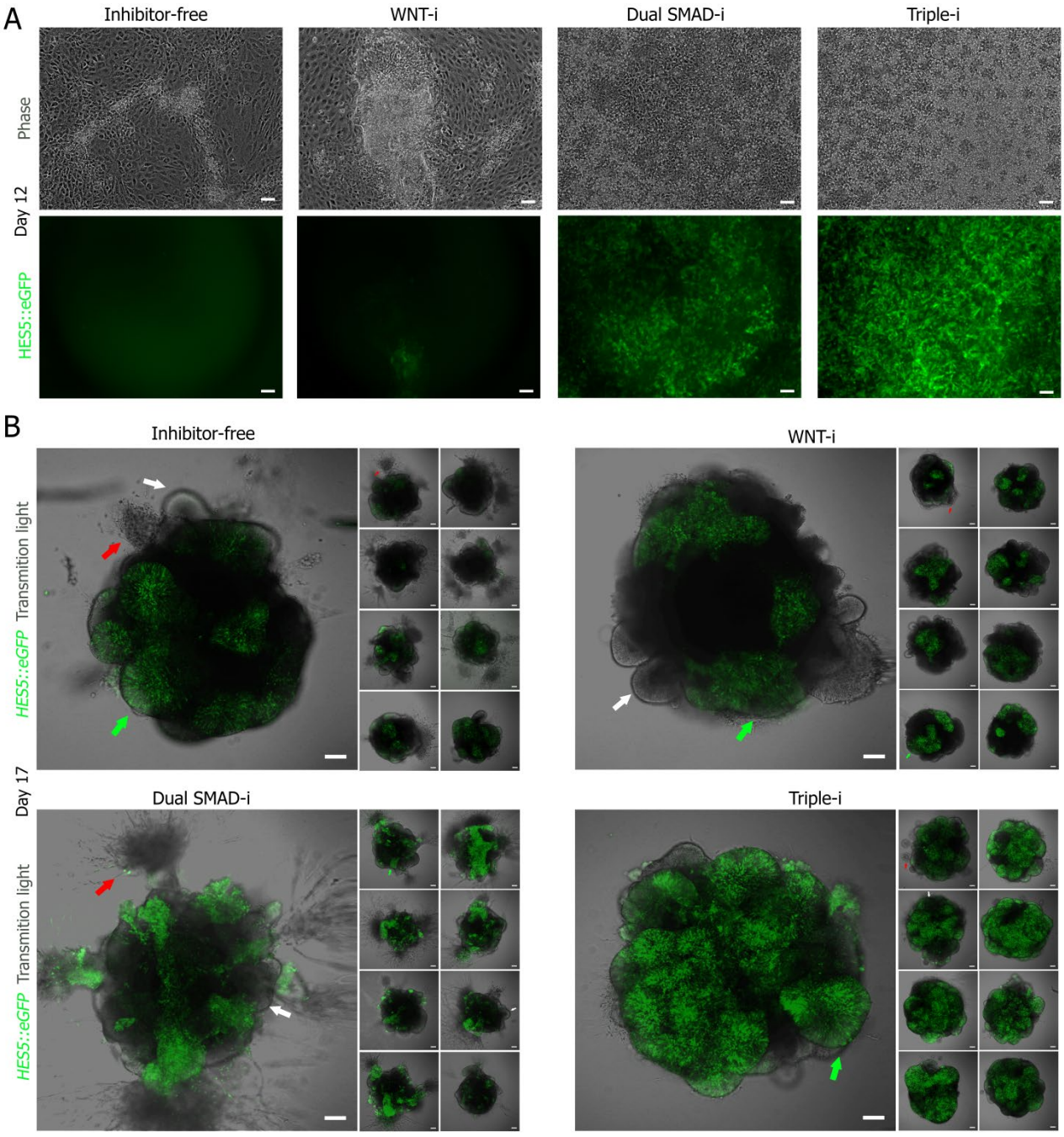

Figure 16: Enhanced Notch activation and efficient radial organization are hallmarks of transition of PSCs towards neocortical fates and require Triple-i.

A. Phase contrast (top) and HES5::eGFP (bottom) images of day 12 neural monolayer progenitors derived from small EBs (sEBs) subjected to neural induction under inhibitor-free conditions (Inhibitor-free), WNT inhibition using XAV-939 (WNT-i), dual SMAD inhibition using SB-431542 and Noggin (dual SMAD-i) and combined dual SMAD and WNT inhibition (Triple-i). Scale bar: 50 µm.

B. Merged bright field images and their matched HES5::eGFP confocal images taken from Day 17 representative organoids (N≥9) derived by indicated treatments. Shown are maximum intensity projections for HES5::eGFP confocal images taken at 15µm intervals across each organoid and collected to a summed image. Green arrows represent enhanced Notch active and radially organized regions (vesicles), white arrows refer to radially organized regions lacking enhanced Notch activation, and red arrows refer to non-neuroepithelial extensions. Note the substantial homogeneity in Notch

activation, radial organization and lack of non-neuroepithelial extension in Triple-i derived organoids. See also organoid size quantification for all treatments in Figure XX. Scale bar: 100 µm

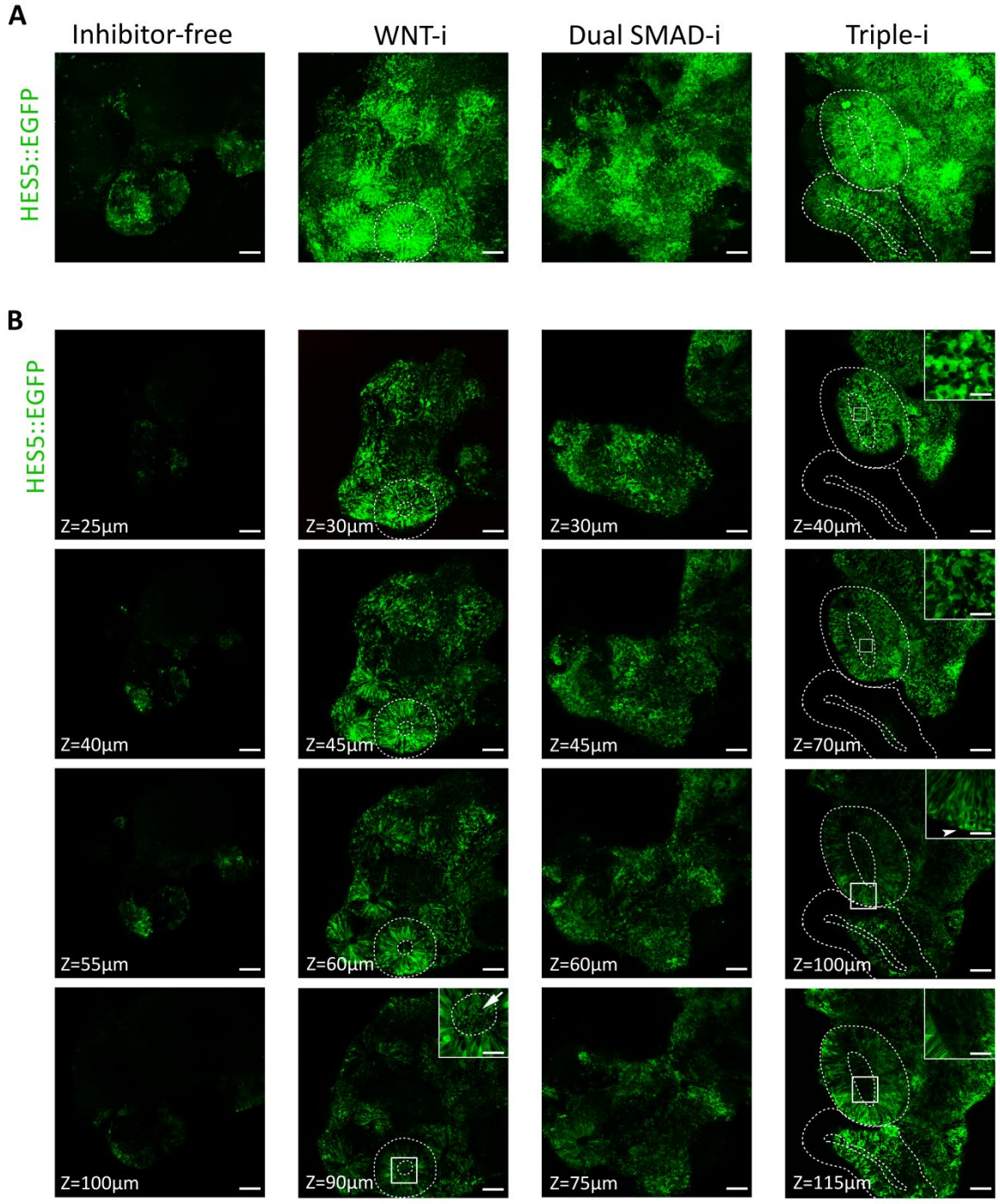

Figure 17: Enhanced radial patterns in cerebral organoids derived by combined dual SMAD and WNT inhibition

A. HES5::eGFP representative confocal images taken from Day 20 organoids derived under defined treatments (N=3 for each day/treatment). Shown is maximum intensity projection of HES5::eGFP confocal images taken at 5µm intervals across each organoid (see corresponding z-sections in B).

Note the sparse HES5::eGFP expression in vesicles of inhibitor-free organoids. Note organization into rosettes but not large vesicles in WNT-i treated organoids (dashed circle). Note irregularity in shape and cytoarchitectural organization of HES5::eGFP expressing cells in dual SMAD-i treated organoids. Note near complete vesicle organization and enhanced Notch activation in Triple-i treated organoids (dashed line). Scale bar: 100 μm.

B. Confocal z-sections of HES5::eGFP across the Day 20 organoids shown in A. Shown are representative images from stacks taken for each treatment, with 33-49 planes collected per stack, depending on treatment. Four representative planes per each organoid are shown. Z-stacks appear from top to bottom images (representing stacks proximal and distal to objective). Triple-i treatment: Basal and apical sites of vesicle ventricular zones are represented by outer and inner dashed lines, respectively. Ventricular zone is represented by HES5::eGFP expressing cells located within outer and inner dashed lines. Vesicle center (surrounded by inner dashed lines) represents from top to bottom to: radial glial cell bodies, radial glial end feet, ventricle of cerebral vesicles. Insets represent enlargements of indicated areas in each image (open squares) corresponding from top to bottom to: radial glial cell bodies, radial glial end feet, radial glial basal processes, ventricle of cerebral vesicles. WNT-i treatment: outer and inner dashed lines represent rosettes that have not developed to vesicles. Inset represents enlarged rosette lumen with apparent radial glial end feet. Scale bars for all large images: 100 μm. Inset scale bars for Triple-i treatment, from top to bottom: 16.7 μm, 16.7 μm, 33 μm, 33 μm. Inset scale bar for WNT-i treatment: 33μm.

3.3.2 Radial Organization of NSCs derived under combined dual SMAD and WNT inhibition coincides with dorsal cortical markers

To further support the link between Notch activation, radial organization and the acquisition of early cortical identity obtained by Triple-i (Figure 12), we performed a series of immunostainings in early 2D and 3D cultures derived under the different paradigms. We began with PAX6 and SOX1, two early neuroepithelial markers for which double staining is highly ambiguous in determining cortical fates. Here, these markers were weakly expressed in inhibitor-free or WNT-i derived monolayer cultures (Figure 18), with WNT-i slightly inducing these markers due to its capacity to attenuate gastrulation and in agreement with in vivo observations [53, 187].

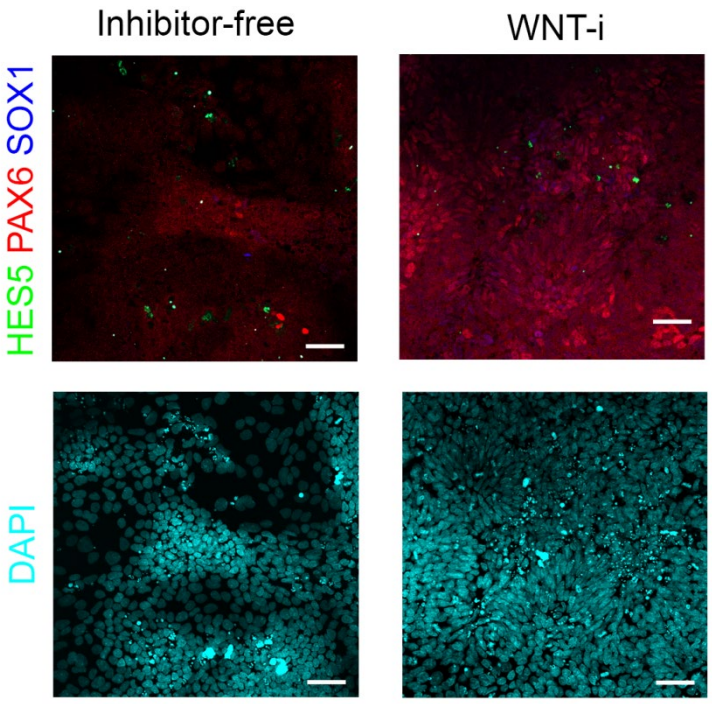

Figure 18: Poor neural induction achieved under inhibitor-free and WNT-i monolayer conditions Combined HES5::eGFP reporter expression and immunostaining of the early neuroepithelial markers PAX6 and SOX1 (top) along with their matched DAPI images (bottom) in day 12 neural progenitors derived under Inhibitor-free (Inhibitor-free) and WNT inhibition using XAV939 (WNT-i). See Figure 18 for images taken for other treatments. Scale bar: 50 µm.

On the other hand, both PAX6 and SOX1 markers were highly expressed under dual SMAD-i and Triple-i derived progenitors. However, only under Triple-i they were homogeneously expressed throughout cultures, co-localized with HES5::eGFP, and coincided with efficient radial organization (Figure 19).

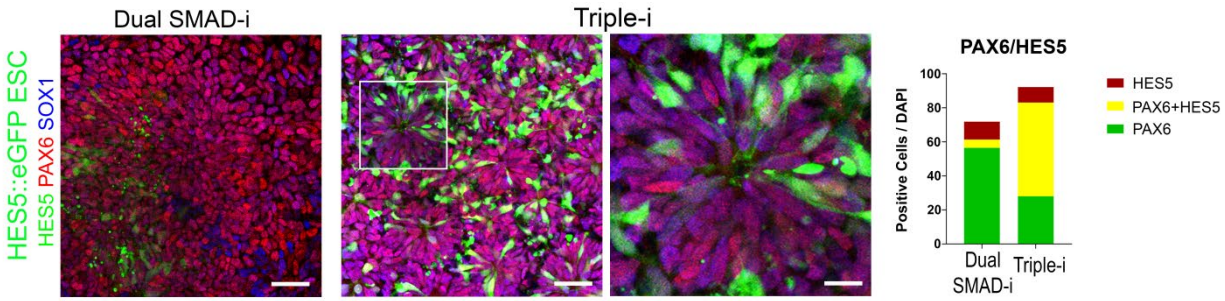

Figure 19: Enhanced Notch activation and efficient radial organization co-localize with neuroepithelial markers in monolayers derived by combined inhibition. Immunostaining of PAX6 and SOX1 with respect to Notch activation (HES5::eGFP) and radial organization in day 12 monolayer neural progenitors derived by indicated treatments. The right image represents a magnified rosette from Triple-i derived progenitors. Scale bar: 50 µm. Note the dramatic shift in marker co-localization together with radial organization under Triple-i. Cell counts and co-localization analysis of markers are presented at the right panel. Note the increased co-localization of PAX6 with HES5::eGFP under Triple-i.

When tested in 3D organoids, early neuroepithelial markers SOX2, PAX6 and SOX1 were comparably expressed under all treatments, again emphasizing ability of organoids to self-induce and maintain neural fates regardless of pathway inhibition. However only under Triple-i – both expression and co-localization of these markers with Notch activation and radial organization was observed (Figure 20A, D). The expression of basal progenitor marker TBR2 and early neuronal marker TBR1 is also comparable under all treatments (Figure 20A). All these results were also confirmed for another human iPSCs (ZIP8K8) derived organoids (Figure 20B). Together with the molecular cortical cell identity revealed in Triple-i conditions (Figure 12), our observations argue that even when markers such as SOX2, PAX6, SOX1 and HES5 are expressed in PSC derived neural cells, it is their co-localization with each other and their overlap with radial organization which together mark cortical cell fate.

To further correlate the process of radial organization and Notch activation to the cortical specification obtained by Triple-i, we looked at the expression of telencephalic/cortical marker FOXG1. In monolayer cultures, this telencephalic marker was upregulated in both dual SMAD-i and Triple-i conditions (Figure 20D), in line with our own observations [119, 127, 146], with observations from the same group [121, 125, 126] as well as others [188]. But only under Tripe-i, this marker was expressed in nearly all neuroepithelial cells, where it also coincided with radial organization and Notch activation (Figure 20C). Organoids derived by Triple-i also exhibited expression of FOXG1 in radially organized regions (vesicle areas) together with Notch activation (Figure 20D), demarcating them as telencephalic/cortical in nature. However, FOXG1 was only partially expressed under inhibitor-free conditions and was completely absent under dual SMAD-i conditions. The lack of FOXG1 in organoids under dual SMAD-i indicated that in the absence of WNT inhibition, self-organizing structures are inherently predisposed towards non-telencephalic fates, while 2D systems exhibit both telencephalic and non-telencephalic cell types.

Finally, we linked Notch activation and radial organization to cortical specification by looking at the expression pattern of PAX6 and EMX2. Within the cortex, PAX6 and EMX2 are expressed rostrally and caudally but share large co-expression regions dorsally [189]. Yet, these markers cannot be simply interpreted as cortical markers as they are also expressed in thalamic regions of the diencephalon as well as in the

hippocampus [190]. Indeed, we found that in both monolayers and organoids expression of PAX6 and EMX2 was induced under both dual SMAD-i and Triple-i (Figure 20C, D). These results were also confirmed for another human iPSCs (ZIP8K8) derived organoids (Figure 20E). However, because most progenitors derived by Triple-i express FOXG1, then such FOXG1+/PAX6+/EMX2+ (Figure 21A) expressing cells seen under Triple-i must represent dorsal cortex progenitors. Compatible with this interpretation, also PAX6 and EMX2 expressing cells were co-localized with radially organized Notch active cells under Triple-i conditions only, providing evidence that enhanced Notch activation coinciding with radial organization are exclusive hallmarks of PSC transition towards cortical fates, rather than towards general CNS or forebrain fates – in a process that requires combined dual SMAD and WNT inhibition.

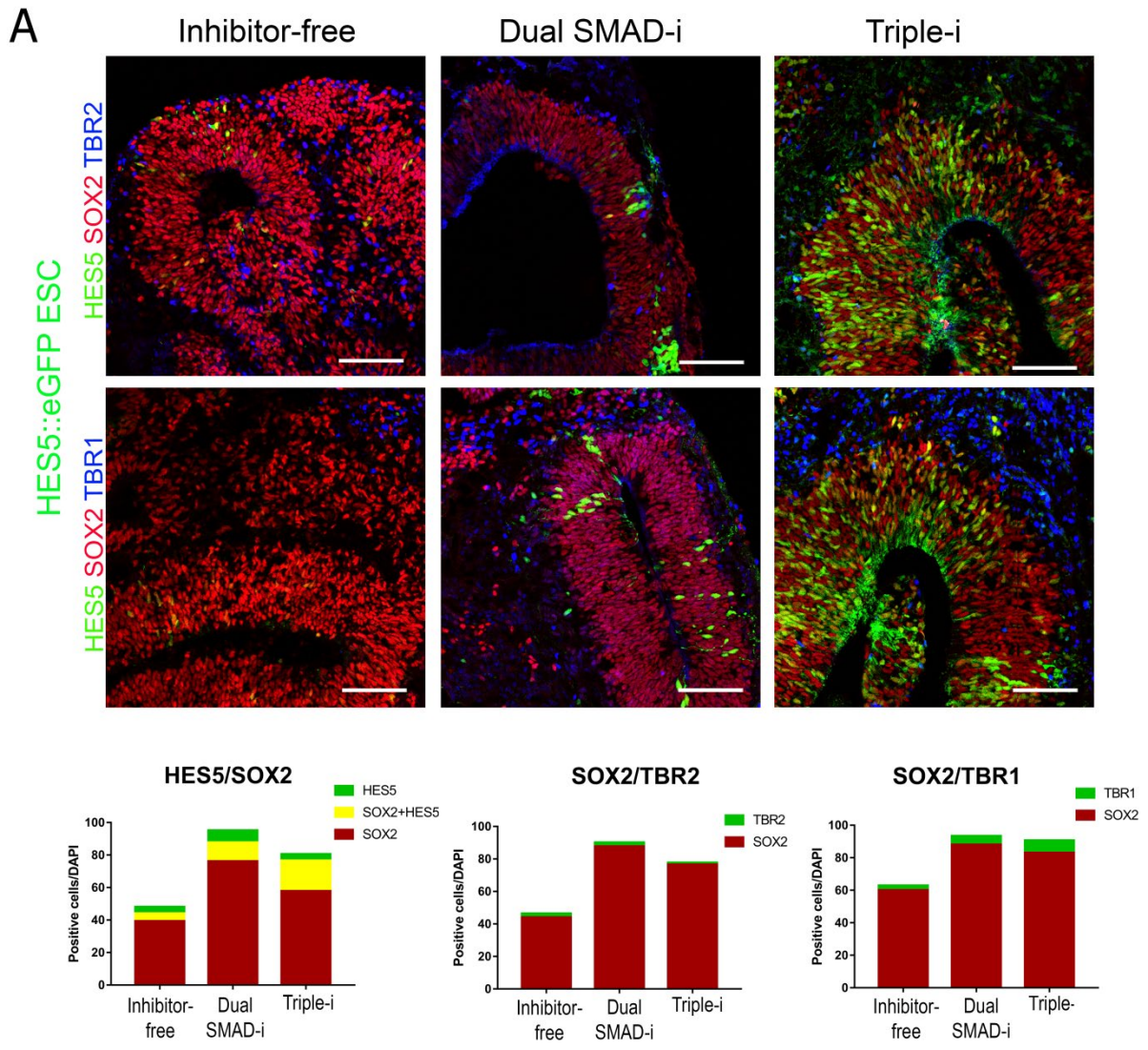

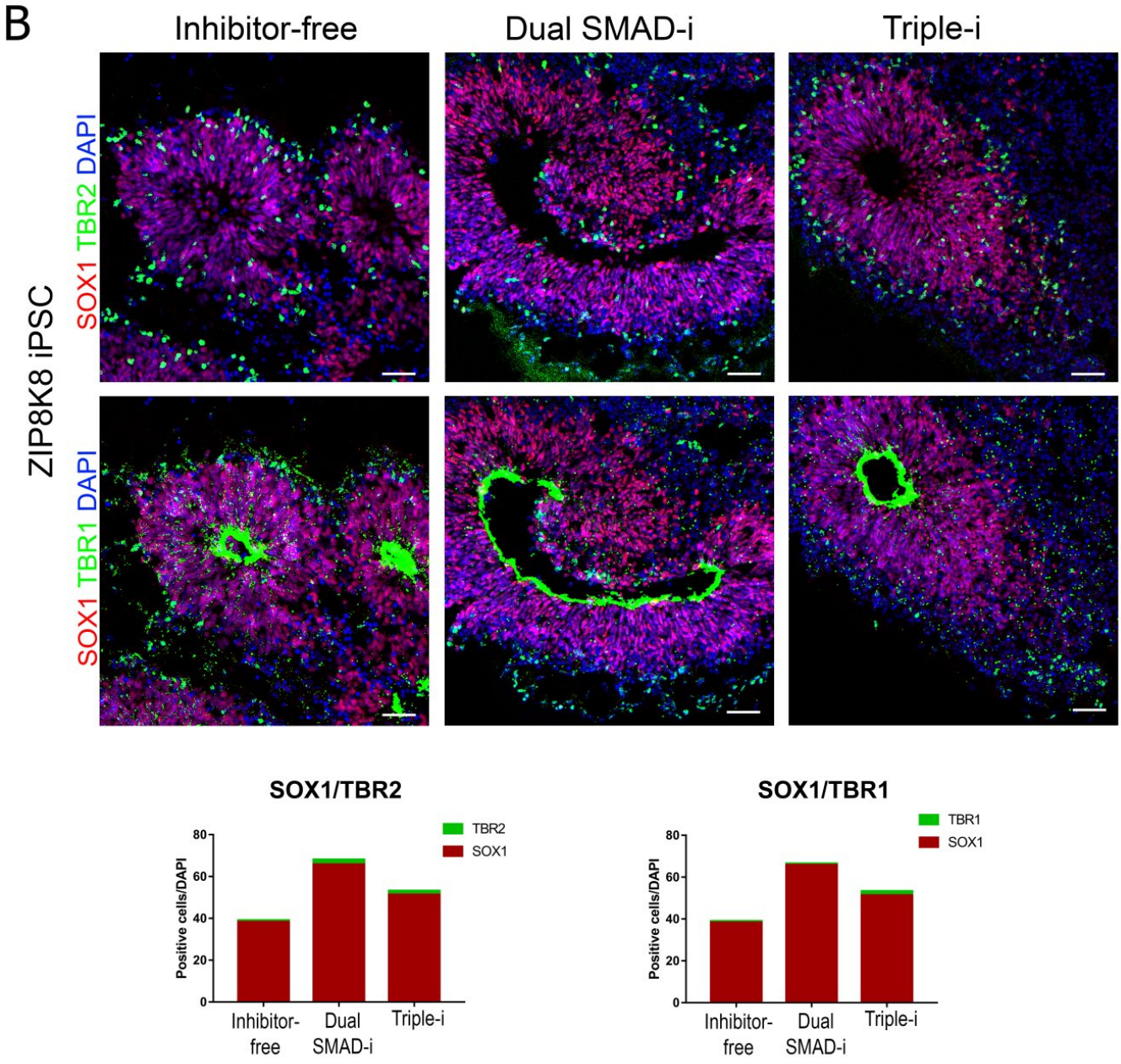
B
Inhibitor-free
Dual SMAD-i
Triple-i
ZIP8K8 iPSC
SOX1 TBR2 DAPI
SOX1 TBR1 DAPI
SOX1/TBR2
TBR2
SOX1
Positive cells/DAPI
80
60
40
20
0
Inhibitor-free
Dual SMAD-i
Triple-i
SOX1/TBR1
TBR1
SOX1
Positive cells/DAPI
80
60
40
20
0
Inhibitor-free
Dual SMAD-i
Triple-i

C

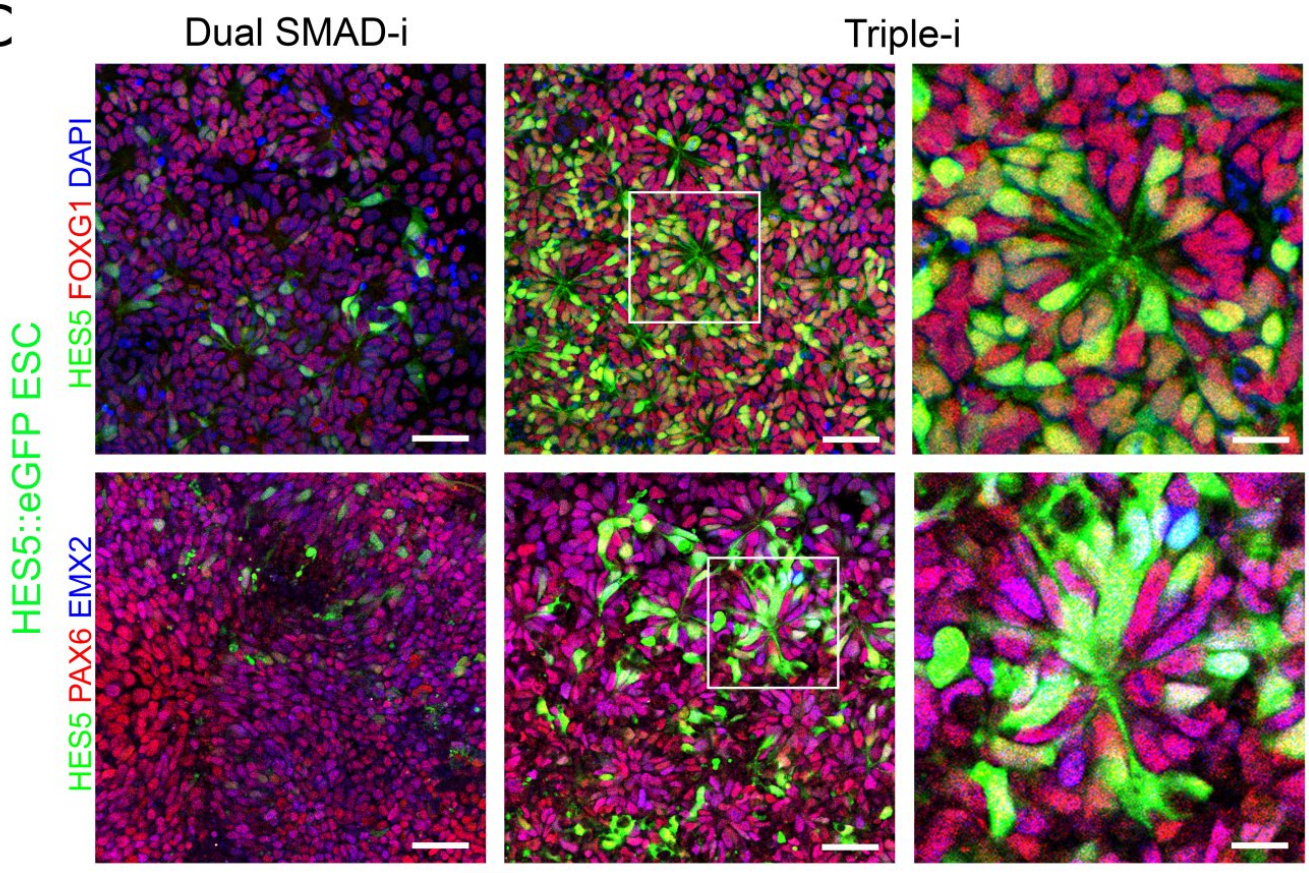
Dual SMAD-i
Triple-i
HES5::eGFP ESC
HES5 FOXG1 DAPI
HES5 PAX6 EMX2

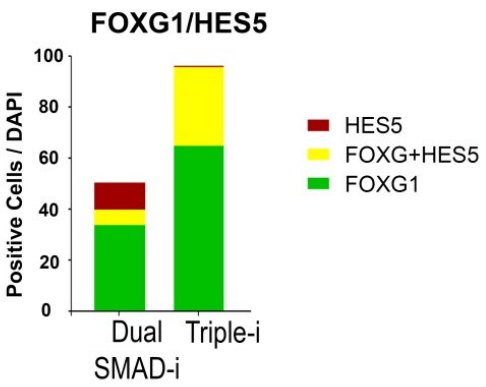
FOXG1/HES5
Positive Cells / DAPI
100
80
60
40
20
0
Dual SMAD-i
Triple-i
HES5
FOXG+HES5
FOXG1

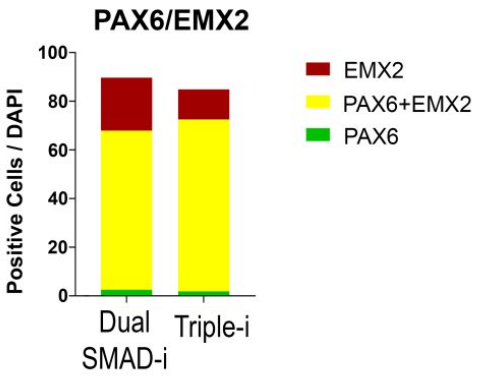
PAX6/EMX2
Positive Cells / DAPI
100
80
60
40
20
0
Dual SMAD-i
Triple-i
EMX2
PAX6+EMX2
PAX6

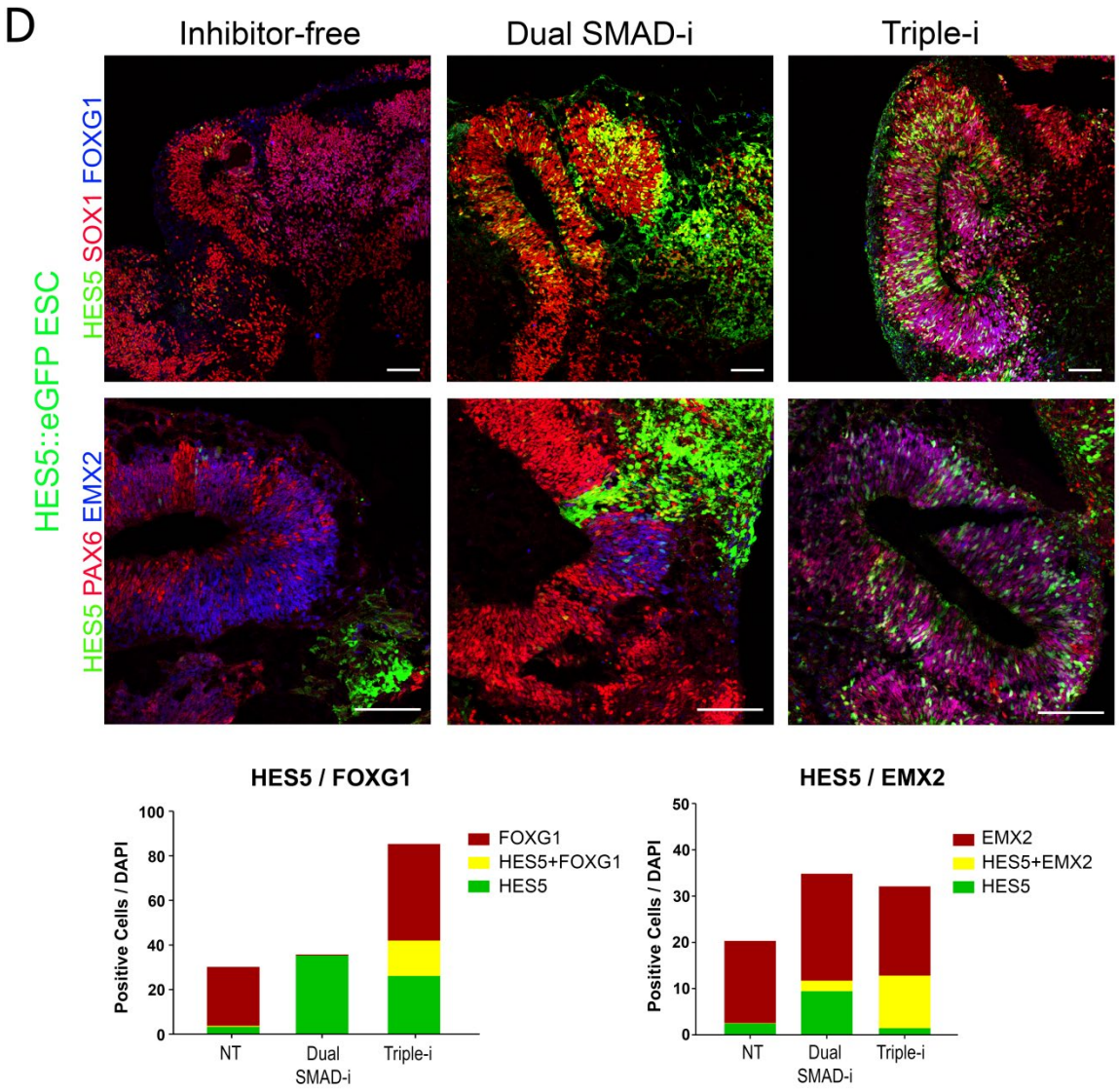
D
Inhibitor-free
Dual SMAD-i
Triple-i
HES5::eGFP ESC
HES5 SOX1 FOXG1
HES5 PAX6 EMX2
HES5 / FOXG1
Positive Cells / DAPI
100
80
60
40
20
0
NT
Dual SMAD-i
Triple-i
FOXG1
HES5+FOXG1
HES5
HES5 / EMX2
Positive Cells / DAPI
50
40
30
20
10
0
NT
Dual SMAD-i
Triple-i
EMX2
HES5+EMX2
HES5

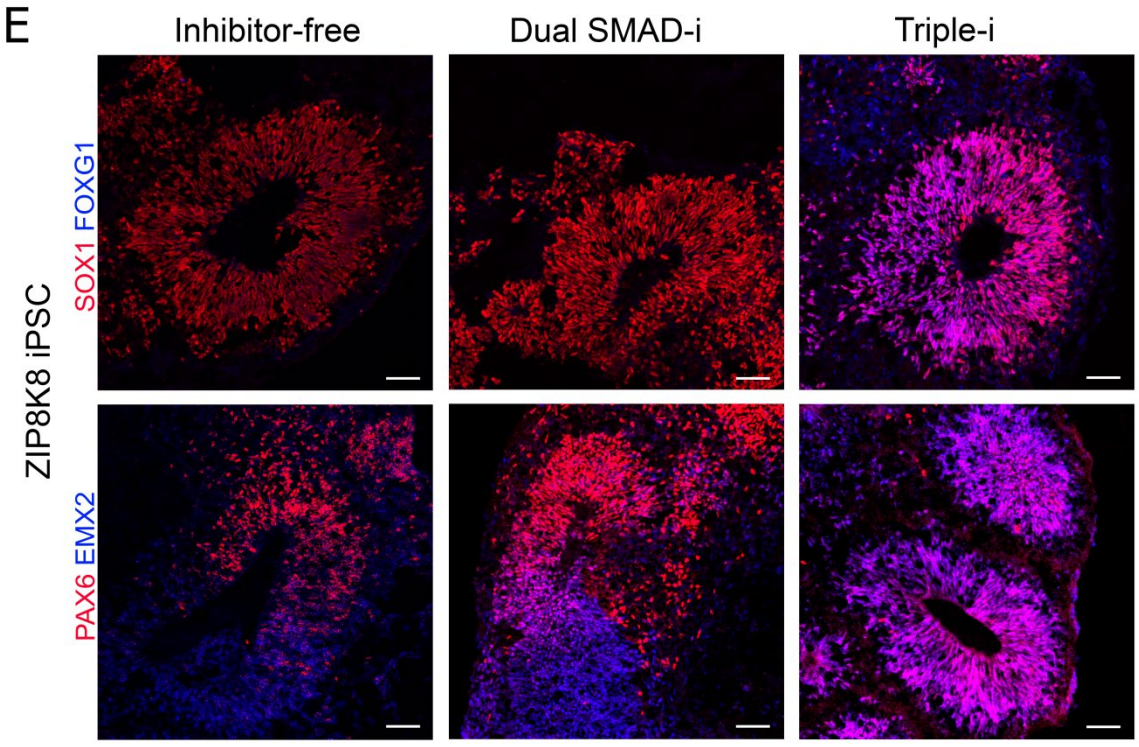
E
Inhibitor-free
Dual SMAD-i
Triple-i
ZIP8K8 iPSC
SOX1 FOXG1
PAX6 EMX2

Figure 20: Enhanced Notch activation and efficient radial organization co-localize with cortical markers in monolayers and organoids derived by combined inhibition.

A. Immunostaining images of SOX2/TBR2 (top) and SOX2/TBR1 (middle), with respect to Notch activation (HES5::eGFP) and radial organization in day 30 organoids derived from HES5::eGFP hESCs under indicated treatments. Note dramatic Notch activation and neural stem cell marker (SOX2) co-localization together with radial organization under Triple-i. Intermediate progenitor marker (TBR2) and deep cortical layer neuronal marker (TBR1) emerges at basal sites of radially organized vesicles in all treatments. Cell counts and co-localization analysis of HES5::eGFP expression and indicated markers are presented at the bottom. Scale bar: 100 μm.

B. Immunostaining images of SOX1/TBR2 (top) and SOX1/TBR1 (middle), with respect to radial organization in day 30 organoids derived from ZIP8K8 iPSCs under indicated treatments. Cell counts of indicated markers are presented at the bottom. Scale bar: 100 μm.

C. Immunostaining images of FOXG1 (top) and PAX6/EMX2 (middle) with respect to Notch activation (HES5::eGFP) and radial organization in day 12 monolayer neural progenitors derived by indicated treatments. The right image represents a magnified rosette from Triple-i derived progenitors. Note the dramatic shift in marker co-localization with Notch coincided with radial organization under Triple-i. Cell counts and co-localization analysis of markers are presented at the right panel. Note the increased co-localization of PAX6 and FOXG1 with HES5::eGFP under Triple-i. Scale bar: 50 μm.

D. Immunostaining images of SOX1/FOXG1 (top) and PAX6/EMX2 (middle) with respect to Notch activation (HES5::eGFP) and radial organization in day 30 organoids derived from HES5::eGFP hESCs under indicated treatments. Cell counts and co-localization analysis of HES5::eGFP expression and indicated markers are presented at the bottom panel. Note the enhanced marker co-localization with Notch activation coincided with radial organization under Triple-i. Scale bar: 100 μm.

E. Immunostaining images of SOX1/FOXG1 (top) and PAX6/EMX2 (middle), with respect to radial organization in day 30 organoids derived from ZIP8K8 iPSCs under indicated treatments. Cell counts of indicated markers are presented in the Figure 21. Scale bar: 100 μm.

We then dissected the cortical areal homogeneity (Figure 21A) of Triple-i derived 2D monolayer progenitors and whole 3D organoids by immunostainings of concerned marker gene expression. While EMX2 is expressed in the cortex dorsally-medially with slight bias caudally, SP8 is an additional marker expressed in the cortex dorso-medially with a bias rostrally. We therefore further characterized cortical progenitors derived by Triple-i by assessing the expression and co-localization of these markers with respect to PAX6 (Figure 21B, C). To better quantify expression proportions, here we performed acute rosette dissociation, fixing and staining, hence the lack of rosette structures. Cells derived by Triple-i abundantly expressed EMX2 (59%) or SP8 (86%), out of which percentages 78% and 69% co-expressed PAX6, respectively (Figure 21B), supporting for dorsal cortical identity. This remarkable

abundance and co-localization of dorsal-medial-caudal (EMX2) and dorsal-medial-rostral (SP8) markers with PAX6 under Triple-i suggested that this treatment mainly induced a pan dorsal-medial cortical identity. This is further supported by the expression of OTX2 and COUP-TF1. In the telencephalon, these markers are expressed only ventrally and laterally, respectively, but not dorsally. Indeed, both markers were poorly expressed in Triple-i derived progenitors (Figure 21B), supporting the presence of dorsal identity. Keeping with these observations in 2D cultures, we confirmed the expression pattern of EMX2, PAX6, SP8 and COUP-TF1 in organoids derived from the same iPSCs (Figure 21C).

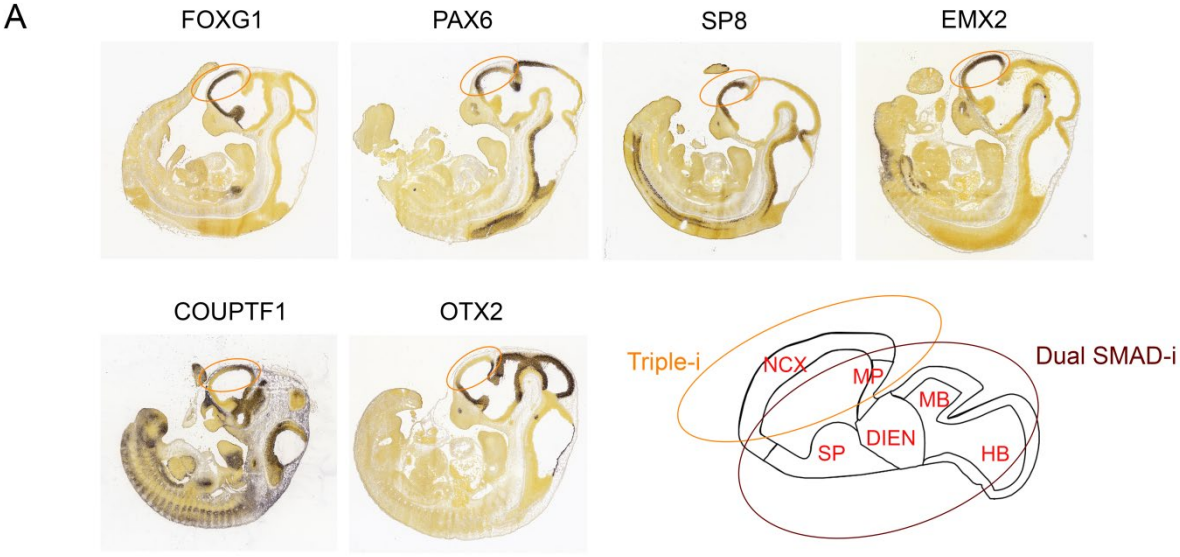
A
FOXG1
PAX6
SP8
EMX2
COUPTF1
OTX2
Triple-i
Dual SMAD-i
NCX
MP
MB
DIEN
SP
HB

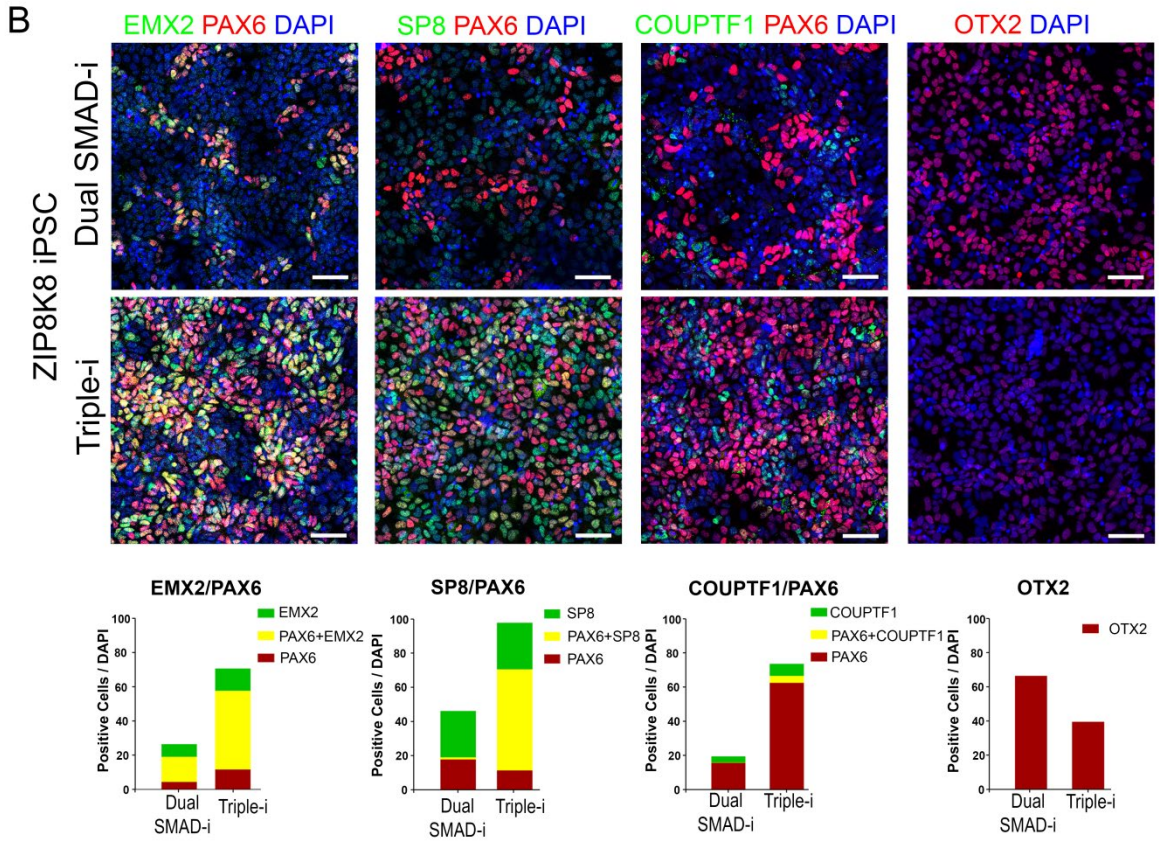
B
ZIP8K8 iPSC
Dual SMAD-i
Triple-i
EMX2 PAX6 DAPI
SP8 PAX6 DAPI
COUPTF1 PAX6 DAPI
OTX2 DAPI
EMX2/PAX6
SP8/PAX6
COUPTF1/PAX6
OTX2
Positive Cells / DAPI
EMX2
PAX6+EMX2
PAX6
SP8
PAX6+SP8
COUPTF1
PAX6+COUPTF1
Dual SMAD-i
Triple-i

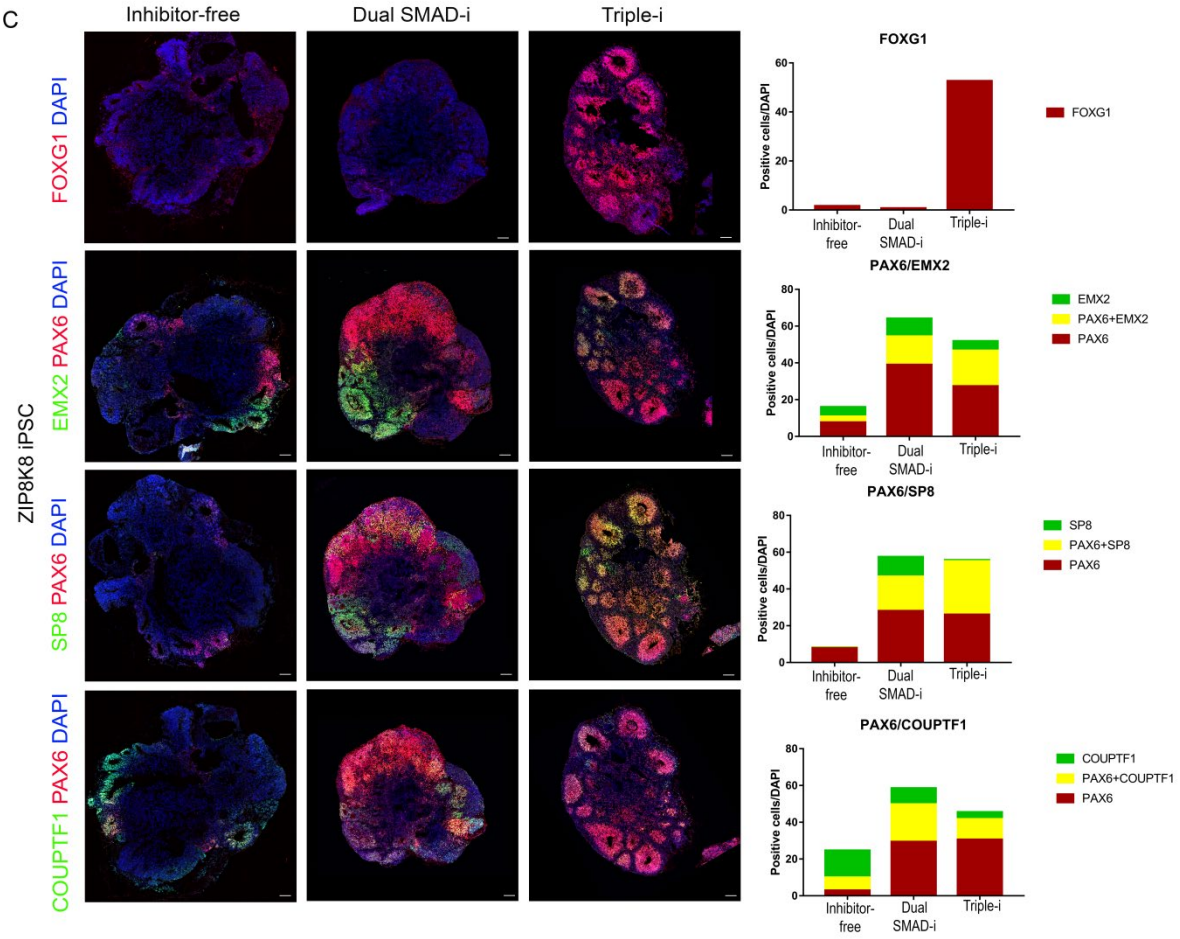

Figure 21: Enriched dorsal cortical fate derivation under combined inhibition.

A. Mouse In-situ hybridization images of Foxg1, Pax6, Sp8, Emx2, Coup-Tf1 and Otx2 obtained from Allen Brain Atlas and illustration depicting regions induced by mentioned treatments. Cortical progenitors entail unique co-expression of all indicated markers (except Otx2 and Coup-Tf1) in discrete as well as shared regions confined within the dorsal telencephalic domain. NCX- Neocortex, MP-Medial pallium, SP-Sub pallium, DIEN-Diencephalon, MB-Midbrain and HB-Hindbrain.

B. Immunostainings of EMX2, SP8 and COUP-TF1 with respect to PAX6, as well as of OTX2, in day 12 dissociated rosette progenitors derived from ZIP8K8 iPSCs by indicated treatments. Cell counts and co-localization analysis are presented at the bottom panel. Scale bar: 50 µm. Note increased co-localization of EMX2 and SP8 with PAX6, as well as reduced OTX2 expression, under Triple-i.

C. Immunostainings of EMX2, SP8 and COUP-TF1 with respect to PAX6, as well as of FOXG1, in day 27 organoids derived from ZIP8K8 iPSCs by indicated treatments. Cell counts and co-localization analysis are presented in the right panel. Note the exclusive expression of FOXG1, as well as increased co-localization of EMX2 and SP8 with PAX6, under Triple-i. Scale bar: 100 µm.

As the current known cortical markers expression is not unambiguous for identifying cortical cell types, we next looked for the expression of novel genes that were enriched in cortical regions and also in non-cortical regions (medial pallium, diencephalon and cerebellum) of Allen human brain regional transcriptional dataset and our organoid transcriptional dataset derived under different treatments (Figure 14) and validated by immunostainings (Figure 22). We confirmed the expression of a novel cortical neuronal marker TIAM2 basally to SOX2 positive vesicles only in the Triple-i generated organoids. MEF2C was another novel cortical marker enriched in Triple-i organoids that was expressed in both VZ progenitors co-localizing with SOX2 and neurons co-localizing with DCX basally to the vesicles. We next also confirmed the expression of non-cortical thalamic markers such as OLIG3 and TCF7L2 and medial pallium/choroid plexus markers such as LMX1A and TTR specific to the organoids generated by Inhibitor-free and dual SMAD-i (Figure 22).

Finally, we confirmed the lack of ventral specification in the absence of WNT by testing the expression of the ventral markers NKX2.1 and NKX2.2 in organoids. We found that these markers were observed in inhibitor-free and dual SMAD-i derived organoids, but not in Triple-i derived organoids (Figure 23A). In accordance, the inhibitory neuronal marker GAD65 was attenuated in Triple-i derived organoids (Figure 23B). Together these results show that combined inhibition is indispensable for obtaining cortical specification.

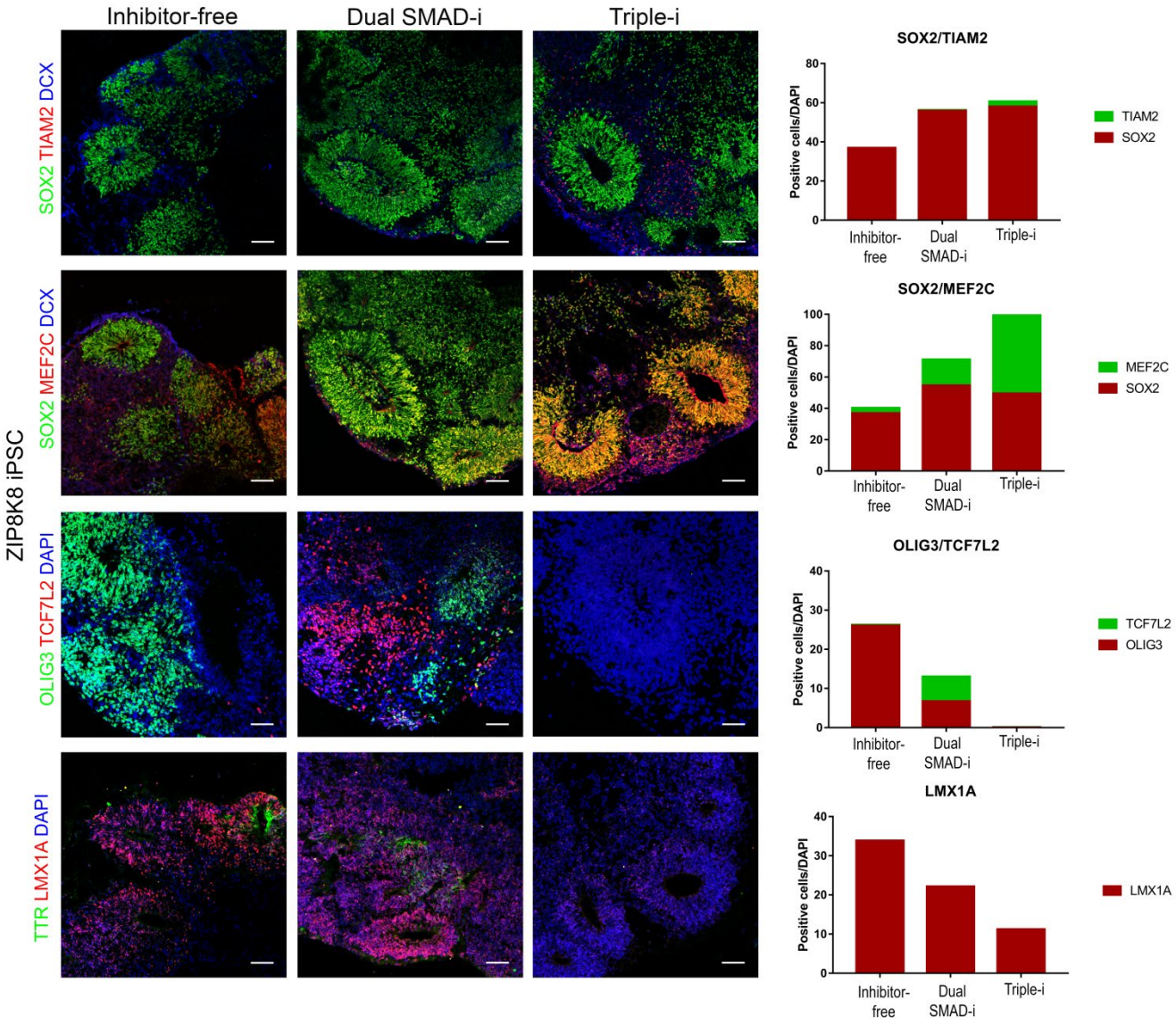

Figure 22: Expression of novel cortical and non-cortical genes in organoids derived under diverse inhibition paradigms

Immunostainings of cortical markers TIAM2, MEF2C with respect to neural stem cell marker SOX2 and neuronal marker DCX and non-cortical markers OLIG3/TCF7L2 (diencephalic markers), TTR/LMX1A (medial pallium markers) in day 27 ZIP8K8 iPSCs organoids derived under indicated treatments. Cell counts analyses are presented at the right panel. Scale bar: 100 µm. Note enrichment of cortical markers in Triple-i generated organoids and non-cortical markers in dual SMAD-i and inhibitor free generated organoids.

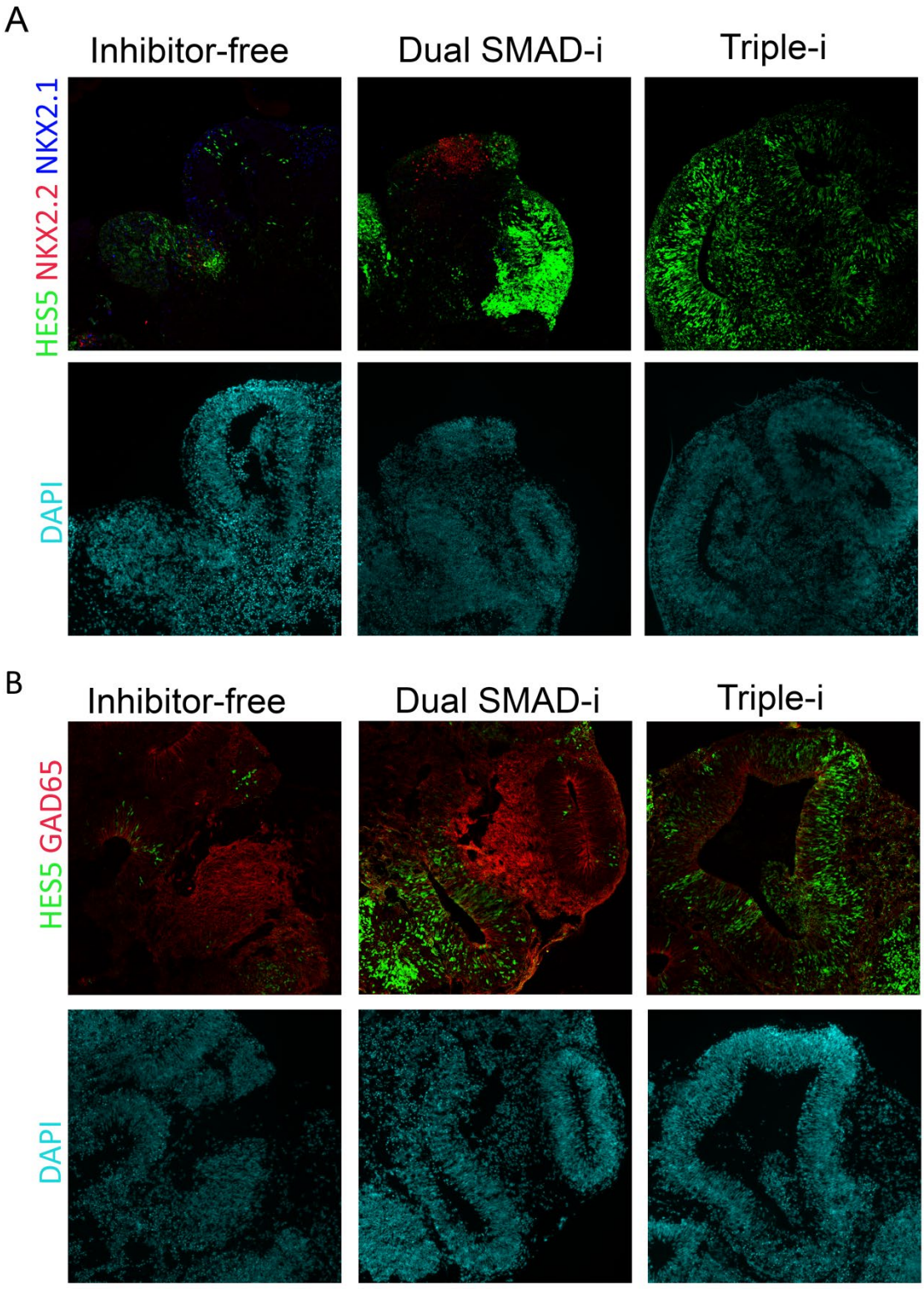

Figure 23: Decreased ventral patterning in Triple-i derived organoids.

A. Combined HES5::eGFP reporter expression and immunostaining for the ventral markers NKX2.1 and NKX2.2 in day 30 organoids derived under indicated treatments. Note lack of expression under Triple-i. Scale bar: 100 µm.

B. Combined HES5::eGFP reporter expression and immunostaining of the GABAergic neuronal marker GAD65 in day 30 organoids derived under indicated treatments. Expression of GAD65 is attenuated in Triple-i organoids. Scale bar: 100 µm.

3.4 Combined dual SMAD and WNT inhibition allows standardized modeling of microcephaly

Our study demonstrates that current derivation methods for cortical fates yield in fact heterogeneous cell populations with distinct identities both molecularly and cellularly, and further argues that only combined dual SMAD and WNT inhibition reproduces neocortical fares. This conclusions postulate that iPSC-based cortical disease modeling systems relying on diverse methods will essentially provide distinct phenotypes. To provide a proof of concept to this idea, we generated a homozygous microcephaly mutation in the same isogenic *HES5::eGFP* human ESC line by Crispr/Cas9 technology. This mutation was generated by a Guanine deletion in 1218 amino acid position of the centriolar gene *STIL,* resulting in a truncated protein (Figure 24) known to eventually cause autosomal recessive microcephaly in humans [152].

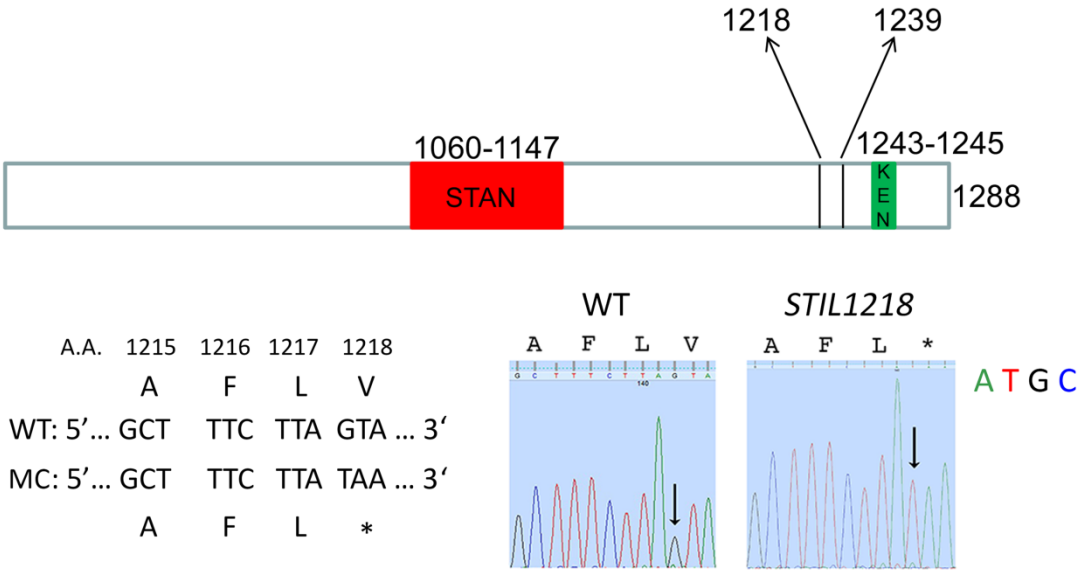

Figure 24: General description on microcephaly mutant cell line.

Description of the STIL protein including the STAN and KEN domains, as well as microcephaly mutations (top). Normal (WT) and planned mutated (STIL) nucleotide sequence adjacent to the region corresponding to the 1218a.a (bottom left). Genome edited sequencing results (bottom right). A-alanine, F-phenylalanine, L-leucine, V-valine and *- stop codon.

We first assessed general microcephaly features in our *STIL* mutated organoids with respect to treatments. Microcephaly organoid size was significantly smaller than that

of WT organoids only when derived by Triple-i (Figure 25), suggesting profound reduction in cortical size compared to non-significant reduction in other brain regions.

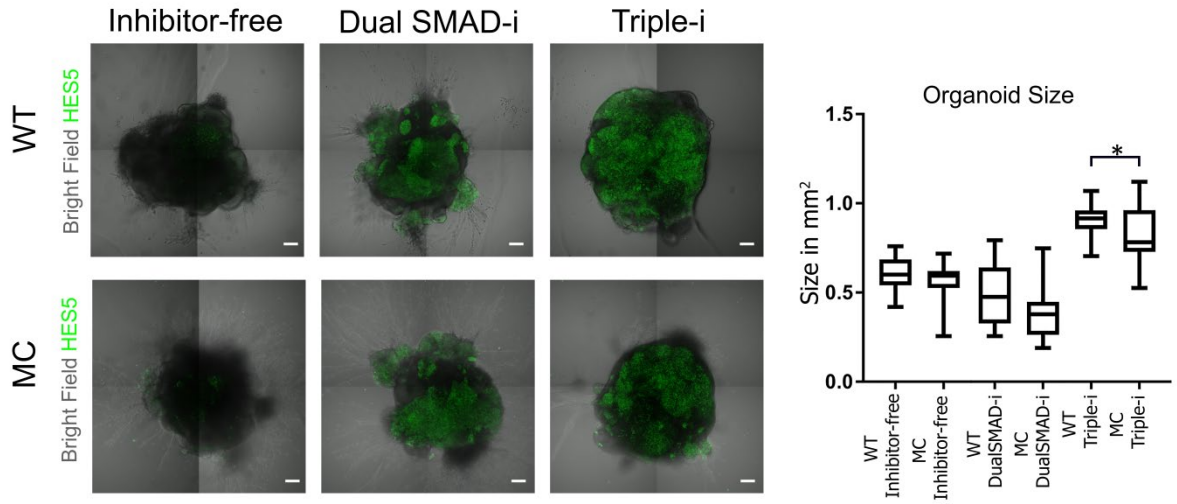

Figure 25: Microcephaly organoids derived under combined inhibition show significant size reduction compared to their wildtype counterparts.

Merged bright field images and their matched HES5::eGFP confocal images obtained from day 17 representative organoids derived from wildtype (WT) or microcephaly (MC) mutant hESCs under indicated treatments. Shown is maximum intensity projection of HES5::eGFP confocal images obtained at 6µm intervals across each organoid. Scale bar: 100 µm. Right: Boxplots representing organoid size obtained from multiple organoids determined by measuring areas of collapsed maximum intensity projection images obtained from day 17 WT and MC mutant organoids derived by different treatments (N>12 for each treatment). MC mutant organoids are significantly smaller than their WT counterparts only if derived by Triple-i. Statistics: Boxplots represent median and interquartile ranges. Statistical test: t-test; *P < 0.05; **P < 0.01 ***P < 0.001; ****P < 0.0001.

In addition, we observed an increase in differentiation compared to proliferation in day 20 organoids based on DCX and SOX2 area thickness ratios (Figure 26A), but this feature was not unique to cortical tissues as it appeared in other derivation methods as well. We also assessed vesicle growth by measuring the net neuroepithelial (vesicle) areas as well as outer and inner lumen perimeters and found significant reduction in both measures in microcephaly organoids (Figure 26B). However, also this reduction was not cortex specific as it occurred in both dual SMAD-i and Triple-i derived organoids. These results suggested that compromised size was caused by loss in progenitor pools, yet not necessarily due to cortex

specific cell loss. We further found that the number of P-VIM+ dividing radial glial cells captured along ventricular linings of microcephaly vesicles was higher compared to those observed for WT vesicles (Figure 26C). This suggested a possible mitotic arrest that could naturally occur in any brain region due to impaired centrosome biogenesis (for Review See [191]. Indeed, on day 30 it was already obvious that ventricular linings were ruptured and contained clustered centrosomes and poor co-localized cilia at basal bodies (Figure 26D). In addition, centrosomes appeared larger in size, reflective of potential centrosome clustering due to excess centrosome duplication, in line with previous studies [165, 192]. Collectively, these results suggested an overall impairment in developmental programs related to all brain regions, hence cannot be advantageously modelled by one derivation method.

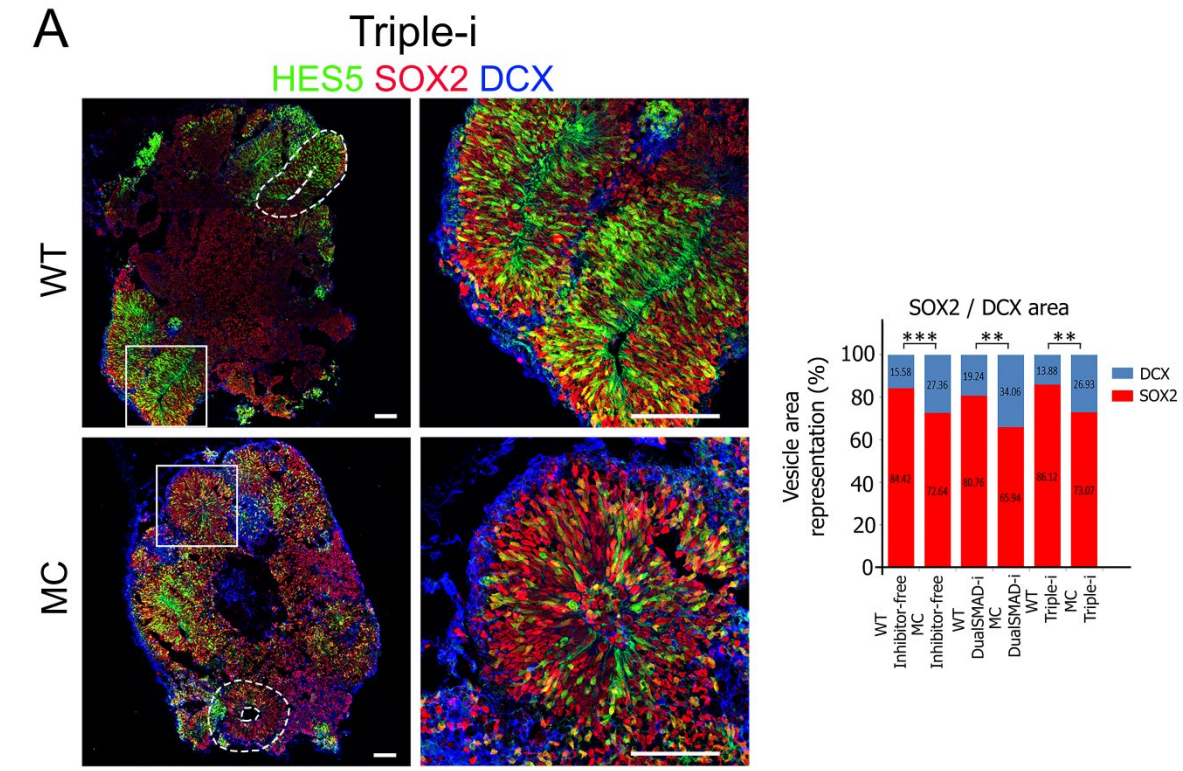

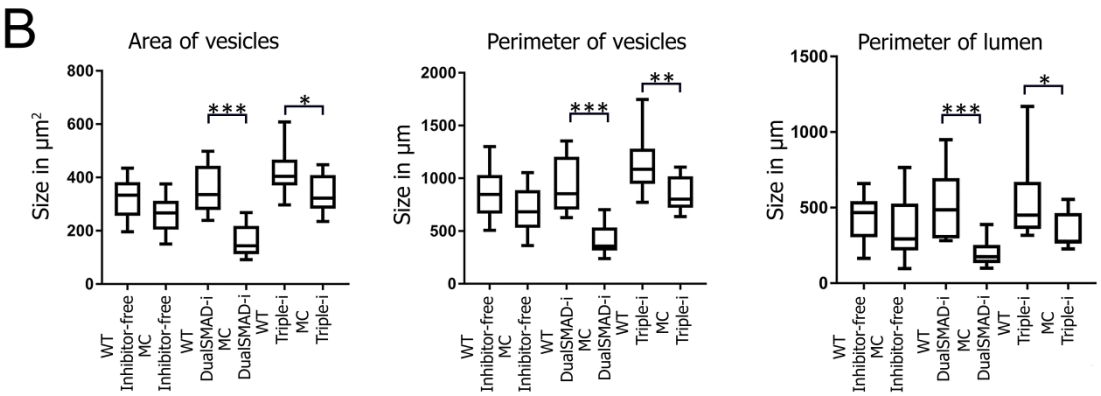

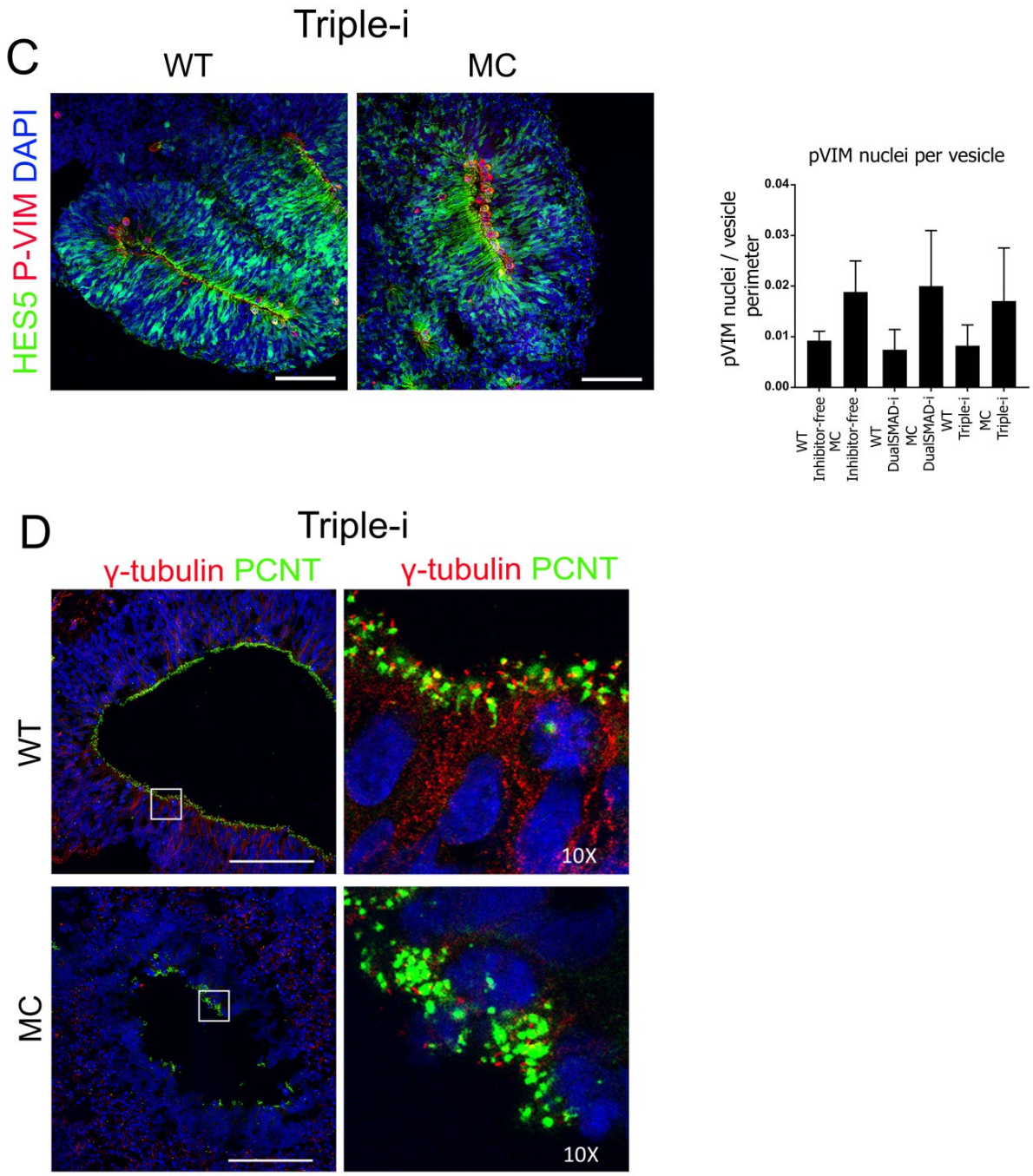

Figure 26: Differential phenotypic modeling of microcephaly in organoids derived by diverse pathway inhibition paradigms.

A. Combined HES5::eGFP expression and immunostaining images for the neural progenitor marker SOX2 and the early neuronal marker DCX in day 20 WT and MC mutant organoids derived under Triple-i conditions. Four-fold magnifications of regions in left images are shown on the right. Quantification of SOX2 and DCX area proportions within vesicles obtained WT or MC organoids derived by indicated treatments. Scale bar: 100 µm. Statistics: Stacked columns represent relative

SOX2 (red) and DCX (blue) expression within selected areas from WT and mutant vesicles. Statistical test: t-test; *P < 0.05; **P < 0.01 ***P < 0.001; ****P < 0.0001.

B. Measurement of ventricular zone areas in WT and mutant organoids. Dashed lines in A mark representative ventricular zone-like areas and luminal areas within vesicles of day 20 WT and MC mutant organoids derived under Triple-i conditions. Boxplots represent measurements for ventricular and luminal areas of organoids derived by indicated treatments. Shown are data representative of at least 10 vesicles extracted from at least 5 representatives WT or MC organoids. Statistics: Boxplots represent median and interquartile range. Statistical test: t-test; *P < 0.05; **P < 0.01 ***P < 0.001; ****P < 0.0001.

C. Combined HES5::eGFP expression and immunostaining images for the dividing radial glial marker P-VIM along with their corresponding DAPI images for day 20 WT and MC mutant organoids derived under Triple-i conditions. Right: cell counts of luminal P-VIM in WT and MC organoids derived by indicated treatments.

D. Immunostaining of the centrosomal marker PERICENTRIN (PCNT) and the ciliary protein marker γ-TUBULIN in day 30 WT and MC organoids derived under Triple-i conditions. Ten-fold magnifications of regions within the left images are shown on the right. Note the ruptured morphology of apical lining as judged by non-continuous centrosome appearance. Note centrosome clustering and attenuated ciliary staining in mutant MC organoids.

3.4.1 Significant reduction in cortical gene expression and massive apoptosis in microcephaly organoids occurs only under combined inhibition

To gain a better insight into disease etiology, we performed RNA-Seq for day 17 and day 30 organoids carrying the homozygous 1218 *STIL* mutation and which were derived by the different protocols. We first integrated the resulting RNA-Seq analyses together with their WT counterparts into the same CA plot generated for Figure 12. We found that microcephaly organoids clustered with their WT counterparts, according to their derivation method. Notably however, day 30 Triple-i derived microcephaly organoids appeared most distally in the entire Triple-i derived organoid cluster, where they were interfacing with day 30 dual SMAD-i derived organoids (Figure 12). Since microcephaly organoids derived by Triple-i were smaller but did not become extinct in culture, these results imply that cortical structures derived under Triple-i were greatly diminished, yet some residual non-cortical fates that could still form under Triple-i remained intact.

Since these results implied that cortical fates were more susceptible than other fates in microcephaly, we looked at genes associated with regional specification throughout WT and microcephaly organoid development. We extracted from day 17

and 30 organoids expression values of gene categorized to groups with distinct regional signatures (neocortex, medial pallium, diencephalon, mid-hindbrain) and compared them across derivation methods and disease state (WT, microcephaly) (Figure 27A). We found that changes in gene expression distributions for the different regional signatures in day 17 organoids were not significant across treatments (Figure 27A), but became so after 30 days in culture, compatible with our global transcriptional analysis for day 30 organoids (Figure 12). The most dramatic differences on day 30 organoids were observed for cortical genes which were significantly reduced in microcephaly organoids generated only under Triple-i. This result strongly confirms the loss of cortical structures in microcephaly organoids generated under Triple-i. However, interestingly expression of posterior fate (diencephalon and mid/hindbrain) genes were upregulated in both Triple-i and inhibitor-free generated microcephaly organoids. This result indicates a major loss of cortical cells accompanying with the promotion of tissues posterior to cortex. Whereas microcephaly generated under dual SMAD-i treatment didn't show any significant changes from its wild type counterparts (Figure 27A). Collectively, these results show that microcephaly development culminates in major reduction of cortical fates and a modest elevation of posterior fates under Triple-i conditions.

To further support the differences observed in the gene expression of microcephaly organoids, we next employed a global gene set enrichment analysis of gene expression data sets generated from both wild type and microcephaly organoids across all treatments using ingenuity analyses. In support to the major loss of cortical gene expression in microcephaly organoids, we observed the downregulation of represented tissues like forebrain, telencephalon, and cerebral cortex in microcephaly organoids generated under all treatments, but much more pronounced in Triple-i generated organoids (Figure 27B). In accordance, we observed the downregulation of pathways related to cell cycle and notch signalling in d30 microcephaly organoids which could be the reason for cortical structures loss (Figure 27C). In addition, we have also observed an increase in neurogenesis in early day 17 microcephaly organoids (Figure 27C) which in turn is reflected in the SOX2/DCX immunostainings of microcephaly organoids (Figure 26A). These results suggest that the compromised size in microcephaly was caused by both the loss of progenitor pool (notch downregulation) accompanied with accelerated differentiation. In line

with the elevation of non-cortical fates in microcephaly organoids (Figure 27A), ingenuity analysis showed the upregulation of tissues such as formation of mesencephalon, eye and sensory system development along with upregulation of canonical pathways like PCP and Wnt/beta-catenin signalling under inhibition-free and Triple-i microcephaly organoids (Figure 27C). Interestingly, only dual SMAD-i microcephaly organoids showed matured neuronal phenotypes like upregulation of neuritogenesis, axonogenesis and canonical pathways such as CREB, glutamate and GABA receptor signalling. This could be resulting from the intact non-cortical structures generated under dual SMAD-i microcephaly organoids.

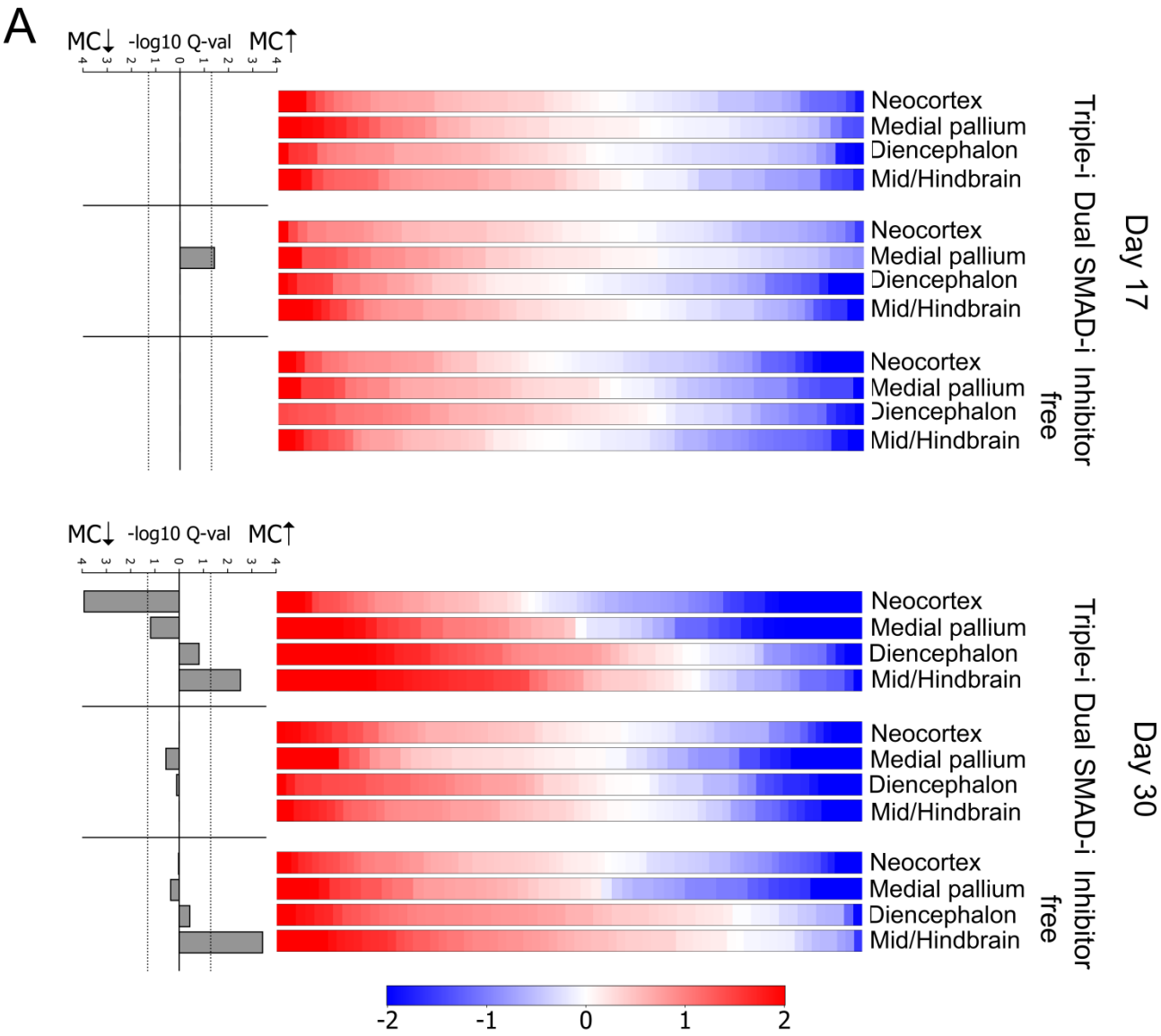

B

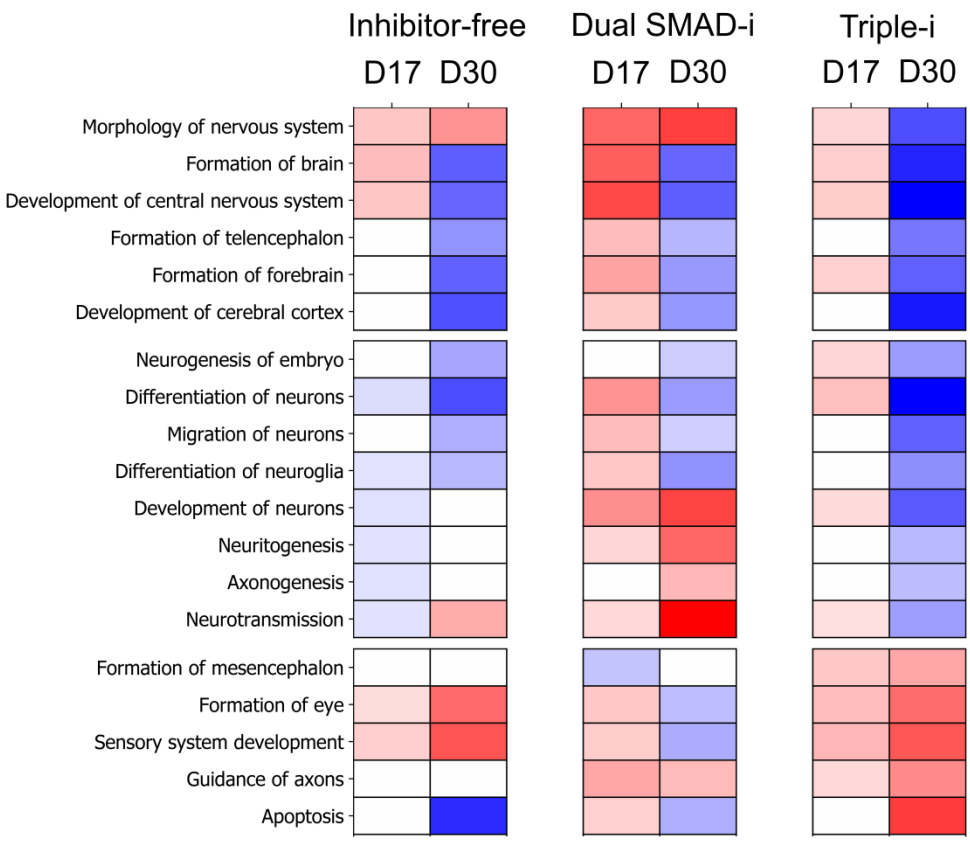
Inhibitor-free
Dual SMAD-i
Triple-i
D17 D30
D17 D30
D17 D30
Morphology of nervous system
Formation of brain
Development of central nervous system
Formation of telencephalon
Formation of forebrain
Development of cerebral cortex
Neurogenesis of embryo
Differentiation of neurons
Migration of neurons
Differentiation of neuroglia
Development of neurons
Neuritogenesis
Axonogenesis
Neurotransmission
Formation of mesencephalon
Formation of eye
Sensory system development
Guidance of axons
Apoptosis

C

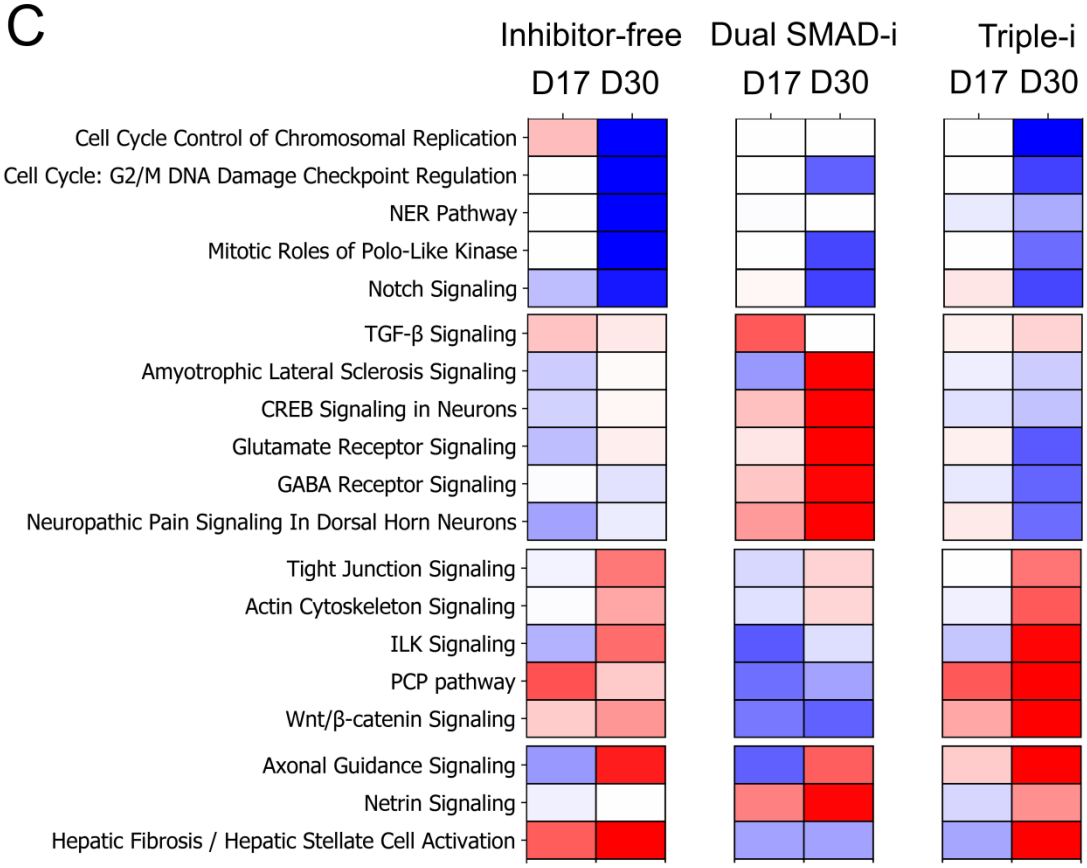
Inhibitor-free
Dual SMAD-i
Triple-i
D17 D30
D17 D30
D17 D30
Cell Cycle Control of Chromosomal Replication
Cell Cycle: G2/M DNA Damage Checkpoint Regulation
NER Pathway
Mitotic Roles of Polo-Like Kinase
Notch Signaling
TGF-β Signaling
Amyotrophic Lateral Sclerosis Signaling
CREB Signaling in Neurons
Glutamate Receptor Signaling
GABA Receptor Signaling
Neuropathic Pain Signaling In Dorsal Horn Neurons
Tight Junction Signaling
Actin Cytoskeleton Signaling
ILK Signaling
PCP pathway
Wnt/β-catenin Signaling
Axonal Guidance Signaling
Netrin Signaling
Hepatic Fibrosis / Hepatic Stellate Cell Activation

Figure 27: Differential molecular phenotypes of microcephaly organoids derived by diverse pathway inhibition paradigms.

A. Differential gene expression and gene set enrichment analysis (bar plot) of brain regions (neocortex, medial pallium, diencephalon and mid/hindbrain) for day 17 (top) and day 30 (bottom) WT vs MC organoids derived under indicated treatments. Note significant reduction in cortical gene expression in day 30 organoids derived under Triple-i condition only.

B. Tissues overrepresented in ingenuity gene enrichment analysis of differentially expressed genes for day 17 and day 30 WT vs MC organoids derived under indicated treatments.

C. Pathways overrepresented in ingenuity gene enrichment analysis of differentially expressed genes for day 17 and day 30 WT vs MC organoids derived under indicated treatments.

We have also observed an upregulation of apoptosis pathway in microcephaly organoids generated under Triple-i in gene enrichment analysis (Figure 27B) and therefore tested for apoptosis by immunostaining. We strikingly found that activated Caspase-3 was substantially expressed in Triple-i derived microcephaly organoids, but absent in inhibitor-free microcephaly organoids and only sparsely present in dual SMAD-i derived microcephaly organoids, demonstrating cortex-specific cell death (Figure 28). Remarkably, cell death under Triple-i was restricted to Notch active and radially organized regions. This finding suggested that execution of programmed cell death possibly initiated in apical radial glial neural stem cells (hence Notch active and radially organized cells) residing within the cortical ventricular zone. This further supported the fact that despite the fact that genetic centrosomal defects existed in all organoid cells, cortical progenitors were exclusively affected. Thus, together with our data on cortical specification under Triple-i, we conclude that combined inhibition is indispensable for precise modeling of microcephaly development.

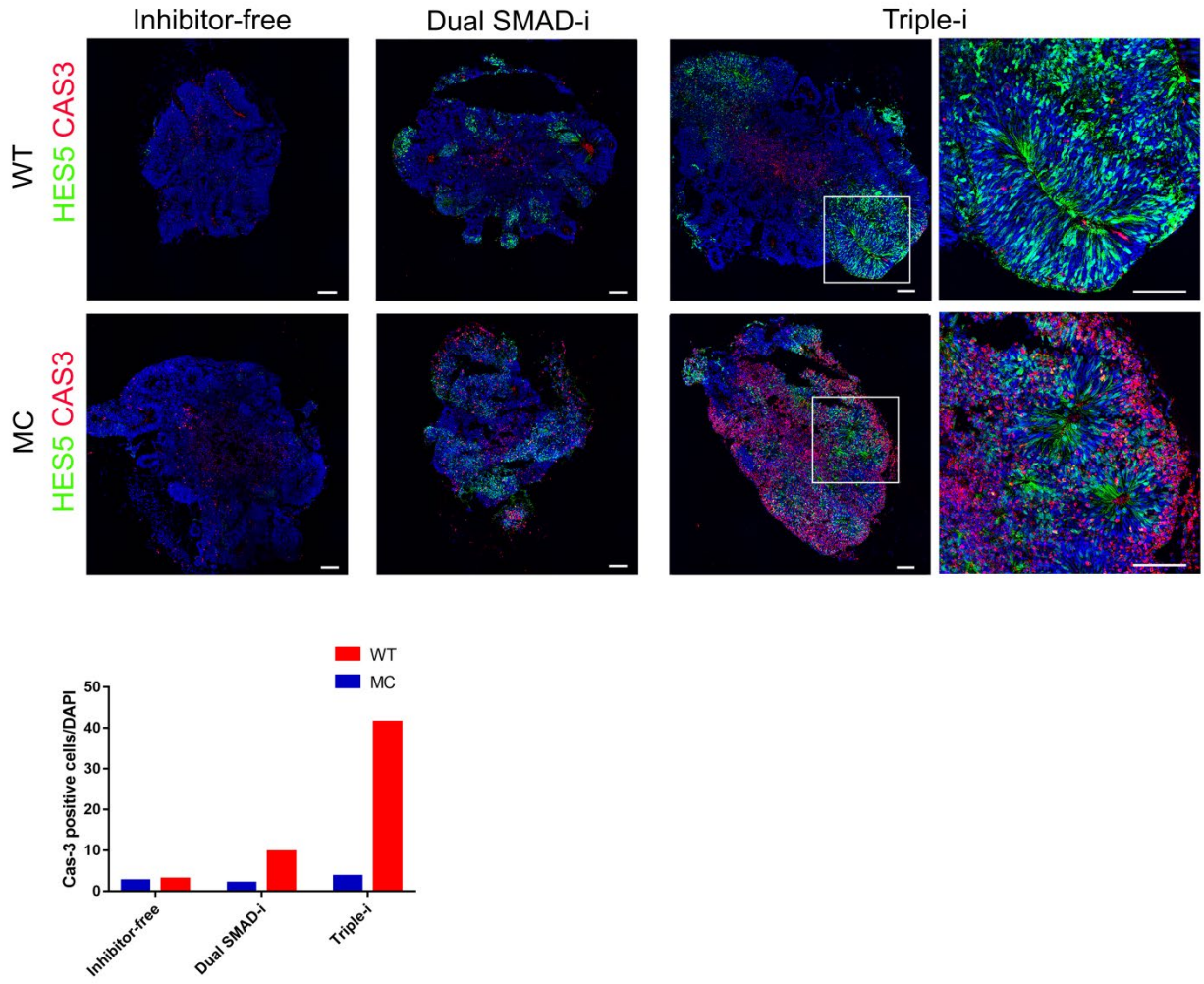

Figure 28: Microcephaly organoids show cortex specific death only when derived under combined inhibition.

Combined HES5::eGFP expression and immunostaining images of the apoptotic marker CAS-3 in day 20 WT and MC mutant organoids derived by indicated treatments. Three-fold magnification images for Triple-i derived organoids are shown on the right. Note the dramatic increase in CAS-3 expression adjacent to HES5::eGFP vesicles under Triple-i. Scale bar: 100 µm.

3.5 Single cell RNA Sequencing of organoids reveals enrichment for cortical fates in organoids derived by combined dual SMAD and WNT inhibition

We next did scRNA sequencing on mature organoids such as day 50 organoids to know about long term regional and differentiation capabilities of organoids generated under all treatments. The average number of genes detected per cell (1040 in Inhibitor-free, 1199 in dual SMAD-i, 1204 in Triple-i, and 1072 in WNT inhibition) were comparable in all treatments. To compare how different day 50 organoids from day 30 organoids in terms of brain regional specifications, we compared relative

expression levels of regional genes across organoids derived by these four different protocols in bulk RNA-Seq of day 30 organoids with scRNA-Seq of day 50 organoids (Figure 29A). We observed preservation of enriched cortical fates in organoids generated under Triple-i with no posterior fate contamination whereas in dual SMAD-i generated day 50 organoids preserved posterior fates along with a medium enrichment of cortical fates. Inhibitor-free organoids show poor and sporadic expression of both cortical and non-cortical gene expression.

We then employed a global gene set enrichment analysis on day 50 organoids simulated bulk RNA-Seq data generated by each treatment (Figure 29B). Overall top over represented tissues in each comparison reveal enriched cortical fates like telencephalon, neocortex in Triple-i, non-cortical fates like thalamic structures, midbrain structures and hindbrain in dual SMAD-i. While inhibitor-free is enriched for mesenchyma, ECM and neural retina fates.

We next looked in to differently expressed genes in stem cell domain (SOX2+HES5+) and neuronal domain (DCX+) cells generated under Triple-i and dual SMAD-i treatments (Figure 29C). We observed that the top 1000 genes that are upregulated under Triple-i condition in both stem cell and neuronal cells are cortical genes like FOXG1, LHX2, SFRP1, NFIA and NFIB whereas dual SMAD-i generated stem cell and neuronal cells are enriched for non-cortical genes like ZIC1, ZIC2, IRX2, PHOX2B and HOXB3.

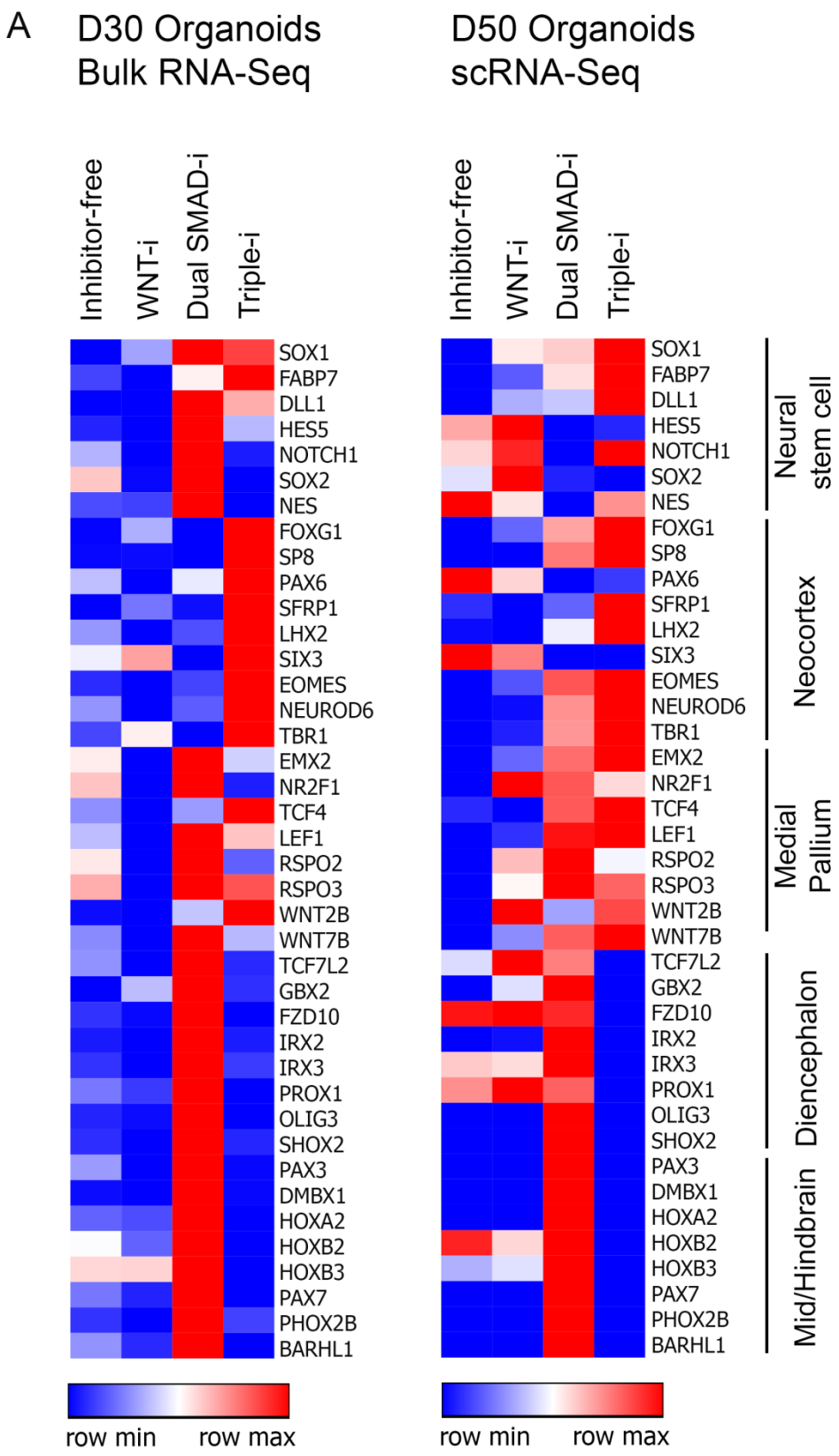
A
D30 Organoids
Bulk RNA-Seq
D50 Organoids
scRNA-Seq
Inhibitor-free
WNT-i
Dual SMAD-i
Triple-i
SOX1
FABP7
DLL1
HES5
NOTCH1
SOX2
NES
FOXG1
SP8
PAX6
SFRP1
LHX2
SIX3
EOMES
NEUROD6
TBR1
EMX2
NR2F1
TCF4
LEF1
RSPO2
RSPO3
WNT2B
WNT7B
TCF7L2
GBX2
FZD10
IRX2
IRX3
PROX1
OLIG3
SHOX2
PAX3
DMBX1
HOXA2
HOXB2
HOXB3
PAX7
PHOX2B
BARHL1
Neural stem cell
Neocortex
Medial Pallium
Diencephalon
Mid/Hindbrain
row min
row max

B

Enrichment analysis in D50 organoids

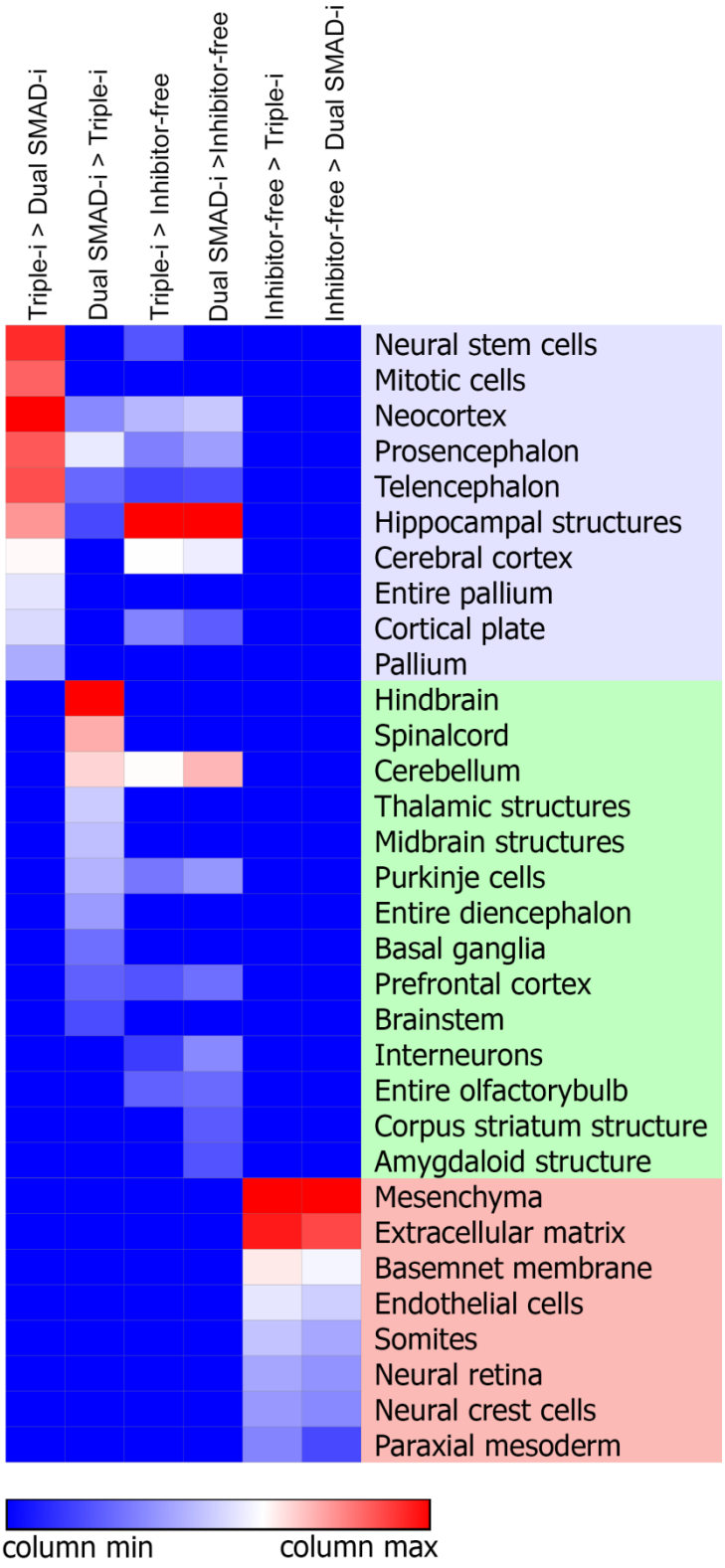

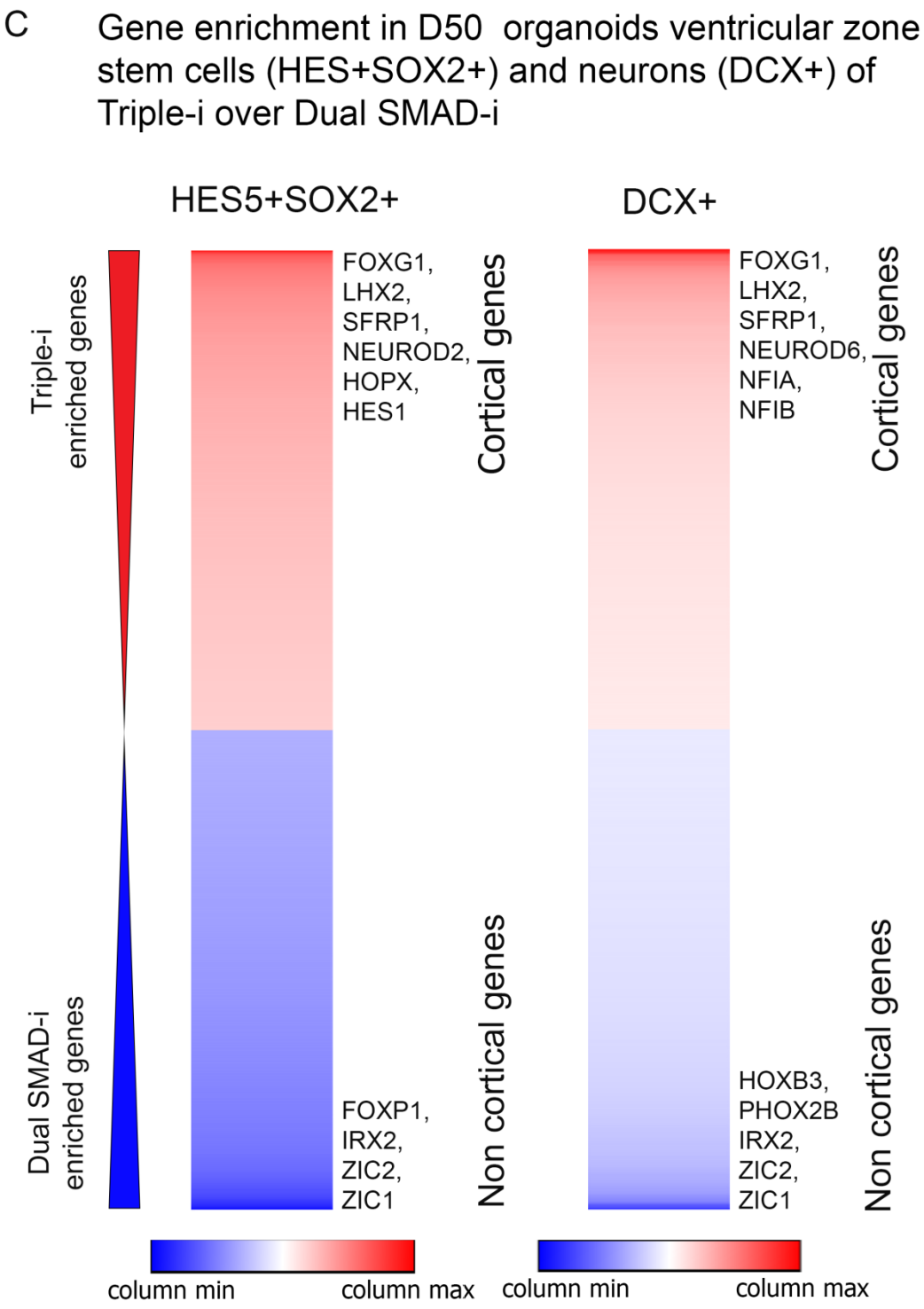

Figure 29: Single cell RNA-Seq reveal cortical cell fate maintenance in mature organoids derived under combined inhibition.

A. A heatmap representing expression values for selected genes categorized according to neural stem cell markers and regional markers (neocortex, medial pallium, diencephalon and midbrain-hindbrain) in day 30 Bulk RNA-Seq and day 50 simulated scRNA-Seq data derived under indicated

treatments. Color-coded scale represents relative expression levels of each gene (row) across treatments. Note the expression of cortical cell markers are maintained without the contamination of non-cortical cell fates in day 50 organoids derived under Triple-i.

B. Genomatix gene enrichment analysis for all pairwise comparison of day 50 organoid RNA-Seq expression data derived under indicated treatments. Color-coded scale represents relative –log p value levels in each comparison (column). Note telencephalic/cortical gene ontology terms enriched in Triple-i derived organoids.

C. A heatmap of log2 fold changes estimated from scRNA-Seq expression levels in neural stem cell (HES5+SOX2+) and neuronal (DCX+) population of day 50 Triple-i derived organoids compared to dual SMAD-i derived organoids. Color-coded scale represents gene expression levels (column). Note cortical genes are enriched in both stem cell and neuronal population of Triple-i derived day 50 organoids with important genes highlighted.

We then clustered cells from inhibitor-free, dual SMAD-i, and Triple-i day 50 organoids together in order to distinguish between similar and distinct cell populations across these three protocols (see methods for details), and identified 12 clusters in total (Figure 30A). The t-SNE map shows that most of the cells generated under dual SMAD-i and Triple-i were clustered together, whereas inhibitor-free generated cells were clustered separately (Figure 30B). FOXG1 expression level was used to distinguish cortical from non-cortical clusters (Figure 30C). A total of 91% of cells in Triple-i organoids and 68% of cells in dual SMAD-i organoids were assigned to cortical clusters. Only 5% of cells in inhibitor-free organoids were assigned to cortical clusters (Figure 30D). We have observed a high percentage of cortical stem cell population (SOX2+HES5+PAX6+FOXG1+) in Triple-i (73%) compared to dual SMAD-i (46%) and inhibitor-free (10%) conditions (Figure 30E). These results clearly show a massive enrichment of cortical cell types under Triple-i treatment.

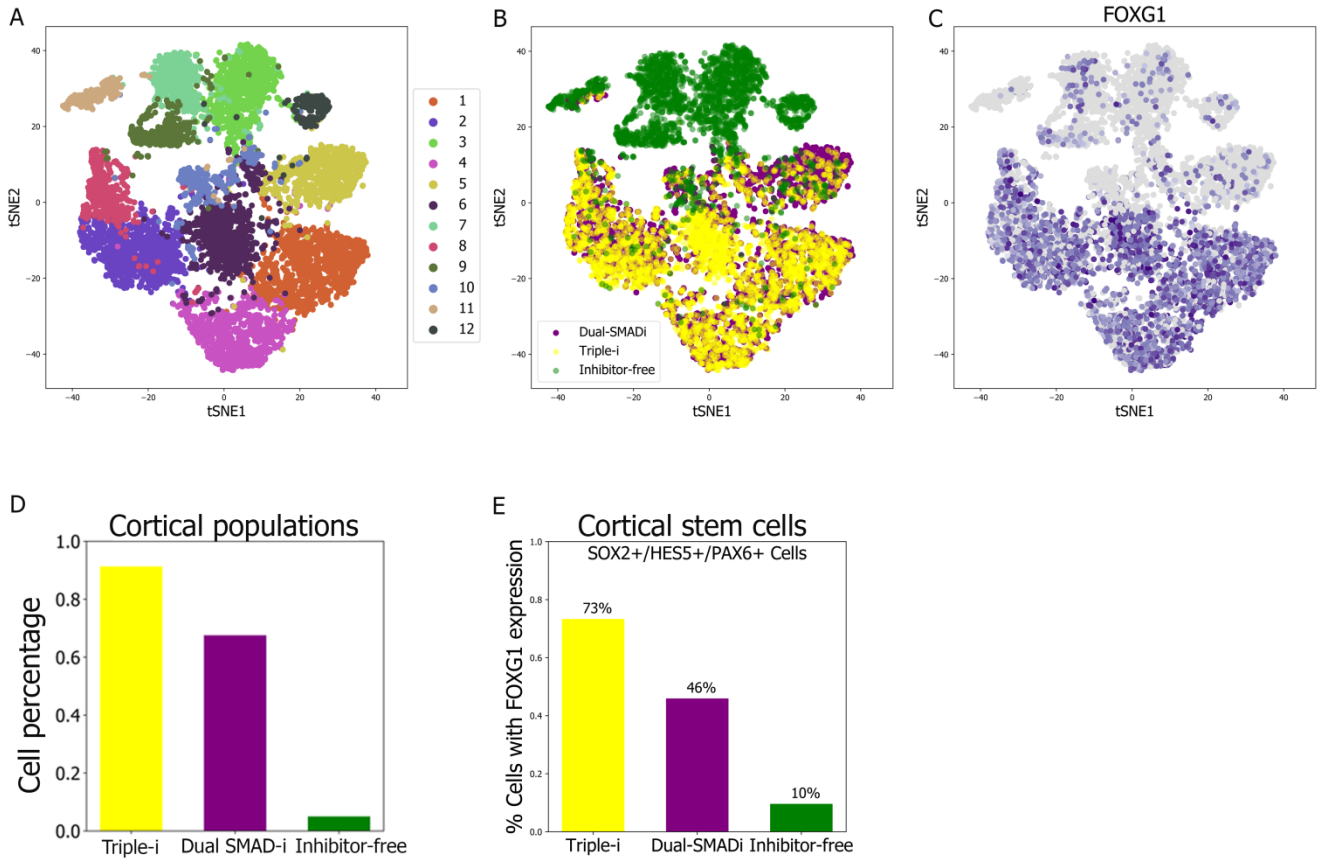

Figure 30: Enriched cortical population (stem cell and their progeny) in organoids derived under combined inhibition.

A. Combined t-distributed stochastic neighbor embedding (tSNE) plots for single cell RNA sequencing data of Day 50 organoids derived under indicated treatments reveals 12 (C1-C12) distinct clusters highlighted in different colors.

B. Combined t-distributed stochastic neighbor embedding (tSNE) plots for single cell RNA sequencing data of Day 50 organoids derived under indicated treatments highlighted in different colors. Color code: yellow-Triple-i, purple-dual SMAD-i and green-inhibitor-free.

C. tSNE plot with telencephalic/cortical marker FOXG1 expression level plotted as a gradient (gray values signify no reads mapping to FOXG1 detected in the respective cell).

D. Bar plot representing percentage of cortical population based on FOXG1 expression in day 50 organoids derived by indicated treatments.

E. Bar plot representing percentage of cortical stem population based on FOXG1, SOX2, HES5 and PAX6 expression in day 50 organoids derived by indicated treatments.

We characterized each cluster based on the expression of marker genes (Figure 31A). We observed five out of twelve clusters (C2, C8, C6, C4 and C1) with high FOXG1 expression levels, and denote these clusters as cortical clusters. From the heatmap (Figure 31B), we validate these clusters as cortical by highlighting the lack

of diencephalic and midbrain/hindbrain genes in these clusters accompanied with high levels of FOXG1 expression. Out of these FOXG1+ cortical clusters, C2 and C8 express neural stem/progenitor markers such as SOX2, SOX1 and HES5. C4 expresses intermediate progenitor marker EOMES, and C1 expresses neuronal markers NEUROD6, TBR1 and DCX. C6 expresses a mixture of both stem cell and neuronal marker genes, signifying that these cells are in a transitory state between stem cell and intermediate progenitor/neuron (Figure 31A). This suggests that the cortical populations observed in these organoids recapitulate the expression patterns observed during in vivo corticogenesis. Out of the seven non-cortical clusters, C10 expresses high levels of the stem cell/progenitor markers SOX2, SOX1 and HES5, as well as posterior markers of medial pallium, diencephalon and mid/hindbrain regions. C5 expresses high levels of the neuronal marker DCX, along with diencephalic and mid/hindbrain regional markers, indicating non-cortical stem cell and neuronal clusters respectively (Figure 31A, B). These clusters were mostly comprised of cells from dual SMAD-i organoids (55% in C10 and 70% in C5), a further indication that dual SMAD-i enriches for diencephalic and mid/hindbrain regions. C9, C3 and C7 express neural retina progenitor markers VSX2, PAX6 and RAX, and C12 expresses retinal pigmental epithelial (RPE) progenitor markers PAX6, OTX2 and RAX [193]. These clusters are mainly comprised of cells generated by inhibitor-free organoids (Figure 31A, B). These findings not only support our results from day 30 organoid bulk RNA-Seq comparisons that Triple-i organoids enrich for cortical marker genes and dual-SMAD-i organoids enrich for thalamic and midbrain/hindbrain genes, but highlight an important finding, that dual-SMAD-i organoids also produce cortical populations which are indistinguishable from the cortical populations generated in Triple-i organoids.

A

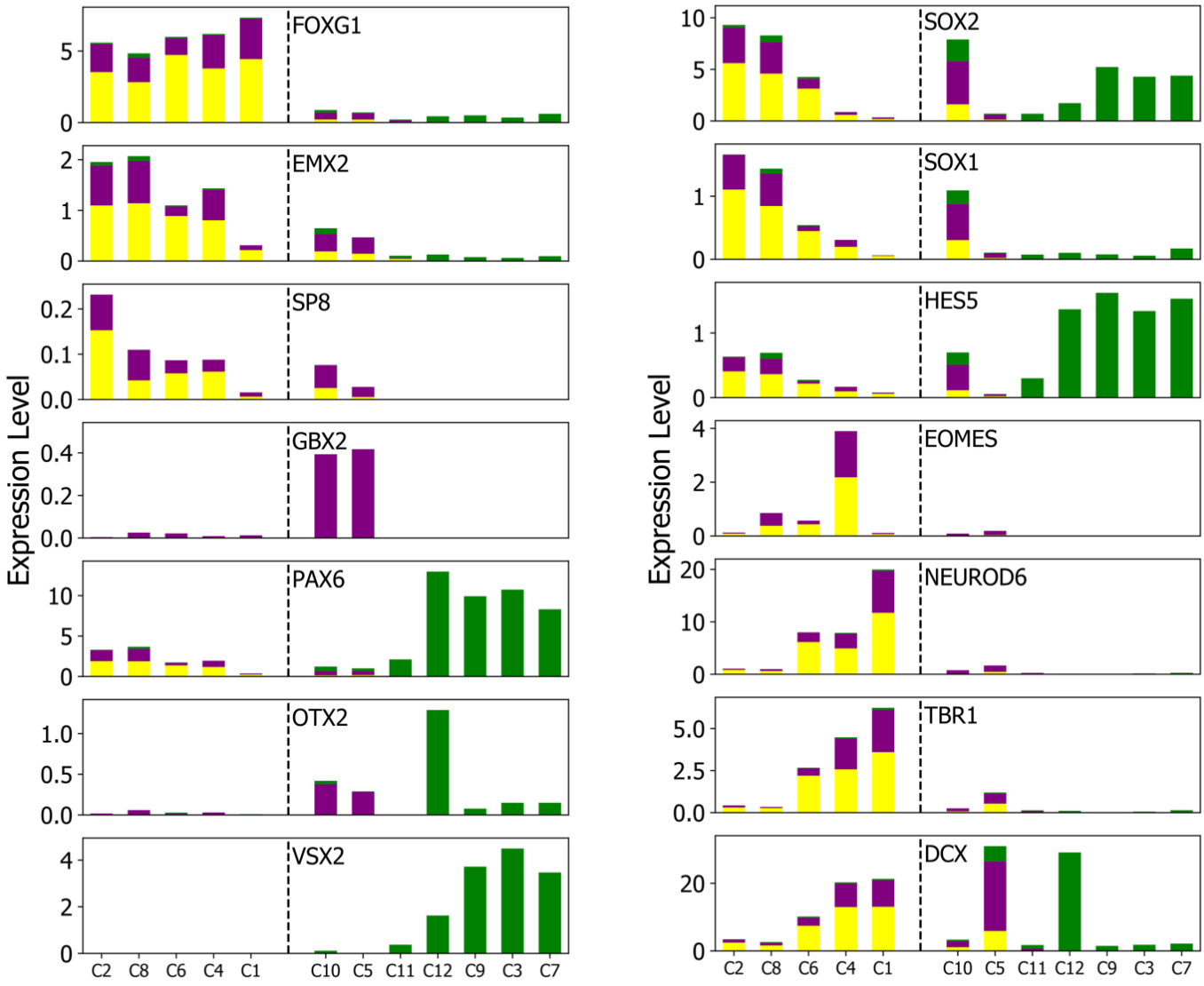
Expression Level
FOXG1
EMX2
SP8
GBX2
PAX6
OTX2
VSX2
SOX2
SOX1
HES5
EOMES
NEUROD6
TBR1
DCX
C2 C8 C6 C4 C1 C10 C5 C11 C12 C9 C3 C7

B

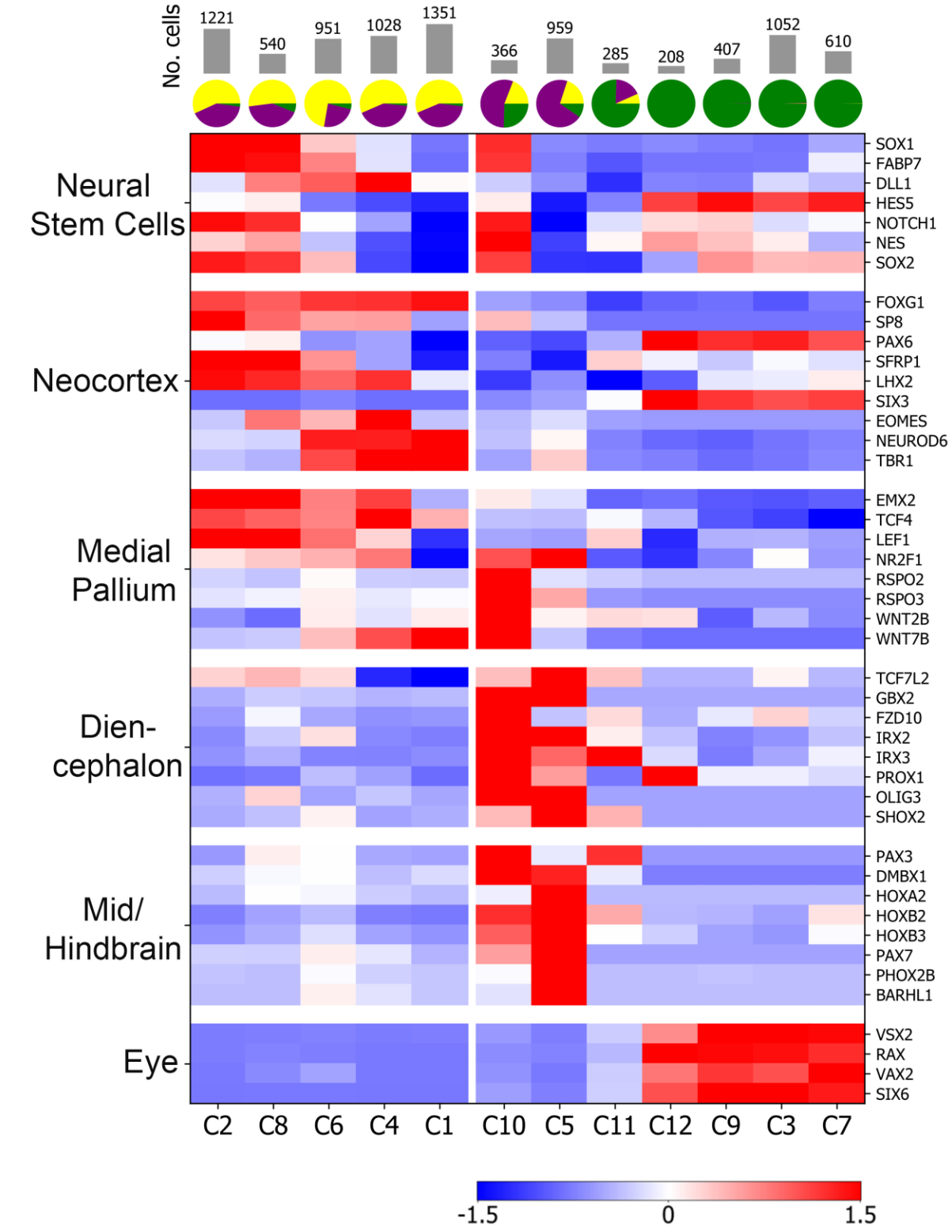

Figure 31: Combined inhibition organoids show homogeneous and increased cortical cellular composition mimicking in vivo corticogenesis.

A. Bar plot representing expression (RP10K) values for selected (brain regional specific and cortex cell type specific) genes in day 50 organoids derived by indicated treatments. The relative height of the stacked bars represents the proportion of reads within each cluster detected in cells across the

indicated treatments. General cortical marker: FOXG1, non-cortical markers: OTX2, GBX2 and VSX2, shared cortical and non-cortical markers: PAX6, EMX2 and SP8, neural stem cell markers: SOX2, SOX1 and HES5, intermediate progenitor marker: EOMES and neuronal markers: NEUROD6, TBR1 and DCX. Color code: yellow-Triple-i, purple-dual SMAD-i and green-inhibitor-free.

B. A heatmap representing expression values for genes marking neural stem cells as well as different brain regions (Neocortex, Medial pallium, Diencephalon and Mid/Hindbrain), with pie charts above displaying percentages of cells from each indicated treatments and bar plots displaying the total number of cells within each cluster. Color-coded scale represents relative expression levels of each gene (row) across clusters. Color code: yellow-Triple-i, purple-dual SMAD-i and green-inhibitor-free. Note the increased cortical cell populations in Triple-i derived organoids.

3.6 Cortical layer markers appear more homogeneously under combined dual SMAD and WNT inhibition

Ultimately, we also assessed cortical lamination capability in Triple-i and dual SMAD-i derived organoids using immunostaining for deep and upper cortical layer markers in day 80 and day 120 organoids. We observed the expression of both deep (TBR1, CTIP2 and to lower extent SATB2) and upper (CUX1, CUX2 and SATB2) layer markers in organoids derived by both treatments in day 80 and day 120 organoids (Figure 32A). Despite these similarities in marker expression between Triple-i and dual SMAD-i, we did observe differences in the cytoarchitectural organization of the corresponding neurons within organoids vicinity. We found that cortical layer neurons populated organoid peripheries much more homogeneously in Triple-i organoids compared to dual SMAD-i organoids, suggesting appropriate cortical layer formation. This was observed qualitatively (Figure 32A), but also validated quantitatively as judged by the more variable apical to basal distribution of deep or upper cortical layer markers in dual SMAD-i derived organoids (Figure 32B). This suggested that only when the correct cortical neuronal types are specified – possibly via Triple-i conditions – these perform efficient migration distally, to properly populate their destined layers. Finally, we also found that although superficial neuronal markers did not yet migrate beyond deep layer neuronal markers in day 80 organoids, they did eventually begin to show some of that migration in day 120 organoids. However again, this phenomenon was obtained regardless of the derivation method. Together, these results propose that the efficient cortical differentiation and lamination, depends on correct cortical fate acquisition at the starting populations and require combined inhibition.

A
Day 80 Organoids
Day 120 Organoids
Dual SMAD-i
Triple-i
DAPI CTIP2 CUX2
DAPI CTIP2 SATB2
DAPI TBR1 CUX1
CUX1
TBR1
SATB2
CTIP2
CUX2

B

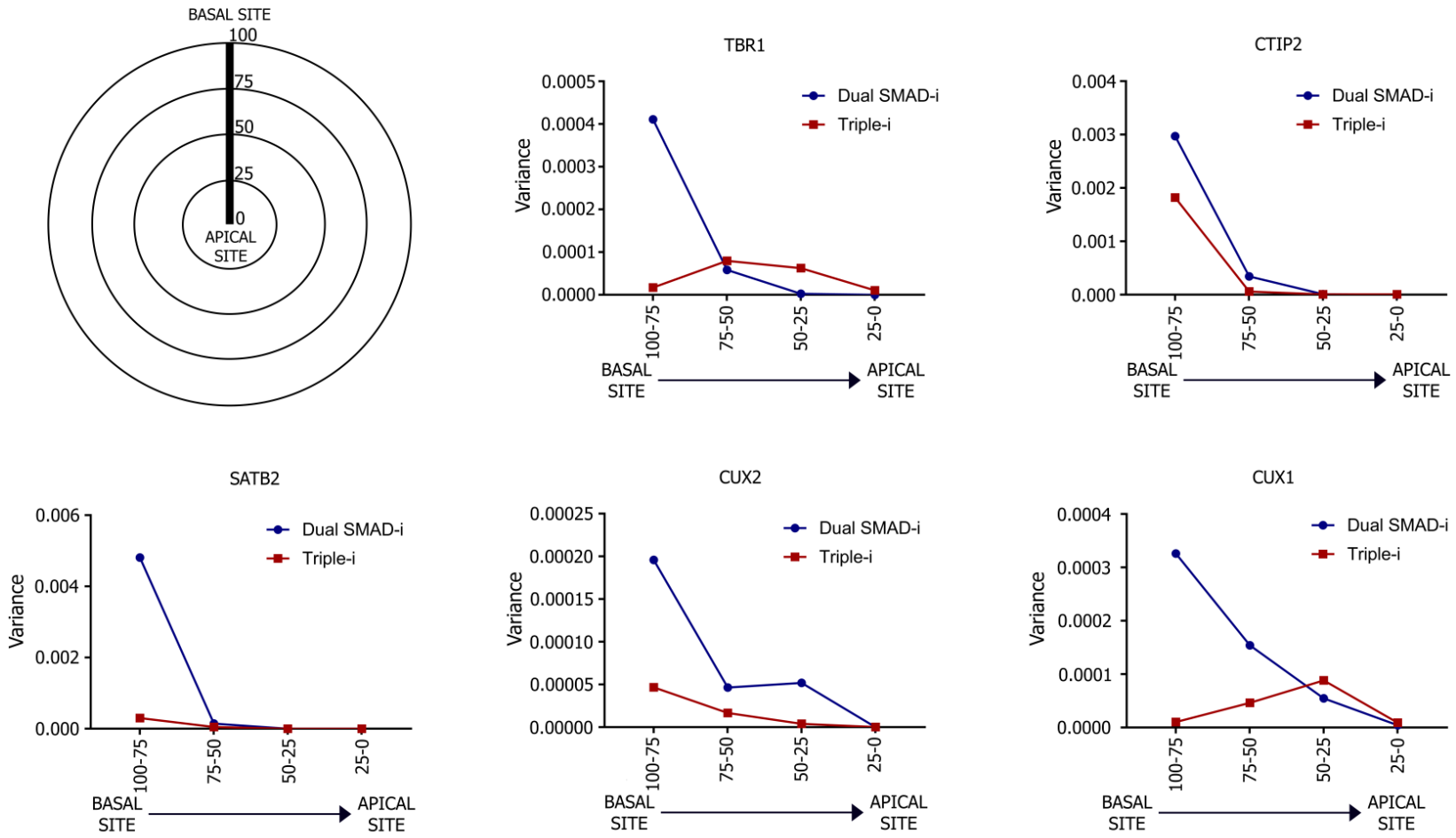
BASAL SITE
100
75
50
25
0
APICAL SITE
TBR1
CTIP2
SATB2
CUX2
CUX1
Dual SMAD-i
Triple-i
Variance
0.0005
0.0004
0.0003
0.0002
0.0001
0.0000
0.004
0.003
0.002
0.001
0.000
0.006
0.00025
0.00020
0.00015
0.00010
0.00005
0.00000
100-75
75-50
50-25
25-0
BASAL SITE
APICAL SITE

Figure 32: Efficient cortical lamination was observed in organoids derived under combined inhibition.

A. Immunostaining images for TBR1/CUX1, CTIP2/CUX2 and CTIP2/SATB2, for day 80 (left) and day 120 (right) organoids derived by indicated treatments. Note the comparable appearance of cortical lamination markers irrespective of the derivation method in both day 80 and day 120 organoids. For day 120 organoids, enlarged regions are shown on the right. Note the beginning cortical layer separation between deep and upper cortical neuronal layers in day 120 organoids. (Landscape orientation)

B. Quantification of apical to basal cortical lamination marker distribution in organoids derived by indicated treatments. Schematic showing whole organoid with apical to basal site, distributed in to four equal sequential radial portions. Charts represent variances calculated for the number of relative marker-expressing cells across selected sub-regions within each of four equally defined sequential radial segments comprising each organoid, from the most basal radial segment (denoted as the most outer segment; 75-100%) to the most apical radial segment (denoted as the most inner segment; 0-25%). Note the highest variances obtained for distribution of all cortical layer markers at basal sites (75-100%) in dual SMAD-i compared to Triple-i derived organoids, suggesting efficient migration and accumulation in the latter. (Landscape orientation)

4. DISCUSSION

The ability of PSCs to differentiate into lineage specific cell types, for example neural lineage, has led to the development of differentiation protocols for the derivation of distinct neuronal and glial subtypes. However it is still difficult to generate clinically relevant cell types such as specific type of cortical neurons at high purity for regenerative medicine due to the enormous heterogeneity that is generated during culture. One of the major obstacles in addressing heterogeneity is revealing how diversity is generated within *starting populations* - the earliest progenitor populations of a given lineage. Starting populations are considered to hold limited heterogeneity with respect to cell identity composition. It is therefore speculated that access to such populations should gain insights into their basic biology and ultimately allow the development of methods to increase their purity and potentially reveal mechanisms governing their self-renewal. In that respect, PSCs still hold the best example for a successfully “captured in time” and considerably homogeneous starting population [70, 194] - a phenomenon that eventually allowed establishment and maintenance of, as well as reprogramming towards distinct pluripotent stem cell states [169, 195-200].

In this study we show that early neocortical neuroepithelial cells—the starting population of neurons and glia of the developing neocortex—can be derived from human PSCs with remarkable regional homogeneity that is also correlated with enhanced radial organization and stem cell state (Notch activation). Numerous protocols to derive neural fates - and particularly early cortical fates - have been proposed, many of which are evenly conceived by the community. However, our study shows that when compared side by side, these methods lead to completely different cellular identities, arguing for distinct cell commitment already at the early neural patterning phase. In 2D monolayer cultures, dual SMAD inhibition produces mixed fates consisting of cortical and non-cortical identities, while combined inhibition induces only dorsal cortical identity. Moreover, we observed that anterior/cortical genes are upregulated on day 8 under both dual SMAD-i and Triple-i conditions. However, only in Triple-i, cortical gene expression is maintained and enriched in subsequent days i.e., day 10 and day 12, while their expression is

declined with concomitant upregulation of posterior/non-cortical genes in dual SMAD-i conditions. This was reminiscent of early studies in frogs where anterior neural axis fates developed first, from which only later transformed to posterior fates (Nieuwkoop's theory) in the absence of WNT inhibitory signal from AVE. Early progenitors derived by dual SMAD-i treatment upregulates diencephalic and midbrain-hindbrain genes already on day 8 and these markers consistently increased up to day 12, demonstrating the early starting populations were heterogeneous with posterior bias. These data in turn suggest that while capacity to develop anterior/cortical bias occurs by default but actual commitment to cortical fates require exogenous WNT inhibition on top of dual SMAD inhibition. In early day 30 organoids, inhibitor-free conditions produce mixed regional fates with moderate efficiency, while dual SMAD inhibition promotes predominantly posterior fates. However, only combined inhibition induces a robust and stable dorsal telencephalic / cortical fate. Thus, our findings propose that many of the obstacles inherent to heterogeneity during differentiation from PSCs can be resolved by correct specification of early starting populations. Also, in analogy to PSCs, such highly specified early cortical progenitors should serve as a convenient platform for addressing self-renewal capabilities and cell fate conversion in culture.

We show here that the generation of such homogeneous cortical starting populations is attributed to addition of WNT inhibition on top of dual SMAD inhibition. While dual SMAD inhibition directs efficient neural conversion, WNT inhibition restricts gastrulation together with specifying the cortical domain. As shown for both monolayers (rosettes) and organoids, only combined inhibition results in the compelling specification towards dorsal cortical fates, demonstrating that WNT inhibition on top of dual SMAD inhibition is imperative for rectifying the heterogeneity generated during neural conversion.

Attributing derivation of cortical fate identity to combined dual SMAD and WNT inhibition, and the induction of diencephalic and mid-hindbrain fates to dual SMAD inhibition in day 30 organoids, was enabled mainly by our corresponding analyses, which compared 10,000 differentially expressed genes among multiple organoids derived by the different treatments and cortical and non-cortical human embryonic CNS samples. This powerful framework showed that this difference between

methods and their outcomes is unequivocal. Gene set enrichment analysis of differentially expressed gene candidates reveal significant enrichment of cortical fates in combined inhibition vs diencephalic and mid-hindbrain fates in dual SMAD-i treatment. Comparing them with Allen human brain regional markers disclose 23 candidate genes enriched in combined inhibition are also highly expressed *in vivo* human cortical tissue. In addition, heatmap comprising 52 genes reflective of distinct regional markers further corroborates the dichotomy between methods and fates and also reveals the heterogeneity between individual organoids derived under same condition. Co-localization of dorsal cortex markers together with neural stem cell markers at the immunostaining and single-cell RNA-Seq levels further confirms homogeneity of cortical cellular identity achieved by combined inhibition. Single cell RNA-Seq shows the homogenous derivation of cortical populations (93%) under combined inhibition vs dual SMAD-i (63%) and inhibitor-free (5%). Dual SMAD-i and inhibitor-free conditions also promotes the generation of non-cortical tissues such as diencephalon, mid/hindbrain and eye tissues, thus making them heterogeneous and difficult to study and interpret with high confidence the exclusive nature of cortical stem cell fates in disease and health. Finally, the reduced variance in neuronal marker distribution in organoids derived by combined inhibition provides an additional discriminative evidence for improved cortical layer organization – a sign for the highly ordered generation of cortical building blocks. These differences could be enabled due to the systematic comparison of several methods performed in parallel, using different culture configurations, testing a number of developmental stages, and further supporting results with an analogous comparison in a disease model. To the best of our knowledge, there has not been any comprehensive comparative study that tackles all these parameters in parallel. While naturally, most studies are inherently limited to one selected derivation method, which is usually sufficient to successfully recapitulate the relevant developmental process and extract related disease phenotype, our study encourages the extension of such experimental model systems to more than one derivation method.

While marked differences in generation of cortical vs non-cortical fates was achieved by the different derivation methods, our study reveals that specification towards medial pallial fates was comparable regardless of the derivation method. The medial pallium is responsible for generation of the cortical hem – a central cortical organizer

that directs specification of hippocampal primordia. In addition, studies portray the cortical hem as potential center responsible for shaping the size and arealization of the cortex itself [201], although this has been debated [189, 202]. The finding that all methods are compatible for cortical hem formation (at least transcriptionally) suggests that it is indifferent to morphogen levels such as TGF and interestingly also WNT. More remarkably, the finding that the generation of this structure is not affected in microcephaly - also here regardless of derivation method - further argues that cortical hem formation is resilient also under severe abnormal developmental circumstances. Therefore, it is tempting to speculate that this novel observation may link early neural patterning with early evolution of cortical organizers. More broadly, one could assume how important organizers such as the hem, which ultimately develop into basic limbic structures such as the hippocampus, have evolved to retain indifference to genetic changes that alter dorsomedial cortical patterning during evolution.

We show here that the generation of homogeneous cortical starting populations requires addition of WNT-i on top of dual SMAD-i. Dual SMAD-i alone has shown to be critical to enhance neural conversion in monolayers and here it is shown to enhance Notch activation in both monolayers and organoids, at the *HES5::eGFP* reporter expression level and at the molecular level, possibly by promoting neurulation [203] and brining major impediment to endodermal and mesodermal lineages [204-206]. However, enhanced Notch activation results also in elevated patterning towards posterior fates, in agreement with high HES5 expression in hindbrain structures as deduced from Allen Brain Atlas expression databases [171]. This suggests that neural cortical cultures derived in the absence of WNT inhibition exhibit insufficient restriction of neural axis elongation / mesoderm formation. The addition of WNT inhibition strongly restricts gastrulation at the outset, thus further reinforcing CNS fates. However, it also specifies the telencephalic/cortical domain, thus rectifying potential residual posterior fate outcomes generated during the acquisition of early CNS fates. Thus, it seems that in vitro, residual mesodermal dedifferentiation is correlated with posterior neural axis patterning, in agreement with reported neuromesodermal progenitors expressing neural and mesodermal markers, and which later develop into posterior neurons [207]. This is less the case for inhibition of WNT alone, which seems sufficient to drive specification towards cortical

progenitor starting populations in organoids, but not in monolayers, supporting the notion of a more robust neural induction mechanism in 3D systems. However, WNT-i alone could not convey robust vesicle expansion in organoids and ensure their endurance during long-term culture, demonstrating the critical role of dual SMAD inhibition in NSC fate specification and proliferation.

This work shows that despite the prevalence of enhanced Notch activation under both dual SMAD and combined inhibition - reflecting high stemness, only when it overlaps with efficient radial organization; it essentially hallmarks transition towards cortical fates. Radial organization of early PSC derived neural progenitors into neural rosettes has been described in many studies since the first description by Zhang and colleagues [116]. We were the first to isolate rosette forming NSCs (R-NSCs) with anterior character from human ESCs and further shown that the rosette formation process depended on Notch activation [119]. Since then, we have been able to specifically correlate rosette formation capacity to Notch activation during cortical fate specification at the cellular, molecular and cytoarchitectural dynamics levels [127, 146, 147]. However, these studies also marked heterogeneity in rosette formation capacity and regional identity [146]. Here we show that radial organization capacity becomes superior under combined inhibition, where it also coincides with enhanced Notch activation – together serving as readout for efficient cortical specification.

We propose that these readouts are linked to actual properties of cortical NSCs. First, radial organization ensures that neuroepithelial cells acquire strong apico-basal cell polarity that is critical for forming a contiguous epithelial lining of the ventricular zone and preserve its unique cytoarchitectural radial organization, which in turn allows proper interkinetic nuclear migration and cell division at apical sites. Enhanced stemness (Notch activation) is required conducting proper cell fate decisions that continue to produce stem cells that progress through the distinct stages during cortical development. While our data does not argue that radial organization capacity is exclusive to cortical progenitors, they do demonstrate that this capacity is always shared by efficiently derived early cortical neuroepithelial cells, while it devoid in posterior early neuroepithelial cells such as diencephalon and mid-hindbrain. We therefore propose that enhanced Notch activation and radial

organization can be assigned as robust hallmarks for corticogenesis, with an emphasis on its early stages – namely creating the starting population for corticogenesis.

The fact that enhanced Notch activation could be induced in two cytoarchitectural contexts - radially organized under combined inhibition or non-radially organized under dual SMAD inhibition - argues that WNT inhibition ensures that the enhanced neural stem cell state (promoted by dual SMAD inhibition) specifically occurs in cortical starting populations. The presence of vesicles in microcephaly organoids exhibiting compromised neuroepithelial cell integrity, substantial cell death in vesicle areas where Notch activation coincided radial organization, and concordant loss in NSC and cortical marker gene expression – all correspond with a model by which combined inhibition is essential for exerting the microcephaly phenotypes and may indeed represent a meaningful pathophysiological component in disease etiology. Conversely, derivation of microcephaly organoids under dual SMAD-i also caused significant reduction in NSC genes, yet apoptosis was hardly present and reduction in posterior fate-specific gene expression was non-significant, suggesting that while stemness is affected in microcephaly in all brain regions, only in the cortex it is deleterious enough to cause dramatic cell loss. Thus, our data propose that it is imperative to run differentiation on both methods for adding important insights to understanding disease pathology.

While the above findings propose that cells committed to cortical fates pursue the apoptotic pathway, while those taking a non-cortical cell fate survive, one could not rule out the possibility that in addition to cortex specific cell death, defects in early neural patterning due to impaired WNT signaling for example, resulted in favored commitment towards posterior fates already at the outset of neural development. This is supported by the increase in posterior gene expression signature in day 17 microcephaly organoids. However, on day 30, microcephaly organoids did not show this preferential expression, suggesting that most of the loss in cortical identity was due to cell death.

Mechanistically, the smaller vesicle size, decrease in proliferation vs. differentiation index during early stages, and the cell cycle arrest at apical sites postulate a disease

model in which centrosome defects cause abnormal cell cycle checkpoint signaling during G2-to-M transition, consequent premature mitotic entry or mitotic arrest at apical sites, and eventual cell death [208, 209]. We were not able to record more asymmetrical cell divisions among P-VIM+ cells in microcephaly organoids and therefore our data could not argue at this point for depletion in stem cells due to increased asymmetric differentiation as mechanism that leads to premature consumption of NSCs. Rather, we propose cell cycle defects leading to cell death at the progenitor but presumably also during last division steps towards differentiation. Since cell death is surrounding Notch active radially organized regions, we propose that apical neural stem cells are primarily affected due to exhaust in cell proliferation, and this may be supported by findings that cerebral cortical ventricular zone progenitors have been shown to undergo some apoptosis in general [210]. It will be interesting to find out whether cortical progenitors are more prone to apoptosis due to increased cell cycle rates compared to posterior fates. This may also explain why cell death in microcephaly occurs primarily in a more active germinal zone, such as the cortical ventricular zone, despite the mutation being shared by all brain cells.
There are several utilities for using Notch activation and radial organization as hallmarks or direct readouts for efficient early cortical specification. First, current readouts require assessment of cortical lamination after many days of differentiation (e.g. >100 days). Second, the use of markers that are less than optimal due to their appearance in other brain regions in vivo as well as under both inhibitory methods in organoids. Given the highly challenging task to compare differentiation efficiencies after 80 days in culture, either between different protocols, different lines, and different labs, our proposed readout specifically aids to standardize differentiation methods and predict overall cortical specification potential already at its early stages. In addition, these readouts may be used to predict the robustness of cytoarchitectural integrity (radial organization) and NSC potential (Notch activation), which so far have not been assessed during the various differentiation paradigms.

Our work further harnesses the already established use of WNT signalling modulation in pluripotent, neural and non-neural lineages, to also standardize cortical differentiation systems. Ample evidence has been accumulated on WNT level modulation. WNT activation participates in maintaining a naïve ground state [169, 197, 199, 211-213], and promotes non-neural differentiation of primed

pluripotent cells [214, 215]. Reciprocally, WNT inhibition promotes priming of naïve PSCs towards epiblast stem cells [213], and is implicated in differentiation towards neural fates [216]. This equilibrium of WNT signaling in variety of pluripotent states [217] is reflected also in the nervous system. WNT activation is implicated in differentiation towards more posterior cell fates [207, 218], while WNT inhibition enhances anterior neural fates [118, 124-126, 133, 134, 136, 188]. Here we show that WNT inhibition is imperative for correct acquisition of cortical progenitor starting populations – which is a critical factor in preventing heterogeneity. Together with SMAD inhibition, enhanced NSC state is achieved in the correct progenitors, enabling the expansion and derivation of appropriate consecutive lineages.

To conclude, we propose that the data generated in this study can serve as valuable and powerful references to model brain development and corticogenesis in particular, under normal and pathogenic conditions. The combined analyses of single organoid and human brain RNA-Seq datasets allow a unique platform for retrieval of critical information on how expression of stem cell, regional and other population-specific genes is reflected by each of the derivation methods and with respect to all brain regions. This also provides a unique opportunity to transcriptionally compare between phenotypes and select the inhibition paradigm that fits clinically relevant cells. For the latter, one could also potentially simulate (in silico) or experiment several related diseases in parallel by different methods, opting out multiple phenotypes depending on treatment. The microcephaly expression profiles bring an additional in-platform, yet standalone data source that sheds light on this highly relevant malformation from which many potential developmental key players can be identified. The single cell dataset for organoids derived by combined inhibition provides a comprehensive in vivo-like snapshot reference of cellular identity composition in the embryonic cortex, particularly for identifying new genes expressed in well-established populations as well as identifying novel populations. Radial organization and Notch activation provide a robust readout for transition of PSCs towards early cortical neural stem cells. While Notch activation reporter is not naturally present in a lab toolbox, a very efficient radial organization serves quite robustly to score cultures transitioning to early cortical linages. Finally, the systematic comparison of organoids and monolayers derived by the different methods with respect to the transcriptional, cytoarchitectural and cell fates provides

another valuable tool to assess which among the 2D or 3D differentiation schemes is suitable for the topic in question.

5. Bibliography

1. Marikawa, Y. and V.B. Alarcon, Establishment of trophectoderm and inner cell mass lineages in the mouse embryo. Mol Reprod Dev, 2009. **76**(11): p. 1019-32.
2. Lumsden, A. and R. Krumlauf, Patterning the vertebrate neuraxis. Science, 1996. **274**(5290): p. 1109-15.
3. Stern, C.D., Initial patterning of the central nervous system: how many organizers? Nat Rev Neurosci, 2001. **2**(2): p. 92-8.
4. SPEMANN, H.u.M., H, Über die Induktion von Embryonalanlagen durch Implantation artfremder Organisatoren. W. Roux' Arch. f. Entw. d. Organis. u. mikrosk. Anat, 1924. **100**: p. 599-638.
5. Hemmati-Brivanlou, A. and D.A. Melton, Inhibition of activin receptor signaling promotes neuralization in Xenopus. Cell, 1994. **77**(2): p. 273-81.
6. Sasai, Y., et al., Regulation of neural induction by the Chd and Bmp-4 antagonistic patterning signals in Xenopus. Nature, 1995. **376**(6538): p. 333-6.
7. Lamb, T.M. and R.M. Harland, Fibroblast growth factor is a direct neural inducer, which combined with noggin generates anterior-posterior neural pattern. Development, 1995. **121**(11): p. 3627-36.
8. Mangold, O., ber die Induktionsf higkeit der verschiedenen Bezirke der Neurula von Urodelen. Die Naturwissenschaften, 1933. **21**(43): p. 761-766.
9. Eyal-Giladi, H., Dynamic aspects of neural induction in amphibia. Arch Biol (Liege), 1954. **65**(2): p. 179-259.
10. Jansen, H.J., et al., The role of the Spemann organizer in anterior-posterior patterning of the trunk. Mech Dev, 2007. **124**(9-10): p. 668-81.
11. Nieuwkoop, P.D., Activation and organization of the central nervous system in amphibians. Part I. Induction and activation. Journal of Experimental Zoology, 1952. **120**(1): p. 1-31.
12. Nieuwkoop, P.D., Activation and organization of the central nervous system in amphibians. Part II. Differentiation and organization. Journal of Experimental Zoology, 1952. **120**(1): p. 33-81.
13. Nieuwkoop, P.D. and G.V. Nigtevecht, Neural Activation and Transformation in Explants of Competent Ectoderm under the Influence of Fragments of

Anterior Notochord in Urodeles. Journal of Embryology and Experimental Morphology, 1954. **2**(3): p. 175-193.

14. Fraser, S.E.a.S., C.D, Early rostrocaudal patterning of the mesoderm and neural plate. In: Gastrulation: from cells to embryo. (ed. C.D. Stern). Cold Spring Harbor Press, 2004: p. 389-402.
15. Cox, W.G. and A. Hemmati-Brivanlou, Caudalization of neural fate by tissue recombination and bFGF. Development, 1995. **121**(12): p. 4349-58.
16. Kiecker, C. and C. Niehrs, A morphogen gradient of Wnt/beta-catenin signalling regulates anteroposterior neural patterning in Xenopus. Development, 2001. **128**(21): p. 4189-201.
17. Durston, A.J., et al., Retinoic acid causes an anteroposterior transformation in the developing central nervous system. Nature, 1989. **340**(6229): p. 140-4.
18. Andoniadou, C.L. and J.P. Martinez-Barbera, Developmental mechanisms directing early anterior forebrain specification in vertebrates. Cell Mol Life Sci, 2013. **70**(20): p. 3739-52.
19. Waddington, C.H., Induction by coagulated organisers in the chick embryo. Nature, 1933. **131**: p. 275-276.
20. Beddington, R.S., Induction of a second neural axis by the mouse node. Development, 1994. **120**(3): p. 613-20.
21. Tam, P.P. and K.A. Steiner, Anterior patterning by synergistic activity of the early gastrula organizer and the anterior germ layer tissues of the mouse embryo. Development, 1999. **126**(22): p. 5171-9.
22. Beddington, R.S. and E.J. Robertson, Anterior patterning in mouse. Trends Genet, 1998. **14**(7): p. 277-84.
23. Beddington, R.S. and E.J. Robertson, Axis development and early asymmetry in mammals. Cell, 1999. **96**(2): p. 195-209.
24. Srinivas, S., The anterior visceral endoderm-turning heads. Genesis, 2006. **44**(11): p. 565-72.
25. Takaoka, K., M. Yamamoto, and H. Hamada, Origin of body axes in the mouse embryo. Curr Opin Genet Dev, 2007. **17**(4): p. 344-50.
26. Acampora, D., et al., Visceral endoderm-restricted translation of Otx1 mediates recovery of Otx2 requirements for specification of anterior neural plate and normal gastrulation. Development, 1998. **125**(24): p. 5091-104.

27. Rhinn, M., et al., Cell autonomous and non-cell autonomous functions of Otx2 in patterning the rostral brain. Development, 1999. **126**(19): p. 4295-304.
28. Perea-Gomez, A., et al., Nodal antagonists in the anterior visceral endoderm prevent the formation of multiple primitive streaks. Dev Cell, 2002. **3**(5): p. 745-56.
29. Yamamoto, M., et al., Nodal antagonists regulate formation of the anteroposterior axis of the mouse embryo. Nature, 2004. **428**(6981): p. 387-92.
30. Hiramatsu, R., et al., External mechanical cues trigger the establishment of the anterior-posterior axis in early mouse embryos. Dev Cell, 2013. **27**(2): p. 131-144.
31. Miura, S., A.P. Singh, and Y. Mishina, Bmpr1a is required for proper migration of the AVE through regulation of Dkk1 expression in the pre-streak mouse embryo. Dev Biol, 2010. **341**(1): p. 246-54.
32. Ho, C.Y., et al., A role for the extraembryonic yolk syncytial layer in patterning the zebrafish embryo suggested by properties of the hex gene. Curr Biol, 1999. **9**(19): p. 1131-4.
33. Jones, C.M., et al., An anterior signalling centre in Xenopus revealed by the homeobox gene XHex. Curr Biol, 1999. **9**(17): p. 946-54.
34. Stern, C.D., Neural induction: old problem, new findings, yet more questions. Development, 2005. **132**(9): p. 2007-21.
35. Foley, A.C., I. Skromne, and C.D. Stern, Reconciling different models of forebrain induction and patterning: a dual role for the hypoblast. Development, 2000. **127**(17): p. 3839-54.
36. Brzica, H., et al., Role of Transporters in Central Nervous System Drug Delivery and Blood-Brain Barrier Protection: Relevance to Treatment of Stroke. J Cent Nerv Syst Dis, 2017. **9**: p. 1179573517693802.
37. Levine, A.J. and A.H. Brivanlou, Proposal of a model of mammalian neural induction. Dev Biol, 2007. **308**(2): p. 247-56.
38. Khokha, M.K., et al., Depletion of three BMP antagonists from Spemann's organizer leads to a catastrophic loss of dorsal structures. Dev Cell, 2005. **8**(3): p. 401-11.
39. Dal-Pra, S., et al., Noggin1 and Follistatin-like2 function redundantly to Chordin to antagonize BMP activity. Dev Biol, 2006. **298**(2): p. 514-26.

40. Di-Gregorio, A., et al., BMP signalling inhibits premature neural differentiation in the mouse embryo. Development, 2007. **134**(18): p. 3359-69.
41. Bachiller, D., et al., The organizer factors Chordin and Noggin are required for mouse forebrain development. Nature, 2000. **403**(6770): p. 658-61.
42. Vallier, L., D. Reynolds, and R.A. Pedersen, Nodal inhibits differentiation of human embryonic stem cells along the neuroectodermal default pathway. Dev Biol, 2004. **275**(2): p. 403-21.
43. Camus, A., et al., Absence of Nodal signaling promotes precocious neural differentiation in the mouse embryo. Dev Biol, 2006. **295**(2): p. 743-55.
44. Bouwmeester, T., et al., Cerberus is a head-inducing secreted factor expressed in the anterior endoderm of Spemann's organizer. Nature, 1996. **382**(6592): p. 595-601.
45. Inui, M., et al., Self-regulation of the head-inducing properties of the Spemann organizer. Proc Natl Acad Sci U S A, 2012. **109**(38): p. 15354-9.
46. Liguori, G.L., et al., Anterior neural plate regionalization in cripto null mutant mouse embryos in the absence of node and primitive streak. Dev Biol, 2003. **264**(2): p. 537-49.
47. Wilson, S.I., et al., An early requirement for FGF signalling in the acquisition of neural cell fate in the chick embryo. Curr Biol, 2000. **10**(8): p. 421-9.
48. Furthauer, M., et al., Fgf signalling controls the dorsoventral patterning of the zebrafish embryo. Development, 2004. **131**(12): p. 2853-64.
49. Davidson, B.P., et al., Exogenous FGF-4 can suppress anterior development in the mouse embryo during neurulation and early organogenesis. Dev Biol, 2000. **221**(1): p. 41-52.
50. Mason, I., Initiation to end point: the multiple roles of fibroblast growth factors in neural development. Nat Rev Neurosci, 2007. **8**(8): p. 583-96.
51. Pera, E.M., et al., Integration of IGF, FGF, and anti-BMP signals via Smad1 phosphorylation in neural induction. Genes Dev, 2003. **17**(24): p. 3023-8.
52. Sheng, G., M. dos Reis, and C.D. Stern, Churchill, a zinc finger transcriptional activator, regulates the transition between gastrulation and neurulation. Cell, 2003. **115**(5): p. 603-13.
53. Kelly, O.G., K.I. Pinson, and W.C. Skarnes, The Wnt co-receptors Lrp5 and Lrp6 are essential for gastrulation in mice. Development, 2004. **131**(12): p. 2803-15.

54. Mukhopadhyay, M., et al., Dickkopf1 is required for embryonic head induction and limb morphogenesis in the mouse. Dev Cell, 2001. **1**(3): p. 423-34.
55. McMahon, A.P., et al., The midbrain-hindbrain phenotype of Wnt-1-/Wnt-1- mice results from stepwise deletion of engrailed-expressing cells by 9.5 days postcoitum. Cell, 1992. **69**(4): p. 581-95.
56. Popperl, H., et al., Misexpression of Cwnt8C in the mouse induces an ectopic embryonic axis and causes a truncation of the anterior neuroectoderm. Development, 1997. **124**(15): p. 2997-3005.
57. Nordstrom, U., T.M. Jessell, and T. Edlund, Progressive induction of caudal neural character by graded Wnt signaling. Nat Neurosci, 2002. **5**(6): p. 525-32.
58. Heisenberg, C.P., et al., A mutation in the Gsk3-binding domain of zebrafish Masterblind/Axin1 leads to a fate transformation of telencephalon and eyes to diencephalon. Genes Dev, 2001. **15**(11): p. 1427-34.
59. Gavalas, A. and R. Krumlauf, Retinoid signalling and hindbrain patterning. Curr Opin Genet Dev, 2000. **10**(4): p. 380-6.
60. Kudoh, T., S.W. Wilson, and I.B. Dawid, Distinct roles for Fgf, Wnt and retinoic acid in posteriorizing the neural ectoderm. Development, 2002. **129**(18): p. 4335-46.
61. Maden, M., The role of retinoic acid in embryonic and post-embryonic development. Proc Nutr Soc, 2000. **59**(1): p. 65-73.
62. Halilagic, A., M.H. Zile, and M. Studer, A novel role for retinoids in patterning the avian forebrain during presomite stages. Development, 2003. **130**(10): p. 2039-50.
63. Jessell, T.M., Neuronal specification in the spinal cord: inductive signals and transcriptional codes. Nat Rev Genet, 2000. **1**(1): p. 20-9.
64. Jessell, T.M. and J.R. Sanes, Development. The decade of the developing brain. Curr Opin Neurobiol, 2000. **10**(5): p. 599-611.
65. Ishibashi, M. and A.P. McMahon, A sonic hedgehog-dependent signaling relay regulates growth of diencephalic and mesencephalic primordia in the early mouse embryo. Development, 2002. **129**(20): p. 4807-19.
66. Chiang, C., et al., Cyclopia and defective axial patterning in mice lacking Sonic hedgehog gene function. Nature, 1996. **383**(6599): p. 407-13.

67. Rowitch, D.H., et al., Sonic hedgehog regulates proliferation and inhibits differentiation of CNS precursor cells. J Neurosci, 1999. **19**(20): p. 8954-65.
68. Goodrich, L.V., et al., Altered neural cell fates and medulloblastoma in mouse patched mutants. Science, 1997. **277**(5329): p. 1109-13.
69. Evans, M.J. and M.H. Kaufman, Establishment in culture of pluripotential cells from mouse embryos. Nature, 1981. **292**(5819): p. 154-6.
70. Martin, G.R., Isolation of a pluripotent cell line from early mouse embryos cultured in medium conditioned by teratocarcinoma stem cells. Proc Natl Acad Sci U S A, 1981. **78**(12): p. 7634-8.
71. Keller, G., Embryonic stem cell differentiation: emergence of a new era in biology and medicine. Genes Dev, 2005. **19**(10): p. 1129-55.
72. Ebert, A.D., P. Liang, and J.C. Wu, Induced pluripotent stem cells as a disease modeling and drug screening platform. J Cardiovasc Pharmacol, 2012. **60**(4): p. 408-16.
73. Sterneckert, J.L., P. Reinhardt, and H.R. Scholer, Investigating human disease using stem cell models. Nat Rev Genet, 2014. **15**(9): p. 625-39.
74. Gurdon, J.B., Adult frogs derived from the nuclei of single somatic cells. Dev Biol, 1962. **4**: p. 256-73.
75. Wilmut, I., et al., Viable offspring derived from fetal and adult mammalian cells. Nature, 1997. **385**(6619): p. 810-3.
76. Tada, M., et al., Nuclear reprogramming of somatic cells by in vitro hybridization with ES cells. Curr Biol, 2001. **11**(19): p. 1553-8.
77. Cowan, C.A., et al., Nuclear reprogramming of somatic cells after fusion with human embryonic stem cells. Science, 2005. **309**(5739): p. 1369-73.
78. Takahashi, K. and S. Yamanaka, Induction of pluripotent stem cells from mouse embryonic and adult fibroblast cultures by defined factors. Cell, 2006. **126**(4): p. 663-76.
79. Robinton, D.A. and G.Q. Daley, The promise of induced pluripotent stem cells in research and therapy. Nature, 2012. **481**(7381): p. 295-305.
80. Hamazaki, T., et al., Concise Review: Induced Pluripotent Stem Cell Research in the Era of Precision Medicine. Stem Cells, 2017. **35**(3): p. 545-550.

81. Bilic, J. and J.C.I. Belmonte, Concise Review: Induced Pluripotent Stem Cells Versus Embryonic Stem Cells: Close Enough or Yet Too Far Apart? Stem Cells, 2012. **30**(1): p. 33-41.
82. Baghbaderani, B.A., et al., Detailed Characterization of Human Induced Pluripotent Stem Cells Manufactured for Therapeutic Applications. Stem Cell Rev, 2016. **12**(4): p. 394-420.
83. Cattaneo, E. and R. McKay, Proliferation and differentiation of neuronal stem cells regulated by nerve growth factor. Nature, 1990. **347**(6295): p. 762-5.
84. Gage, F.H., Mammalian neural stem cells. Science, 2000. **287**(5457): p. 1433-8.
85. Sauer, F.C., Mitosis in the neural tube. The Journal of Comparative Neurology, 1935. **62**(2): p. 377-405.
86. Frantz, G.D. and S.K. McConnell, Restriction of late cerebral cortical progenitors to an upper-layer fate. Neuron, 1996. **17**(1): p. 55-61.
87. Temple, S., The development of neural stem cells. Nature, 2001. **414**(6859): p. 112-7.
88. Gage, F.H. and S. Temple, Neural stem cells: generating and regenerating the brain. Neuron, 2013. **80**(3): p. 588-601.
89. Taverna, E. and W.B. Huttner, Neural progenitor nuclei IN motion. Neuron, 2010. **67**(6): p. 906-14.
90. Lee, H.O. and C. Norden, Mechanisms controlling arrangements and movements of nuclei in pseudostratified epithelia. Trends Cell Biol, 2013. **23**(3): p. 141-50.
91. Gotz, M. and W.B. Huttner, The cell biology of neurogenesis. Nat Rev Mol Cell Biol, 2005. **6**(10): p. 777-88.
92. Kriegstein, A.R. and M. Gotz, Radial glia diversity: a matter of cell fate. Glia, 2003. **43**(1): p. 37-43.
93. Campbell, K. and M. Gotz, Radial glia: multi-purpose cells for vertebrate brain development. Trends Neurosci, 2002. **25**(5): p. 235-8.
94. Hansen, D.V., et al., Neurogenic radial glia in the outer subventricular zone of human neocortex. Nature, 2010. **464**(7288): p. 554-561.
95. LaMonica, B.E., et al., OSVZ progenitors in the human cortex: an updated perspective on neurodevelopmental disease. Curr Opin Neurobiol, 2012. **22**(5): p. 747-53.

96. Dehay, C., H. Kennedy, and K.S. Kosik, The outer subventricular zone and primate-specific cortical complexification. Neuron, 2015. **85**(4): p. 683-94.
97. Molyneaux, B.J., et al., Neuronal subtype specification in the cerebral cortex. Nat Rev Neurosci, 2007. **8**(6): p. 427-37.
98. Kwan, K.Y., N. Sestan, and E.S. Anton, Transcriptional co-regulation of neuronal migration and laminar identity in the neocortex. Development, 2012. **139**(9): p. 1535-46.
99. D'Arcangelo, G., et al., A protein related to extracellular matrix proteins deleted in the mouse mutant reeler. Nature, 1995. **374**(6524): p. 719-23.
100. Hirata, T., et al., Zinc finger gene fez-like functions in the formation of subplate neurons and thalamocortical axons. Dev Dyn, 2004. **230**(3): p. 546-56.
101. Arlotta, P., et al., Neuronal subtype-specific genes that control corticospinal motor neuron development in vivo. Neuron, 2005. **45**(2): p. 207-21.
102. Chen, B., L.R. Schaevitz, and S.K. McConnell, Fezl regulates the differentiation and axon targeting of layer 5 subcortical projection neurons in cerebral cortex. Proc Natl Acad Sci U S A, 2005. **102**(47): p. 17184-9.
103. McEvilly, R.J., et al., Transcriptional regulation of cortical neuron migration by POU domain factors. Science, 2002. **295**(5559): p. 1528-32.
104. Sugitani, Y., et al., Brn-1 and Brn-2 share crucial roles in the production and positioning of mouse neocortical neurons. Genes Dev, 2002. **16**(14): p. 1760-5.
105. Alcamo, E.A., et al., Satb2 regulates callosal projection neuron identity in the developing cerebral cortex. Neuron, 2008. **57**(3): p. 364-77.
106. Cubelos, B., et al., Cux-2 controls the proliferation of neuronal intermediate precursors of the cortical subventricular zone. Cereb Cortex, 2008. **18**(8): p. 1758-70.
107. Nieto, M., et al., Expression of Cux-1 and Cux-2 in the subventricular zone and upper layers II-IV of the cerebral cortex. J Comp Neurol, 2004. **479**(2): p. 168-80.
108. Franco, S.J., et al., Fate-restricted neural progenitors in the mammalian cerebral cortex. Science, 2012. **337**(6095): p. 746-9.

109. Fame, R.M., J.L. MacDonald, and J.D. Macklis, Development, specification, and diversity of callosal projection neurons. Trends Neurosci, 2011. **34**(1): p. 41-50.
110. Molyneaux, B.J., et al., Novel subtype-specific genes identify distinct subpopulations of callosal projection neurons. J Neurosci, 2009. **29**(39): p. 12343-54.
111. Grunz, H. and L. Tacke, Neural differentiation of Xenopus laevis ectoderm takes place after disaggregation and delayed reaggregation without inducer. Cell Differ Dev, 1989. **28**(3): p. 211-7.
112. Wilson, P.A. and A. Hemmati-Brivanlou, Induction of epidermis and inhibition of neural fate by Bmp-4. Nature, 1995. **376**(6538): p. 331-3.
113. Kelava, I. and M.A. Lancaster, Stem Cell Models of Human Brain Development. Cell Stem Cell, 2016. **18**(6): p. 736-48.
114. Kawasaki, H., et al., Induction of midbrain dopaminergic neurons from ES cells by stromal cell-derived inducing activity. Neuron, 2000. **28**(1): p. 31-40.
115. Tropepe, V., et al., Direct neural fate specification from embryonic stem cells: a primitive mammalian neural stem cell stage acquired through a default mechanism. Neuron, 2001. **30**(1): p. 65-78.
116. Zhang, S.C., et al., In vitro differentiation of transplantable neural precursors from human embryonic stem cells. Nat Biotechnol, 2001. **19**(12): p. 1129-33.
117. Ying, Q.L., et al., Conversion of embryonic stem cells into neuroectodermal precursors in adherent monoculture. Nat Biotechnol, 2003. **21**(2): p. 183-6.
118. Watanabe, K., et al., Directed differentiation of telencephalic precursors from embryonic stem cells. Nat Neurosci, 2005. **8**(3): p. 288-96.
119. Elkabetz, Y., et al., Human ES cell-derived neural rosettes reveal a functionally distinct early neural stem cell stage. Genes Dev, 2008. **22**(2): p. 152-65.
120. Elkabetz, Y. and L. Studer, Human ESC-derived neural rosettes and neural stem cell progression. Cold Spring Harb Symp Quant Biol, 2008. **73**: p. 377-87.
121. Chambers, S.M., et al., Highly efficient neural conversion of human ES and iPS cells by dual inhibition of SMAD signaling. Nat Biotechnol, 2009. **27**(3): p. 275-80.

122. Gaspard, N., et al., Generation of cortical neurons from mouse embryonic stem cells. Nat Protoc, 2009. **4**(10): p. 1454-63.
123. Boissart, C., et al., Differentiation from human pluripotent stem cells of cortical neurons of the superficial layers amenable to psychiatric disease modeling and high-throughput drug screening. Transl Psychiatry, 2013. **3**: p. e294.
124. Mariani, J., et al., Modeling human cortical development in vitro using induced pluripotent stem cells. Proc Natl Acad Sci U S A, 2012. **109**(31): p. 12770-5.
125. Qi, Y., et al., Combined small-molecule inhibition accelerates the derivation of functional cortical neurons from human pluripotent stem cells. Nat Biotechnol, 2017. **35**(2): p. 154-163.
126. Maroof, A.M., et al., Directed differentiation and functional maturation of cortical interneurons from human embryonic stem cells. Cell Stem Cell, 2013. **12**(5): p. 559-72.
127. Edri, R., et al., Analysing human neural stem cell ontogeny by consecutive isolation of Notch active neural progenitors. Nat Commun, 2015. **6**: p. 6500.
128. Camp, J.G., et al., Human cerebral organoids recapitulate gene expression programs of fetal neocortex development. Proc Natl Acad Sci U S A, 2015. **112**(51): p. 15672-7.
129. Lancaster, M.A., et al., Cerebral organoids model human brain development and microcephaly. Nature, 2013. **501**(7467): p. 373-9.
130. Quadrato, G., et al., Cell diversity and network dynamics in photosensitive human brain organoids. Nature, 2017. **545**(7652): p. 48-53.
131. Pasca, A.M., et al., Functional cortical neurons and astrocytes from human pluripotent stem cells in 3D culture. Nat Methods, 2015. **12**(7): p. 671-8.
132. Qian, X., et al., Brain-Region-Specific Organoids Using Mini-bioreactors for Modeling ZIKV Exposure. Cell, 2016. **165**(5): p. 1238-1254.
133. Bershteyn, M., et al., Human iPSC-Derived Cerebral Organoids Model Cellular Features of Lissencephaly and Reveal Prolonged Mitosis of Outer Radial Glia. Cell Stem Cell, 2017. **20**(4): p. 435-449 e4.
134. Eiraku, M., et al., Self-organized formation of polarized cortical tissues from ESCs and its active manipulation by extrinsic signals. Cell Stem Cell, 2008. **3**(5): p. 519-32.

135. Iefremova, V., et al., An Organoid-Based Model of Cortical Development Identifies Non-Cell-Autonomous Defects in Wnt Signaling Contributing to Miller-Dieker Syndrome. Cell Rep, 2017. **19**(1): p. 50-59.
136. Kadoshima, T., et al., Self-organization of axial polarity, inside-out layer pattern, and species-specific progenitor dynamics in human ES cell-derived neocortex. Proc Natl Acad Sci U S A, 2013. **110**(50): p. 20284-9.
137. Ishibashi, M., et al., Targeted disruption of mammalian hairy and Enhancer of split homolog-1 (HES-1) leads to up-regulation of neural helix-loop-helix factors, premature neurogenesis, and severe neural tube defects. Genes & Development, 1995. **9**(24): p. 3136-3148.
138. Tomita, K., et al., Mammalian hairy and Enhancer of split homolog 1 regulates differentiation of retinal neurons and is essential for eye morphogenesis. Neuron, 1996. **16**(4): p. 723-34.
139. de la Pompa, J.L., et al., Conservation of the Notch signalling pathway in mammalian neurogenesis. Development, 1997. **124**(6): p. 1139-48.
140. Gaiano, N., J.S. Nye, and G. Fishell, Radial glial identity is promoted by Notch1 signaling in the murine forebrain. Neuron, 2000. **26**(2): p. 395-404.
141. Ohtsuka, T., et al., Roles of the basic helix-loop-helix genes Hes1 and Hes5 in expansion of neural stem cells of the developing brain. J Biol Chem, 2001. **276**(32): p. 30467-74.
142. Hatakeyama, J. and R. Kageyama, Notch1 expression is spatiotemporally correlated with neurogenesis and negatively regulated by Notch1-independent Hes genes in the developing nervous system. Cereb Cortex, 2006. **16 Suppl 1**: p. i132-7.
143. Basak, O. and V. Taylor, Identification of self-replicating multipotent progenitors in the embryonic nervous system by high Notch activity and Hes5 expression. Eur J Neurosci, 2007. **25**(4): p. 1006-22.
144. Takahashi, T., R.S. Nowakowski, and V.S. Caviness, Jr., Cell cycle parameters and patterns of nuclear movement in the neocortical proliferative zone of the fetal mouse. J Neurosci, 1993. **13**(2): p. 820-33.
145. Kornack, D.R. and P. Rakic, Radial and horizontal deployment of clonally related cells in the primate neocortex: relationship to distinct mitotic lineages. Neuron, 1995. **15**(2): p. 311-21.

146. Ziller, M.J., et al., Dissecting neural differentiation regulatory networks through epigenetic footprinting. Nature, 2015. **518**(7539): p. 355-359.
147. Ziv, O., et al., Quantitative Live Imaging of Human Embryonic Stem Cell Derived Neural Rosettes Reveals Structure-Function Dynamics Coupled to Cortical Development. PLoS Comput Biol, 2015. **11**(10): p. e1004453.
148. Jackson, A.P., et al., Identification of microcephalin, a protein implicated in determining the size of the human brain. Am J Hum Genet, 2002. **71**(1): p. 136-42.
149. Bond, J., et al., ASPM is a major determinant of cerebral cortical size. Nat Genet, 2002. **32**(2): p. 316-20.
150. Moynihan, L., et al., A third novel locus for primary autosomal recessive microcephaly maps to chromosome 9q34. Am J Hum Genet, 2000. **66**(2): p. 724-7.
151. Leal, G.F., et al., A novel locus for autosomal recessive primary microcephaly (MCPH6) maps to 13q12.2. J Med Genet, 2003. **40**(7): p. 540-2.
152. Kumar, A., et al., Mutations in STIL, encoding a pericentriolar and centrosomal protein, cause primary microcephaly. Am J Hum Genet, 2009. **84**(2): p. 286-90.
153. Mlakar, J., et al., Zika Virus Associated with Microcephaly. N Engl J Med, 2016. **374**(10): p. 951-8.
154. Tang, H., et al., Zika Virus Infects Human Cortical Neural Progenitors and Attenuates Their Growth. Cell Stem Cell, 2016. **18**(5): p. 587-90.
155. Garcez, P.P., et al., Zika virus impairs growth in human neurospheres and brain organoids. Science, 2016. **352**(6287): p. 816-8.
156. Liang, Q., et al., Zika Virus NS4A and NS4B Proteins Deregulate Akt-mTOR Signaling in Human Fetal Neural Stem Cells to Inhibit Neurogenesis and Induce Autophagy. Cell Stem Cell, 2016. **19**(5): p. 663-671.
157. Aplan, P.D., D.P. Lombardi, and I.R. Kirsch, Structural characterization of SIL, a gene frequently disrupted in T-cell acute lymphoblastic leukemia. Mol Cell Biol, 1991. **11**(11): p. 5462-9.
158. Tang, C.J., et al., The human microcephaly protein STIL interacts with CPAP and is required for procentriole formation. Embo j, 2011. **30**(23): p. 4790-804.
159. Vulprecht, J., et al., STIL is required for centriole duplication in human cells. J Cell Sci, 2012. **125**(Pt 5): p. 1353-62.

160. Arquint, C., et al., Cell-cycle-regulated expression of STIL controls centriole number in human cells. J Cell Sci, 2012. **125**(Pt 5): p. 1342-52.
161. Izraeli, S., et al., The SIL gene is required for mouse embryonic axial development and left-right specification. Nature, 1999. **399**(6737): p. 691-4.
162. Zitouni, S., et al., CDK1 Prevents Unscheduled PLK4-STIL Complex Assembly in Centriole Biogenesis. Curr Biol, 2016. **26**(9): p. 1127-37.
163. Ohta, M., et al., Direct interaction of Plk4 with STIL ensures formation of a single procentriole per parental centriole. Nat Commun, 2014. **5**: p. 5267.
164. David, A., et al., Molecular basis of the STIL coiled coil oligomerization explains its requirement for de-novo formation of centrosomes in mammalian cells. Sci Rep, 2016. **6**: p. 24296.
165. Arquint, C. and E.A. Nigg, STIL microcephaly mutations interfere with APC/C-mediated degradation and cause centriole amplification. Curr Biol, 2014. **24**(4): p. 351-60.
166. Placantonakis, D.G., et al., BAC transgenesis in human embryonic stem cells as a novel tool to define the human neural lineage. Stem Cells, 2009. **27**(3): p. 521-32.
167. Okita, K., et al., A more efficient method to generate integration-free human iPS cells. Nat Methods, 2011. **8**(5): p. 409-12.
168. Beers, J., et al., Passaging and colony expansion of human pluripotent stem cells by enzyme-free dissociation in chemically defined culture conditions. Nat Protoc, 2012. **7**(11): p. 2029-40.
169. Gafni, O., et al., Derivation of novel human ground state naive pluripotent stem cells. Nature, 2013. **504**(7479): p. 282-6.
170. Lancaster, M.A. and J.A. Knoblich, Generation of cerebral organoids from human pluripotent stem cells. Nat Protoc, 2014. **9**(10): p. 2329-40.
171. Kang, H.J., et al., Spatio-temporal transcriptome of the human brain. Nature, 2011. **478**(7370): p. 483-9.
172. Dobin, A., et al., STAR: ultrafast universal RNA-seq aligner. Bioinformatics, 2013. **29**(1): p. 15-21.
173. Li, H., et al., The Sequence Alignment/Map format and SAMtools. Bioinformatics, 2009. **25**(16): p. 2078-9.
174. Anders, S., P.T. Pyl, and W. Huber, HTSeq--a Python framework to work with high-throughput sequencing data. Bioinformatics, 2015. **31**(2): p. 166-9.

175. Johnson, W.E., C. Li, and A. Rabinovic, Adjusting batch effects in microarray expression data using empirical Bayes methods. Biostatistics, 2007. **8**(1): p. 118-27.
176. Leek, J.T., et al., The sva package for removing batch effects and other unwanted variation in high-throughput experiments. Bioinformatics, 2012. **28**(6): p. 882-3.
177. Fellenberg, K., et al., Correspondence analysis applied to microarray data. Proc Natl Acad Sci U S A, 2001. **98**(19): p. 10781-6.
178. Klein, A.M., et al., Droplet barcoding for single-cell transcriptomics applied to embryonic stem cells. Cell, 2015. **161**(5): p. 1187-1201.
179. Zilionis, R., et al., Single-cell barcoding and sequencing using droplet microfluidics. Nat Protoc, 2017. **12**(1): p. 44-73.
180. Macosko, E.Z., et al., Highly Parallel Genome-wide Expression Profiling of Individual Cells Using Nanoliter Droplets. Cell, 2015. **161**(5): p. 1202-1214.
181. Huelsken, J., et al., Requirement for β-Catenin in Anterior-Posterior Axis Formation in Mice. The Journal of Cell Biology, 2000. **148**(3): p. 567-578.
182. Liu, P., et al., Requirement for Wnt3 in vertebrate axis formation. Nat Genet, 1999. **22**(4): p. 361-5.
183. Yoshikawa, Y., et al., Evidence that absence of Wnt-3a signaling promotes neuralization instead of paraxial mesoderm development in the mouse. Dev Biol, 1997. **183**(2): p. 234-42.
184. Gunhaga, L., et al., Specification of dorsal telencephalic character by sequential Wnt and FGF signaling. Nat Neurosci, 2003. **6**(7): p. 701-7.
185. Backman, M., et al., Effects of canonical Wnt signaling on dorso-ventral specification of the mouse telencephalon. Dev Biol, 2005. **279**(1): p. 155-68.
186. Wrobel, C.N., et al., Persistent expression of stabilized beta-catenin delays maturation of radial glial cells into intermediate progenitors. Dev Biol, 2007. **309**(2): p. 285-97.
187. Mishina, Y., et al., Bmpr encodes a type I bone morphogenetic protein receptor that is essential for gastrulation during mouse embryogenesis. Genes Dev, 1995. **9**(24): p. 3027-37.
188. Yao, Z., et al., A Single-Cell Roadmap of Lineage Bifurcation in Human ESC Models of Embryonic Brain Development. Cell Stem Cell, 2017. **20**(1): p. 120-134.

189. O'Leary, D.D., S.J. Chou, and S. Sahara, Area patterning of the mammalian cortex. Neuron, 2007. **56**(2): p. 252-69.
190. Simeone, A., et al., Nested expression domains of four homeobox genes in developing rostral brain. Nature, 1992. **358**(6388): p. 687-90.
191. Delaval, B. and S.J. Doxsey, Pericentrin in cellular function and disease. J Cell Biol, 2010. **188**(2): p. 181-90.
192. David, A., et al., Lack of centrioles and primary cilia in STIL(-/-) mouse embryos. Cell Cycle, 2014. **13**(18): p. 2859-68.
193. Eiraku, M., et al., Self-organizing optic-cup morphogenesis in three-dimensional culture. Nature, 2011. **472**(7341): p. 51-6.
194. Thomson, J.A., et al., Embryonic stem cell lines derived from human blastocysts. Science, 1998. **282**(5391): p. 1145-7.
195. Tesar, P.J., et al., New cell lines from mouse epiblast share defining features with human embryonic stem cells. Nature, 2007. **448**(7150): p. 196-9.
196. Takahashi, K., et al., Induction of pluripotent stem cells from adult human fibroblasts by defined factors. Cell, 2007. **131**(5): p. 861-72.
197. Ying, Q.L., et al., The ground state of embryonic stem cell self-renewal. Nature, 2008. **453**(7194): p. 519-23.
198. Rais, Y., et al., Deterministic direct reprogramming of somatic cells to pluripotency. Nature, 2013. **502**(7469): p. 65-70.
199. Theunissen, T.W., et al., Systematic identification of culture conditions for induction and maintenance of naive human pluripotency. Cell Stem Cell, 2014. **15**(4): p. 471-487.
200. Theunissen, T.W., et al., Molecular Criteria for Defining the Naive Human Pluripotent State. Cell Stem Cell, 2016. **19**(4): p. 502-515.
201. Caronia-Brown, G., et al., The cortical hem regulates the size and patterning of neocortex. Development, 2014. **141**(14): p. 2855-65.
202. Yoshida, M., et al., Massive loss of Cajal-Retzius cells does not disrupt neocortical layer order. Development, 2006. **133**(3): p. 537-45.
203. Xu, R.H., et al., BMP4 initiates human embryonic stem cell differentiation to trophoblast. Nat Biotechnol, 2002. **20**(12): p. 1261-4.
204. D'Amour, K.A., et al., Efficient differentiation of human embryonic stem cells to definitive endoderm. Nat Biotechnol, 2005. **23**(12): p. 1534-41.

205. Laflamme, M.A., et al., Cardiomyocytes derived from human embryonic stem cells in pro-survival factors enhance function of infarcted rat hearts. Nat Biotechnol, 2007. **25**(9): p. 1015-24.
206. Munoz-Sanjuan, I. and A.H. Brivanlou, Neural induction, the default model and embryonic stem cells. Nat Rev Neurosci, 2002. **3**(4): p. 271-80.
207. Gouti, M., et al., In vitro generation of neuromesodermal progenitors reveals distinct roles for wnt signalling in the specification of spinal cord and paraxial mesoderm identity. PLoS Biol, 2014. **12**(8): p. e1001937.
208. Griffith, E., et al., Mutations in pericentrin cause Seckel syndrome with defective ATR-dependent DNA damage signaling. Nat Genet, 2008. **40**(2): p. 232-6.
209. Tibelius, A., et al., Microcephalin and pericentrin regulate mitotic entry via centrosome-associated Chk1. J Cell Biol, 2009. **185**(7): p. 1149-57.
210. Thomaidou, D., et al., Apoptosis and Its Relation to the Cell Cycle in the Developing Cerebral Cortex. The Journal of Neuroscience, 1997. **17**(3): p. 1075-1085.
211. Sato, N., et al., Maintenance of pluripotency in human and mouse embryonic stem cells through activation of Wnt signaling by a pharmacological GSK-3-specific inhibitor. Nat Med, 2004. **10**(1): p. 55-63.
212. Marson, A., et al., Wnt signaling promotes reprogramming of somatic cells to pluripotency. Cell Stem Cell, 2008. **3**(2): p. 132-5.
213. ten Berge, D., et al., Embryonic stem cells require Wnt proteins to prevent differentiation to epiblast stem cells. Nat Cell Biol, 2011. **13**(9): p. 1070-5.
214. Kurek, D., et al., Endogenous WNT signals mediate BMP-induced and spontaneous differentiation of epiblast stem cells and human embryonic stem cells. Stem Cell Reports, 2015. **4**(1): p. 114-128.
215. Davidson, K.C., et al., Wnt/beta-catenin signaling promotes differentiation, not self-renewal, of human embryonic stem cells and is repressed by Oct4. Proc Natl Acad Sci U S A, 2012. **109**(12): p. 4485-90.
216. Aubert, J., et al., Functional gene screening in embryonic stem cells implicates Wnt antagonism in neural differentiation. Nat Biotechnol, 2002. **20**(12): p. 1240-5.

217. Blauwkamp, T.A., et al., Endogenous Wnt signalling in human embryonic stem cells generates an equilibrium of distinct lineage-specified progenitors. Nat Commun, 2012. **3**: p. 1070.
218. Kriks, S., et al., Dopamine neurons derived from human ES cells efficiently engraft in animal models of Parkinson's disease. Nature, 2011. **480**(7378): p. 547-51.

6. Abbreviations

A-P — Anterior-Posterior

APC/C — Anaphase promoting complex / cyclosome

AVE — Anterior visceral endoderm

bHLH — Basic helix-loop-helix

BMP — Bone morphogenetic protein

bRG — Basal radial glial

CC — Coiled coil

CNS — Central nervous system

CP — Cortical plate

Dkk1 — Dickkopf 1

D-V — Dorso-ventral

EB — Embryoid body

ESC — Embryonic stem cells

FACS — Fluorescence activated cell sorting

FGF — Fibroblast growth factor

hESC — Human embryonic stem cells

ICM — Inner cell mass

INM — Interkinetic nuclear migration

IP — Intermediate progenitors

iPSC — Induced pluripotent stem cell

MCPH — Microcephaly primary hereditary (Autosomal recessive primary microcephaly)

MEF — Mouse embryonic fibroblast

mESC — Mouse embryonic stem cells

mPSC — Mouse pluripotent stem cell

NE — Neuroepithelial

NECD — Notch extracellular domain

NICD — Notch intra cellular domain

NPC — Neural progenitor cell

NSC — Neural stem cells

OSVZ — Outer sub-ventricular zone

PSC — Pluripotent stem cells

RA — Retinoic acid

RG — Radial glial

R-NSC — Rosette neural stem cell

SHH — Sonic Hedgehog

SVZ — Sub-ventricular zone

TACE — TNF-α ADAM metalloprotease converting enzyme

TE — Trophoectoderm

TM — Transmembrane domain

VZ — Ventricular zone

ZIKV — Zika virus

7. List of publications

- **Mutukula N***, Rotem Volkman*, Sneha Arora, Elzbieta Gralinska, Ramon Vidal, Björn Brändl, Stefan Börno, Bernd Timmermann, Franz-Josef Müller, Sascha Sauer, Martin Vingron and Yechiel Elkabetz “Combinatorial Pathway Inhibition in Brain Organoids Dictates Distinct Regional, Stem Cell and Cytoarchitectural Signatures in Health and Disease” (Manuscript in communication)

- **Mutukula N**, Elkabetz Y "Neural Killer" Cells: Autologous Cytotoxic Neural Stem Cells for Fighting Glioma.” **Cell Stem Cell.** 2017 Apr 6;20(4):426-428. doi: 10.1016/j.stem.2017.03.019.

- Ziv O, Zaritsky A, Yaffe Y, **Mutukula N**, Edri R, Elkabetz Y “Quantitative Live Imaging of Human Embryonic Stem Cell Derived Neural Rosettes Reveals Structure-Function Dynamics Coupled to Cortical Development.” **PLoS Comput Biol**. 2015 Oct 16;11(10):e1004453

- Edri R, Yaffe Y, Ziller MJ, **Mutukula N**, Volkman R, David E, Jacob-Hirsch J, Malcov H, Levy C, Rechavi G, Gat-Viks I, Meissner A, Elkabetz Y “Analysing human neural stem cell ontogeny by consecutive isolation of Notch active neural progenitors.” **Nat Commun**. 2015 Mar 23; 6:6500.

- Sharma T, Kumari P, Pincha N, **Mutukula N**, Saha S, Jana SS, Ta M “Inhibition of Non Muscle Myosin II Leads to G0/G1 Arrest of Wharton’s Jelly-derived Mesenchymal Stem Cells” **Cytotherapy**. 2014 May; 16(5):640-52.